1-28-2019

Exploration of the Lean Limit in a Split-Cycle Engine

Steven Dal Bello
University of Windsor

Exploration of the Lean Limit in a Split-Cycle Engine

By:

Steven Dal Bello

A Thesis
Submitted to the Faculty of Graduate Studies
Through the Department of Mechanical, Automotive and Materials Engineering
in Partial Fulfillment of the Requirements for
the Degree of Master of Applied Science
at the University of Windsor

Windsor, Ontario, Canada

Exploration of the Lean Limit in a Split-Cycle Engine

by

Steven Dal Bello

APPROVED BY:

D. Green

Department of Mechanical, Automotive and Materials Engineering

---

M. Zheng

Department of Mechanical, Automotive and Materials Engineering

---

A. Sobiesiak, Advisor

Department of Mechanical, Automotive and Materials Engineering

January 15, 2019

Declaration of Originality

I hereby certify that I am the sole author of this thesis and that no part of this thesis has been published or submitted for publication.

I certify that, to the best of my knowledge, my thesis does not infringe upon anyone's copyright nor violate any proprietary rights and that any ideas, techniques, quotations, or any other material from the work of other people included in my thesis, published or otherwise, are fully acknowledged in accordance with the standard referencing practices. Furthermore, to the extent that I have included copyrighted material that surpasses the bounds of fair dealing within the meaning of the Canada Copyright Act, I certify that I have obtained a written permission from the copyright owner(s) to include such material(s) in my thesis and have included copies of such copyright clearances to my appendix.

I declare that this is a true copy of my thesis, including any final revisions, as approved by my thesis committee and the Graduate Studies office, and that this thesis has not been submitted for a higher degree to any other University or Institution.

Abstract

With increasing focus on efficiency and reduction of greenhouse gases, combustion processes need to be improve. Whether through use of alternative fuel or alternative combustion cycles, improvements to the combustion process are desired. Natural gas composed primarily of methane is an alternative fuel for internal combustion engines that has a potential to meet these goals. It has a high octane number, reduced CO_2 output and lower emissions than other gases. Natural gas has a low laminar flame speed, making its implementation in internal combustion engines challenging.

A split-cycle engine has been constructed at the University of Windsor to address issues typical of natural gas combustion. The architecture promotes intense turbulence leading to improved burn rates. Testing on the split-cycle has shown burn durations under 30°CA, amongst the fastest for natural gas engines presented in literature.

This work will address two issues with the split-cycle engine, the high lean limit of operation and the low loads achieved by the engine. The lean limit of operation is extended using a dual coil ignition strategy, increasing energy input to the kernel, thereby increasing stability. Secondly, it has been shown that early exhaust valve closure results in excessive combustion products being in-cylinder, resulting in 15-25% charge dilution. A change in exhaust valve timing is shown to effect the lean limit of operation.

Low loads are attempted to be addressed with a change of valve timing. The valve timing change results in improved combustion parameters yet poorer indicated output. This cause of this issue is determined using a mass balance analysis which shows that the mass flow rate through the system is partially dependent on the mass transfer from the crossover passage, which should be optimized for the best performance for this type of engine. A new parameter that is used to characterize split-cycle engine performance, the mass compressed ratio, is defined in this work.

Acknowledgements

I would like to thank my Supervisor Dr. Sobiesiak for his guidance and support throughout this project. His patience and feedback on the work I have performed is greatly appreciated. I would also like to thank Dr. Green and Dr. Zheng for being on my committee and for the useful feedback and input they have provided.

I would also like to thanks the technicians at the University for their technical assistance and fulfilling my machining requests. Specifically I would like to thank Andy Jenner, Dean Poublon, Bruce Durfy, Kevin Harkai, Ram Barakat and Frank Cicchello for there assistance with various parts of this thesis.

Finally, I would like to thank Dr. Iain Cameron, the initial fabricator of the split-cycle engine for his assistance with the various inquiries I have had for him and providing me with the resources I needed to successfully complete this thesis.

Contents

List of Tables

List of Figures

Abbreviations

AFR Air-to-Fuel Ratio.

BAT Best Achievable Ignition Timing.

BBDC Before Bottom Dead Center.

BMEP Brake Mean Effective Pressure.

BTDC Before Top Dead Center.

CA Crank Angle.

CNG Compressed Natural Gas.

CO Carbon Monoxide.

CO_2 Carbon Dioxide.

COV Coefficient of Variation.

cRIO CompactRIO.

DAQ Data Acquisition.

EGR Exhaust Gas Recirculation.

EVC Exhaust Valve Closing.

FPGA Field Programmable Gate Array.

HCPC Homogeneous Charge Progressive Combustion.

ICE Internal Combustion Engines.

IGR Internal Gas Recirculation.

IMEP Indicated Mean Effective Pressure.

isfc Indicated Specific Fuel Consumption.

LFE Laminar Flow Element.

LHV Lower Heating Value.

LPP Location of Peak Pressure.

MAF Mass Air Flow.

MC$_r$ Mass Compressed Ratio.

MFB Mass Fraction Burned.

MFF Mass Fuel Flow Rate.

NG Natural Gas.

NO$_x$ Nitrous Oxides.

OVC Overhead Valve Camshaft.

PM Particulate Matter.

PR Pressure Ratio.

PR$_n$ Normalized Pressure Ratio.

RPV Reverse Poppet Valve-Train.

SI Spark Ignition.

TDC Top Dead Center.

TDMS Technical Data Management Solution.

UEGO Universal Exhaust Gas Oxygen.

UHC Unburnt Hydrocarbons.

VI Virtual Instrument.

XOVI Crossover Passage Inlet Valve.

XOVO Crossover Passage Outlet Valve.

XOVO-c Crossover Passage Outlet Valve Closing.

XOVR Crossover Passage.

Chapter 1

Introduction

1.1 Overview

Increasingly stringent emissions requirements for internal combustion engines has led to a need to improve the combustion process. Emission regulations from governments have typically measured four major components in exhaust gas; Carbon Monoxide (CO), Nitrous Oxides (NO_x), Unburnt Hydrocarbons (UHC) and Particulate Matter (PM) [2]. Future regulations of combustion engines are to include restrictions on production of CO_2 [3], meaning reductions in CO_2 emissions is an area of great concern to combustion researchers and engine designers. As CO_2 is a product of complete combustion, decreasing CO_2 emissions will require an improvement of the overall efficiency of an engine through an improvement of the combustion process. Typical methods of improving engine efficiency have included better combustion chamber design, use of alternative fuels, and the running engines at leaner equivalence ratios.

The use of Natural Gas (NG) consisting mostly of pure methane is explored due to some of its favourable properties. The components of NG vary depend on the source of the fuel. NG produced in Canada has a high methane content and is therefore the content explored in this work [4]. NG has a high octane rating of 130 making it more resistant to knock while being run at higher compression ratios. Engines fueled by NG are also more tolerant to lean mixtures. Running a converted engine on NG has been shown to be a method of reducing emission compared to gasoline counterparts; up to 53% CO and 22% CO_2 reductions have been achieved [5]. However this reduction in tailpipe emissions is often accompanied by a decrease in output of the engine, with typical reductions ranging from 10-35% [6]. The reduction is due to the lower laminar flame speed of NG when compared to conventional gasoline. This results in

spark timing being advanced by up to 10° Crank Angle (CA)[7]. Also presenting an issue with NG engines is the gaseous fuel displacing air in the intake, thereby reducing volumetric efficiency. Previous works have shown to reduce volumetric efficiency up to 10% when converting a port injected engine to NG[8].

In-cylinder turbulence has been shown to increase the rates of combustion for both NG and gasoline fuels [7, 9, 10]. In-cylinder turbulence with large velocity fluctuations and small scale turbulent eddies are desired. Typically, in order to achieve this amount of turbulence large squish areas, high engine speeds, and compact combustion chambers are needed [1].

Another approach that has been used in order to achieve the high level of turbulence needed for rapid combustion is through the use of a split-cycle engine [11, 12]. Split-cycle operation is an engine where one cylinder performs intake and compression strokes while a second performs expansion and exhaust. This arrangement will be reviewed in depth in Chapter 2. A split-cycle engine has been constructed at the University of Windsor and evaluated for its performance [11]. Quick burn durations for a natural gas engine have been achieved, however several issues exist limiting the performance of the engine. One of the most significant factors impacting the engine performance is the lean limit of the engine. At this time a lean limit of $\Phi = 0.85$ is the minimum achievable equivalence ratio for this engine, which is high compared to other natural gas engines. In this work reasons for this lean limit are explored along with techniques for extending this lean limit. The applicability of this work extends to not just this engine, but any engine with large amounts of turbulence generation, engines running at lean limit or engines with high amounts of charge dilution.

1.2 Research Objectives

The objective of this work is to continue development and research of the split-cycle engine at the University of Windsor. The previous work on this engine has presented multiple issues with the operation of the engine [11]. The three following points have been chosen as the main focus of this research.

1. To explore performance at the lean limit of operation and develop methods for extending it. A better understanding of the causes of the lean limit will be developed and used to implement techniques for better lean limit performance. The two main methods for extension will be:

   (a) Changing the exhaust valve closing (EVC) to reduce in-cylinder trapped mass

   (b) Use of an alternative and/or high energy ignition system to improve ignition at lean limits

2. Change the cam profiles on the crossover passage (XOVR) to improve engine output. Values previously tested were those of the first design iteration where little information was known on the engine operation. Effects of changing the XOVR opening duration are explored with a new set of cam profiles that are tested and validated.

3. Use the implemented changes and the amassed data to further characterize the split-cycle engine. Data can be compared with results from the first iteration of valve timing to better characterize the operation of the engine.

1.3 Thesis Organization

This thesis is organized into seven chapters. The first chapter is the introduction. The Second chapter will go over the split-cycle engine design. Operating principles of the split-cycle are discussed, followed by a description of the engine and data acquisition constructed at the University of Windsor. Chapter 3 is a quick review of the operating parameters used to evaluate the performance of the engine. Chapter 4 gives an operational benchmark of the engine to be compared to improvements made later in the work. The split-cycle engines most impressive operating characteristic is the short burn durations it achieves. In this section the failure of the initial engine head gasket is discussed. Chapter 5 shows the results of the engine with implemented multiple coil strikes and dual coil ignition strategy. In Chapter 6 valve timing is changed on the engine and performance characteristics of the engine are discussed. Chapter 7 is a summary of the conclusions of this work.

Chapter 2

Split-Cycle Engine

In this section an overview of the split-cycle engine is presented. A literature review on the split-cycle engine and use of natural gas as a fuel is given. An overview of the split-cycle engine that has been constructed at the University of Windsor is given, with sections covering the design, control and data acquisition of the engine.

2.1 Operating Principles

A split-cycle engine is an engine in which the four engine strokes are separated into two separate cylinders. In this arrangement the first cylinder will perform the intake and compression strokes while the second will perform expansion and exhaust. In this work the first cylinder will be referred to as the compression cylinder and the second as the expansion cylinder. The two cylinders must be connected by an intermediary volume to allow for the transfer of charge from the compression to the expansion cylinder. This arrangement is beneficial to engine operation as the entire cycle can be completed in one engine revolution. A split-cycle engine would be comparable to a two cylinder four-stroke in terms of the strokes occurring during each revolution of the crankshaft.

The concept of a split-cycle engine or engines that operates on similar principles to one have been discussed in literature. Examples of designs that have been discussed in literature are the Scuderi Split-Cycle Engine [12], the Homogeneous Charge Progressive Combustion (HCPC) [13], the Tour engine [14], and the two-stroke engine concept developed by Tiainen et. al [15]. The design for each of these engine concepts varies, however all function via a previously compressed charge entering an expansion cylinder. The design that has been studied in this work is the split-cycle engine design

proposed by American engineer Carmelo Scuderi [16].

The Scuderi split-cycle engine consists of 2 cylinders connected by a high pressure crossover passage (XOVR). There is an offset between the compression and expansion cylinders with the expansion cylinder approaching engine top dead center TDC before the compression cylinder. In this arrangement the XOVR passage will ideally remain isobaric throughout the engine cycle. Figure 2.1 shows the arrangement of the split-cycle cylinders and XOVR.

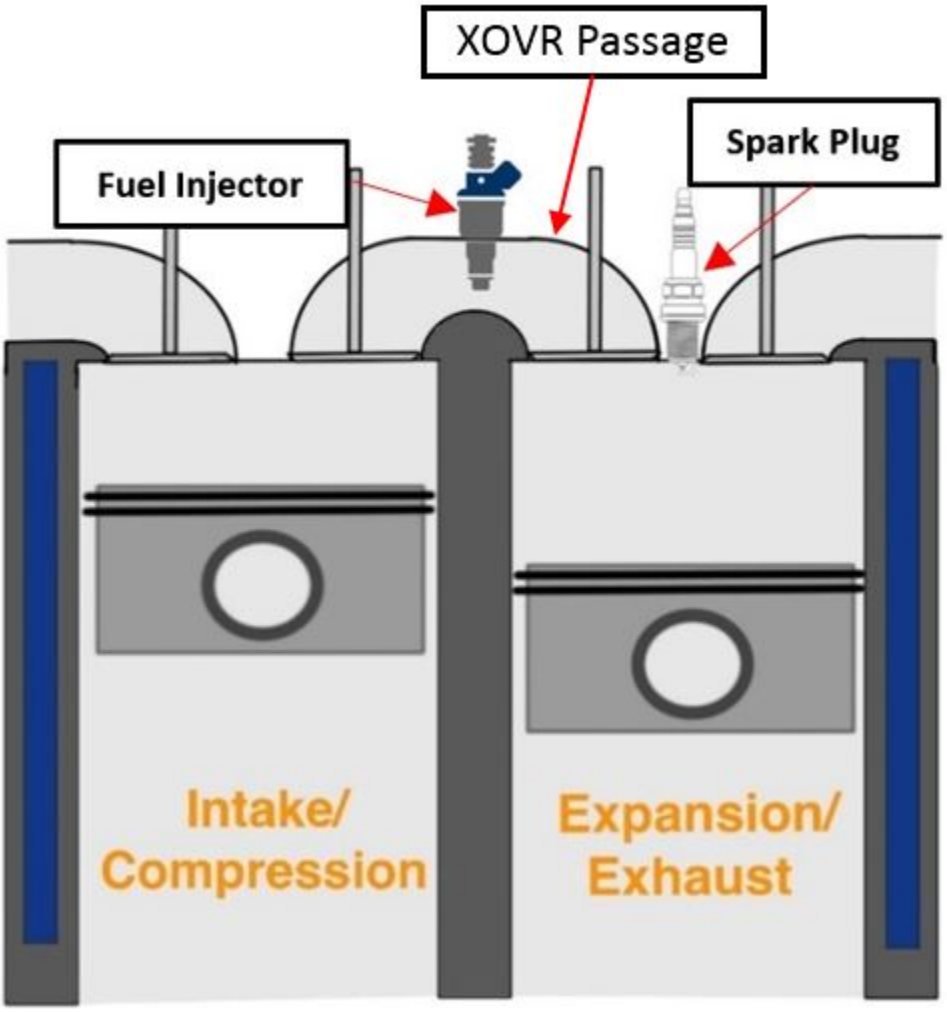

Figure 2.1: Illustration of the Split-Cycle Engine Arrangement

Fuel is injected into the XOVR while the inlet and outlet valves are both closed. Injection occurs at 270°before top dead center (BTDC), ensuring that a homogeneous charge is transferred to the cylinder. The valves from the XOVR are both open while

the engine is at TDC. At this time the charge is transferred from the high pressure XOVR to the expansion cylinder. Mass transfer occurs rapidly at sonic velocities leading to intense small scale turbulence at the time of ignition. This is due in part to the expansion cylinder being at TDC, restricting the size of the largest turbulent eddies that can be formed. Also the limited valve height of less than 4mm results in small scale turbulence generated by the flow passing over the valves. This turbulence leads to short burn durations faster than those achieved in a typical four-stroke arrangement, potentially leading to greater efficiencies.

The thermodynamic cycles can be observed to better understand the operation of the split-cycle engine. In Figure 2.2 the ideal thermodynamic cycle is shown on a Pressure-Crank Angle basis.

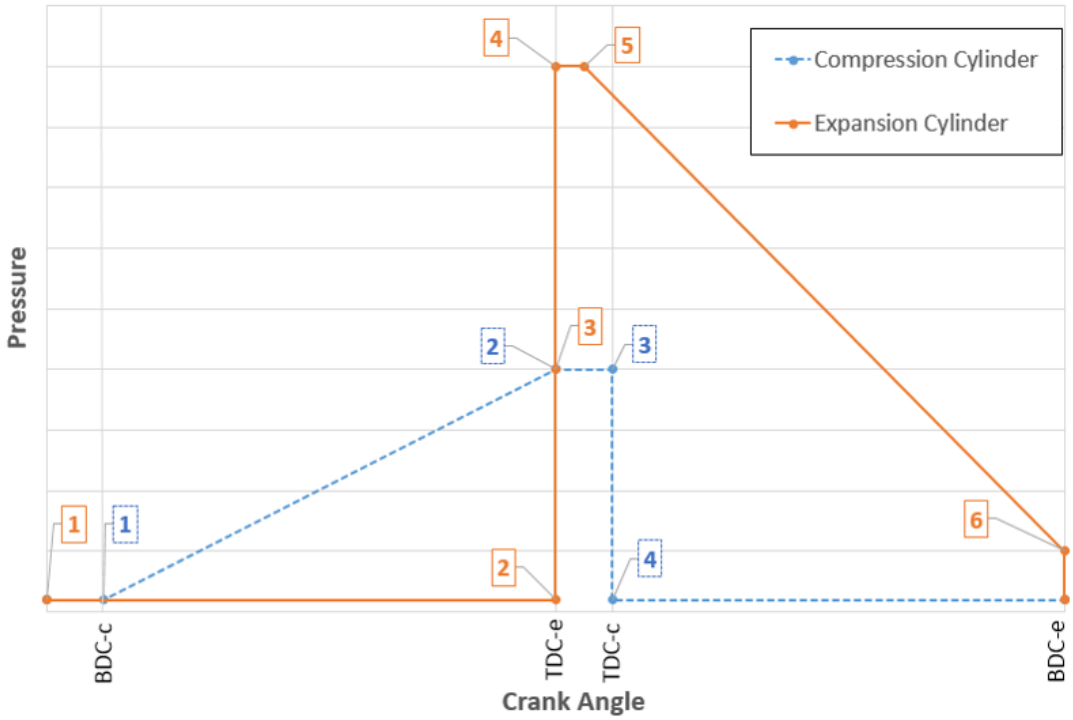

Figure 2.2: Ideal Split-Cycle Thermodynamic Cycle

It should be noted that the two traces are for both cylinders and that the processes are being performed simultaneously. The compression cylinder is the work inputted to the engine and the expansion cylinder is the work output. The processes for each cylinder will be explained.

Compression Cylinder

1-2 Polytropic Compression

2-3 Mass Transfer to XOVR

3-4 Re-expansion of trapped mass due to mechanical clearances

4-1 Fresh Air Intake

Expansion Cylinder

1-2 Exhaust Stroke

2-3 Mass Transfer from XOVR

3-4 Constant Volume Heat Release

4-5 Constant Pressure Heat Release

5-6 Polytropic Expansion

6-1 Blow Down

The compression cylinder behaves as a compressor operating on a standard compression cycle. In this engine the expansion pressure trace will differ from the theoretical one. Mass transfer does not happen instantaneously in steps **2-3**. Mass transfer will take a finite amount of time. As well any valve train will also require a finite amount of time for valves to open and close, further increasing the duration of this event. Furthermore, ignition must be delayed in order to ensure the flame does not travel into the XOVR. This results in ignition occurring after TDC. How these realities affect engine performance will be later described in Section 2.3

2.2 Natural Gas Use as a Fuel

NG is particularly advantageous as a fuel due to its reduced CO_2 emissions per unit energy output. Work by Dondero and Goldemberg [5] has shown that in an engine converted to NG the CO_2 emissions for the same power output as gasoline were reduced by 22%. This reduction in CO_2 is makes NG an attractive fuel in places where cap and trade systems have been implemented. The higher energy output of NG per mass of CO_2 make it attractive in the cap and trade systems which charge

base on carbon output [17]. Further advantages of NG are due to its high octane rating of 130. This will allow for higher compression ratios to be run in a NG Spark Ignition (SI) engine. In turn, this will lead to higher thermal efficiencies, which can be understood by looking at Equation 2.1.

$$n_{th} = 1 - \frac{1}{r_c^{k-1}} \tag{2.1}$$

In this equation r_c is the compression ratio and k is the ratio of specific heat. With an increasing compression ratio the thermal efficiency will increase.

Natural gas composition varies depending on the origin of the gas. Its major constituent is typically methane, which typically makes up 80-95% of the gas composition. Other components vary, often containing ethane, propane, butane, nitrogen gas and CO_2. The Lower Heating Value (LHV) of methane is typically 50 MJ/kg. In comparison to a more common fuel, the LHV of gasoline is typically 42MJ/kg [4].

A further advantage of NG in engines is that it can be run at lean equivalence ratios. Research has shown the ability to run NG engines at a equivalence ratio of up to $\phi = 0.6$. [6, 18] Lean equivalence ratios are desirable in SI engines due to the reductions in NO_x and CO that accompany lean burn conditions [1]. The decrease in undesired combustion products can be seen in Figure 2.3 as a function of equivalence ratio ϕ.

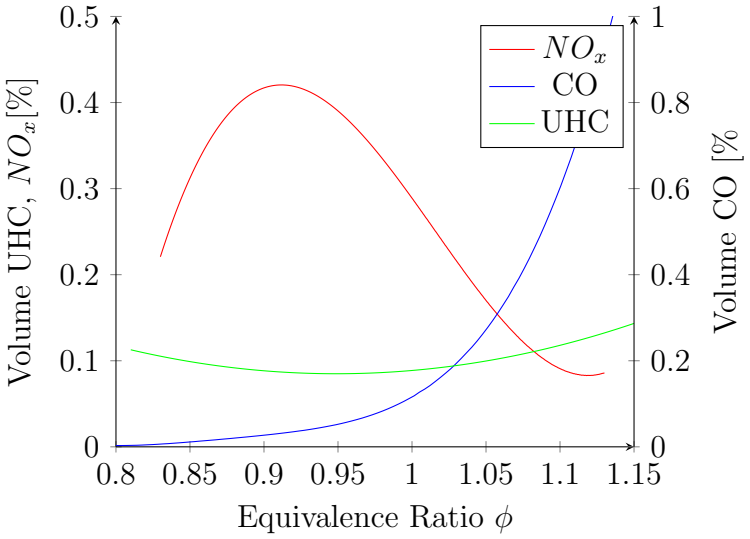

Figure 2.3: Typical variation in emissions with ϕ from Stone [1]

Issues that arise from the use of NG come from the transport, storage and burning of the fuel. The storage of NG is challenging due to the gaseous state and low density of the fuel. In an automotive application where volume available for fuel storage is extremely limited, storage systems often require complex solutions to increase storage density [19]. Further adding to complications with NG is the primary component of methane which is a significantly more potent greenhouse gas than CO_2 [20]. If leakage of methane occurs during production or delivery, it can offset any gain made by using it as a fuel. This results in a necessity to design production facilities to minimize effects of potential leakage occurring during NG production.

Issues that arise for use in internal combustion engines ICE are due to the fuel properties of NG. The laminar flame speed of methane is $U_L \approx 0.37 cm/s$, which is the slowest amongst hydrocarbon fuels [21]. This results in lower flame speeds and longer burn durations in-cylinder. In order to improve rates of combustion turbulence is needed to wrinkle the flame front and increase the burning velocity. The positive influence of increasing turbulence on the flame speed is well documented in literature [1, 22]. The slower flame speed of NG mixtures results in some performance inhibiting behaviour in engines when compared to SI engines fueled with traditional hydrocarbon fuels such as gasoline. Spark timing must be advanced in order to compensate for the longer burn durations [6]. This results in combustion being initiated further before engine TDC, which results in lower overall work output due to the pressure rise on the compression stroke.

Lower laminar flame speed can be compensated for by designing combustion chambers and intake systems to optimize in-cylinder turbulence generation. Specialized combustion chambers with large squish areas [23], and specially designed intake ports to optimize swirl generation [24] have been used as methods of increasing combustion rates through turbulence generation. Both of these methods have been shown to sufficiently increase the rate of combustion in SI NG engines. It should be noted that it has been shown that excessive turbulence can be detrimental to engine operation. Excessive turbulence can lead to extra heat transfer through the cylinder walls and therefore the engine should be designed with these limits in mind [25].

Further issues exist with NG as a fuel due to its gaseous state. Due to the fuel being gaseous it displaces air when port injected, decreasing volumetric efficiency up to 10% [26]. Furthermore, this gaseous fuel is often less homogeneous when entering

the combustion cylinder, resulting in variations in the local air-to-fuel ratio and thus lower combustion stability.

2.3 University of Windsor Split-Cycle Engine

In this section an overview on the constructed split-cycle engine is given. Important and distinguishing design features are reviewed as they directly relate to the performance of the engine. A detailed overview of the construction can be found in the dissertation of Dr. Iain Cameron [11]. Modifications discussed in Sections 2.6.3 and 4.3 should be noted for their relevant to the future operation and use of the engine.

2.3.1 Constructed Engine

The split-cycle engine constructed at the University of Windsor is based on a *Kubota Z482* 2-cylinder diesel engine. Engine components were reused during construction in order to save on cost and time during construction. Components modified and reused use in the split-cycle include the cylinder block, engine oil pan, crankshaft, pistons and the cam shaft for the intake and exhaust valves. Table 2.1 gives the specifications on the geometry of the engine.

Table 2.1: Split-Cycle Engine Specifications

Bore	67 mm
Stroke	68 mm
Connecting Rod Length	98.2 mm
Cylinder Displacement	240 cm^3
Geometric Compression Ratio	108:1
Geometric Expansion Ratio	86:1
Piston Offset Angle	20°
Spark Plug	Single Iridium, Centrally Located

An interesting feature of the split-cycle engine is the high expansion and compression ratios, significantly higher than what is used by a normal engine. These are the geometric compression ratios for the engine and are not representative of the pressures achieved with the engine due to the valve timing. The valves to the XOVR open before the pistons reach TDC, reducing the effective compression ratio. Valves also close after TDC resulting in lower expansion ratios as well. These high compression ratios are achieved using very small head clearance of $h_c = 0.5mm$. It would be

impossible to achieve this small head clearance with a typical valve train and highlights the reason for the construction of the reverse poppet valve train which will be discussed in the following section.

Reverse Poppet Valves

In order to minimize clearance volume the unique inward opening valve train has been developed, referred to as the Reverse Poppet Valve-Train (RPV). As opposed to a conventional valve train where valves are opened into the cylinder, these valves are pulled away from the cylinder and into the XOVR passage. The cam shaft is an Overhead Valve Camshaft (OVC) that operates separate from the conventional valve train for intake and exhaust. A drawing of the cross section of the valve arrangement can be seen in Figure 2.4 [11]

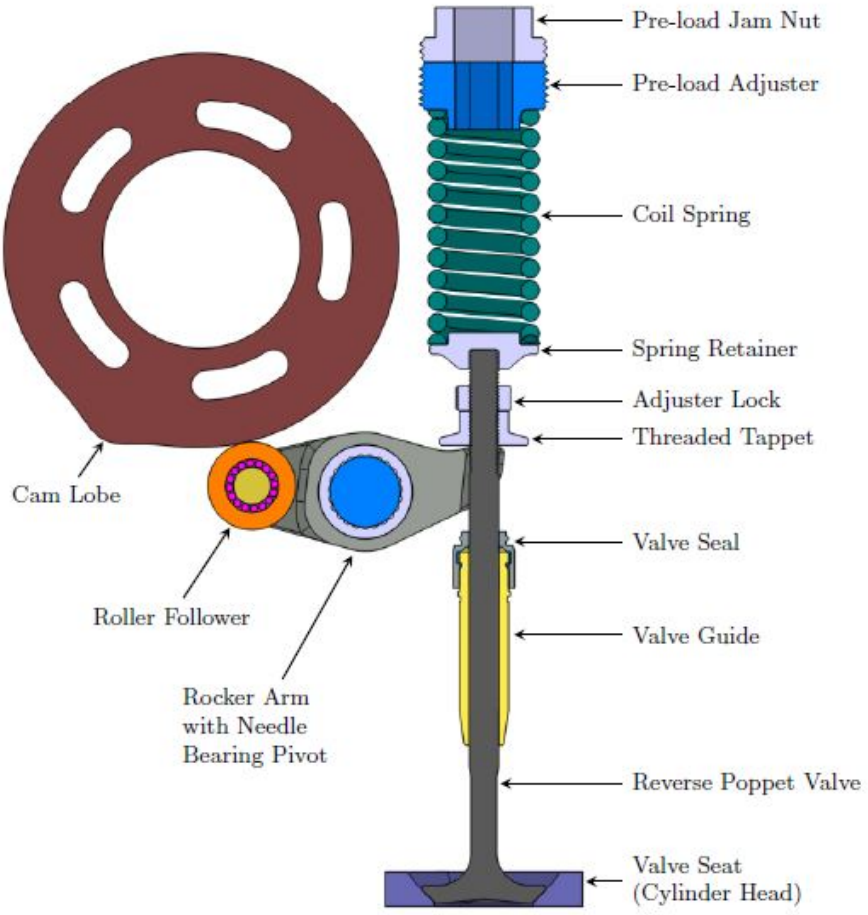

Figure 2.4: Cross-Section of RPV OHC

This is a unique arrangement only seen in the split-cycle engine. All components had to be designed and fabricated at te University of Windsor and the process is documented in the thesis of Dr.Iain Cameron [11].

Another item of note with the valve train is the low valve lift and short opening duration of the valves. Nominal valve opening duration is 50°CA, significantly shorter than durations of typical 4-stroke engine. Maximum lift was initially designed with a 3.5mm lift on both intake and exhaust, however has it been minimized based on results from testing tests. The short opening duration and low valve lift are only needed due to the high pressure of the XOVR passage. Since flow is occurring at sonic velocities large lifts and durations are not required to fill the cylinder. The arrangement of the sonic flow passing through the valves with low lift also leads to intense, small scale turbulence at the time of ignition.

Engine Head Construction

In order to accommodate the RPV discussed in the previous section a custom engine head needed to be constructed. During design precedence was given to existing components from the stock Kubota engine. The design that was chosen was a two piece cylinder head. The lower mates with the deck of the engine block using the stock Kubota gasket. In the top of the lower head the crossover passage is machined. To seal this high pressure volume a copper gasket is constructed to seal between the upper and lower head. The failure of the original design of this gasket is documented in Section 4.3. The upper head contains all valvetrain components and seals the XOVR passage.

Fuel System

The split-cycle engine is fuelled by Compressed Natural Gas (CNG). The CNG is injected into the XOVR at a pressure of 1000psi ($\approx 68bar$). Injection into the XOVR passage solves one of the major issues with the usage of CNG in that it allows for adequate mixture preparation as injection occurs significantly before TDC. The large volume of the XOVR allows for adequate mixing of the fuel before delivery into the expansion cylinder.

2.3.2 Engine Dynamometer

The split-cycle engine is connected to an 15V AC dynamometer, often shortened to dyno. The dyno is used for both energy dissipation and motoring of the engine. The engines output shaft is connected to the AC dyno using a belt drive. Due to the frictional losses caused by a belt, the presented values for indicated performance of this work will be the Indicated Mean Effective Pressure (IMEP), obtained from the in-cylinder pressure. An image of the set-up is given in Figure 2.5.

Figure 2.5: Engine Dynamometer Set-Up

2.4 Split-Cycle Engine Operating Characteristics

With the split-cycle engine there is a significant difference in what can be achieved in theory versus what happens in reality. The limitations of the practical implementation of a split-cycle engine can be seen in the operating pressure traces in Figure 2.6.

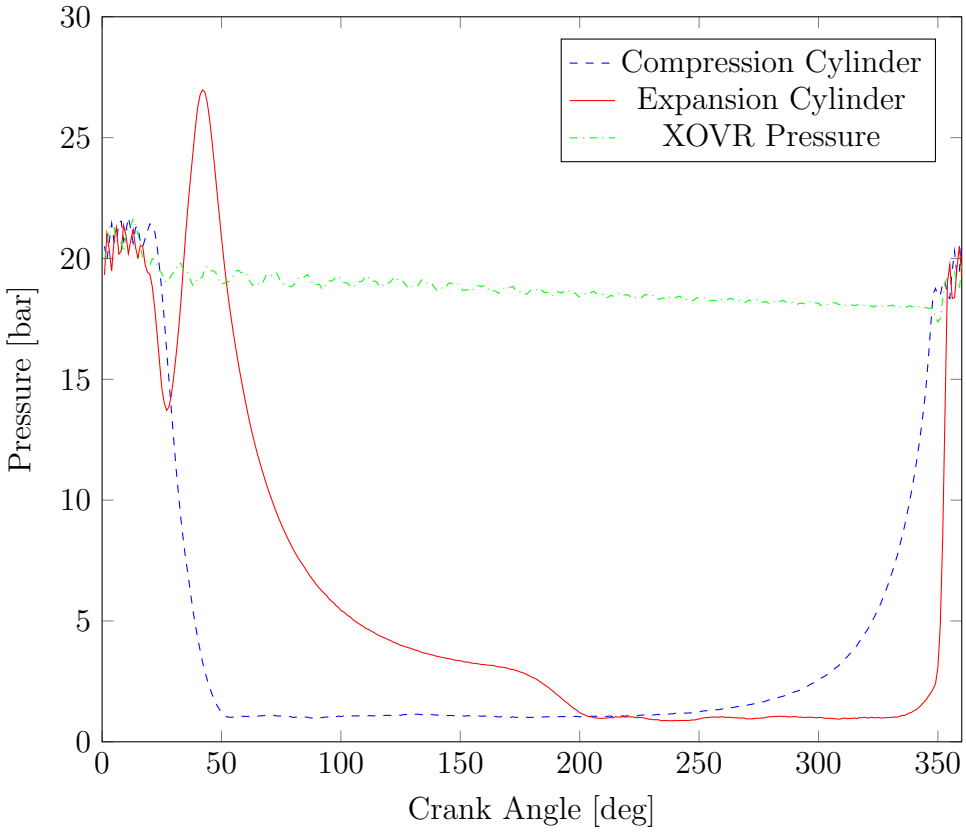

Figure 2.6: Pressure Traces for Split-Cycle Engine During Normal Operation

This figure shows many of the realities of the actual split-cycle engine cycle. It should be noted that the XOVR pressure is decreasing slightly throughout the cycle. This pressure drop is partially attributed to heat transfer losses, but is also due to mass loss occurring in the XOVR. The second characteristic to note is the opening duration of the compression and expansion cylinder, from roughly 350°(10°BTDC) to 30°ATDC. Mass transfer from the compression cylinder and to the expansion cylinders take a finite amount of time, limiting the operation of the engine. The last characteristic to note is the effect of the late ignition timing. A unique characteristic of the split-cycle engine is the pressure drop that occurs before the heat release begins in-cylinder (from 25-35°ATDC). Ignition timing is limited by the closing of the XOVR outlet valve, as any earlier ignition would result in flame propagating into the XOVR passage.

2.5 Split-Cycle Advantages and Disadvantages

The split-cycle engine has been constructed in an attempt to address some of the short comings of burning NG and of SI engines in general. The advantages and

disadvantages of the split-cycle engine constructed at the University of Windsor are given in this section.

2.5.1 Advantages of Split-Cycle Architecture

- Engine only takes one crankshaft revolution (360°) to complete an entire engine cycle.
- A power stroke occurs on every cycle. This results in the split-cycle having performance characteristics similar to a 2-stroke engine without the problems associated with two strokes, such as short circuiting and burning of engine oil.
- Fuel is injected into the XOVR passage allowing for good mixing of air and fuel, creating a well pre-mixed charge.
- No risk of knocking on the compression stroke as only air is compressed.
- Turbulence generation is decoupled from engine speed, not requiring higher engine speeds for turbulence generation. Allows for quick burn to occur at all conditions, including part load.
- Mixture transfer from the XOVR to the combustion cylinder occurs at TDC of expansion cylinder. Causes intense small scale turbulence at the time of ignition, leading to fast burn rates.

2.5.2 Disadvantages of Split-Cycle Architecture

- The split-cycle engine with its two valvetrains and the RPV is more complex than a traditional 2-stroke or 4-stroke engine
- Ignition occurs after TDC, resulting in an expanding volume during the entire flame development and main burn periods.
- Ignition timing is limited by the closing of the XOVR outlet valve, which retards ignition timing.
- The XOVR is a significant source of heat loss from compressed charge at high temperature remaining in the XOVR for an extended period of time. Furthermore, flows into and out of the XOVR are non-isentropic, resulting in further heat losses.

2.6 Data Acquisition, Control and Post-Processing

2.6.1 Data Acquisition and Control

Data acquisition is done using three separate data acquisition cards. The acquisition can be divided into three classifications:

1. Temperature Data Acquisition
2. Low Speed Data Acquisition for mass flow meters and lambda measurement
3. High Speed Data Acquisition for crank angle dependent variables and Low Level Control

NI-9213 Thermocouple DAQ Device

Designed for use with thermocouple measurements. Records all of the thermocouple channels with cold junction temperature compensation.

NI-6210 USB DAQ Device

The NI-6210 Data Acquisition (DAQ) device is a multi-use DAQ device capable of 250 kS/s aggregate sampling. In previous work on this engine it was used as the data acquisition device for the emissions bench. Since the emissions bench is no longer in use this device has been re-purposed for general data acquisition. Slower sampled, non-time dependent variables have been acquired with this device. This arrangement opens up acquisition channels on the high speed NI-6356 USB device and reduces the size of the saved data files. A list of signals and the channel locations are given in Table 2.2.

Table 2.2: Channel Allocation NI-6210

Channel	Signal
AI1	Mass Fuel Flow
AI2	Mass Air Flow
AI3	λ Horiba MEXA-730
AI4	Room Relative Humidity

NI-6356 X-Series USB DAQ

The NI-6356 device is a multi-use DAQ device capable of multiple types of data acquisition and low level control. It acquires analogue data at 1.25Ms/s/ch, which

is sufficient speed for acquiring the data at the rates needed for 0.1 CA resolution. The device is also used to acquire the digital input signal from the rotary crank angle encoder.

The device is also capable of analogue output which is used for low level control. The device is used to control the dyno speed, throttle position and fan control. A full list of the inputs and outputs of the data acquisition card are given in Table 2.3.

Table 2.3: Channel Allocation NI-6356

Channel	**Signal**
AI0	Intake Pressure
AI1	In-Cylinder Pressure 1
AI2	In-Cylinder Pressure 2
AI3	Crossover Pressure
AI4	Exhaust Pressure
AI5	Torque
AO0	Dyno Speed Control
AO1	Throttle Control
Port2:Line3	Fan Control
ctr3	Encoder Channel

Engine Control

As the split-cycle is a custom-built engine there is no existing control program to for the ignition system and fuel injection. As such, a program had to be developed. In order to control the engine a LabView CompactRIO (cRIO) device with a Field Programmable Gate Array (FPGA) was chosen. The FPGA allows for fast data refresh rates (40MHz). The control program which is written in LabView is converted to a Xilinx file. The program is written to the cRIO device, allowing it to operate without directly relying on a computer. This is a desirable arrangement as it allows the engine to run without fear of a computer program causing latency during operation and potentially causing damage to the set-up.

A NI-9074 cRIO Chassis was selected for use. A NI-9401 module is used for crank angle measurements and to control ignition timing. The NI-9751 is used to drive the injection events and the NI-9215 is used for low level monitoring of exhaust and fuel system pressure.

2.6.2 Instrumentation

Pressure Transducers

The split-cycle engine has been instrumented with multiple pressure transducers in order to monitor and characterize the performance of the engine. Pressure transducers are used to monitor operation of both cylinders and the XOVR passage, and then used to analyze engine performance. All pressure transducers used in the experimental set-up have been purchased from Kistler. In-cylinder pressure measurements for the compression and expansion cylinders are made with piezoelectric sensors and require zero-level correction. This correction is made with transducers located on the intake and exhaust ports. A list of the sensors is given in Table 2.4.

Table 2.4: Engine Pressure Transducers

Location	Transducer	Type	Cooling	Range	Amplifier
Intake Port	Kistler 4043A5	Piezoresistive	Uncooled	0-5 bar	Kistler 4618A0
In-Cylinder	Kistler 6052C	Piezoelectric	Uncooled	0-100 bar	Kistler 5064
Crossover Passage[1]	Kistler 4260A	Piezoresistive	Uncooled	0-51 bar	Internal
Exhaust Port[2]	Kistler 4049B	Piezoresistive	Water Cooled	0-5 bar	Kistler 4665

[1] Updated pressure transducer from previous work
[2] Additional pressure transducer for this work

Crank Angle Position Measurement

Crank angle position was measured with a BEI H25 crank angle encoder mounted directly to the crankshaft. Measurements are made at a resolution of 0.1° CA, a commonly used measurement resolution for IC engines research. This resolution is sufficient to capture all characteristics of normal combustion. The data can be down sampled for analysis if required [27].

Alignment of the encoder to indicate engine TDC was performed. Accurately indicating TDC is crucial to accurate data analysis. Davis and Patterson have shown that an offset of 1°CA can result in an error of $4-5\%$ for the calculation of IMEP [28]. Three methods of alignment are typically used in combustion analysis.

- **Mechanical Alignment:** The encoder is manually aligned by finding engine TDC and setting the z-pulse of the encoder to correspond with engine TDC. This is the least accurate method.

- **Motoring Cylinder Pressure Trace:**The engine is motored without firing and engine TDC can be found by plotting pressure and volume logarithmically. On this plot, TDC will be represented by a sharp peak. This is not practical with the split-cycle engine as neither of the cylinders valves are closed at TDC, and thus this peak pressure is not achieved.

- **TDC Sensor:** Use of a commercially available TDC indicating system with accuracy of $\pm 0.1^\circ$ CA [29]. The high cost of these sensors often makes it impractical to implement.

The engine was indicated to TDC using the mechanical alignment method described by Lancaster et al. [30] This method would achieve accuracies of TDC setting within ± 3°CA. While this would result in large errors with respect IMEP and MFB, since all tests are performed with this same error all results would carry the same bias. While a TDC sensor is significantly more accurate, its high cost has made it cost prohibitive to use for this work.

Air-to-Fuel Ratio Measurements

Air flow rate and mass fuel flow rate were monitored in this work. Mass Air Flow (MAF) is measured using a Meriam Z50MC2-2F Laminar Flow Element (LFE) and a Dwyer Instruments Series 616 Weatherproof Differential Pressure Transmitter. A pressure drop will occur over the precisely manufactured LFE which will be measured by the pressure meter. The pressure drop is used to calculate the MAF by converting the measured pressure drop to the MAF. The total uncertainty of the system is $\pm 0.54\%$.

Mass Fuel Flow Rate (MFF) is measured using a Sierra Smart-Trak M100L mass flow meter. The flow meter is capable of measuring MFF at the high pressures of the fuel delivery system with a full scale accuracy of $\pm 1\%$ [31].

The most common way to measure the Air-to-Fuel Ratio (AFR) is to use the measured mass flows and determine the AFR by dividing MAF/MFF. However, the previous work on this engine showed a large amount of blow-by, making calculations using this method inaccurate. The exact location of the blow-by has not been isolated, thus making any measurements of AFR inaccurate. Therefore, a Horiba Mexa-700 meter was used with a Universal Exhaust Gas Oxygen (UEGO) sensor to measure the Excess Air Ratio (λ) of the mixture. This was done to be consistent with the

measurements made in previous works on this engine. The Horiba meter gives a reading of λ, the value which is the inverse of the equivalence ratio (ϕ). The definition of AFR is given in equation 2.2.

$$\phi = \frac{1}{\lambda} = \frac{AFR_{Stoich}}{AFR_{Actual}} \tag{2.2}$$

Where the air-to-fuel ratio is defined in Equation 2.3.

$$AFR = \frac{MAF}{MFF} \tag{2.3}$$

Temperature Measurements

Thermocouples were also used to measure the temperature of various points on the engine. All outfitted thermocouples are K-Type thermocouples purchased from Omega®Engineering. K-Type thermocouples have been selected for use due to their large operating range (up to 1260° C), low cost and ability to function in rugged conditions caused by the engine. The standard accuracy of a K-type thermocouple is ±2.2°C or ±0.75%, whichever is greater [32]. Thermocouples of 1/16 inch diameter are used and are sampled at 10Hz. The slower sampling rate is used due to the long response time of thermocouples in air flow which can be up to 4s in a flow of 3m/s. [33].

2.6.3 Data Acquisition Sensors Modifications

Throughout the work on the engine various components of the engine have been upgraded or replaced. This has been due to certain components failure or in order to improve operation. The modifications will be listed and the rational behind the changes discussed.

Crossover Passage Transducer

A Kistler-4260A piezoresistive transducer was used to measure the XOVR pressure in this work. The new pressure transducer is connected to the XOVR via a quick connect fitting.

Exhaust Pressure Transducer

A Kistler 4049B water-cooled pressure transducer has been added to the exhaust system of the set-up. The transducer is located roughly 50mm upstream of the exhaust valve between the engine and the exhaust thermocouple. It is capable of measuring pressures ranging from 0-5bar with accuracy of $\pm 0.3\% FSO$. The new transducer location is shown in Figure 2.7

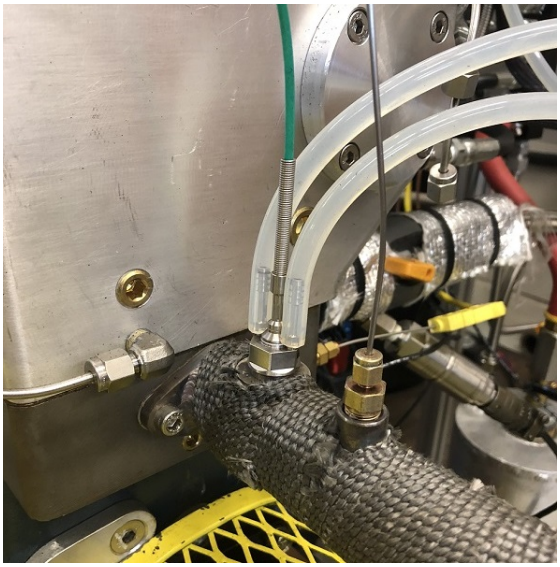

Figure 2.7: Exhaust Pressure Transducer Location

The exhaust pressure transducer is cooled using the existing cooling set-up that was used with the old XOVR passage transducer. With this transducer the exhaust pressure can be monitored and used to accurately pegging the expansion cylinder transducer.

2.6.4 LabView^{TM} Code

A LabView^{TM} Virtual Instrument (VI) has been used as the method of low level control and data acquisition for the split-cycle engine. The main structure of the LabView^{TM} code remains unchanged from the previous work on this engine [11]. The acquisition occurs within the main low level control and acquisition program. Data is acquired on a crank angle basis for crank angle dependent variables. Non-crank angle position variable are acquired at 10 Hz.

Changes to the LabView^{TM} VI have been made in order to ease the burden on the author for the processing of data. Data acquisition files are now saved in a procedurally generated folder based on the date of the test. Network acquired variables are now enabled with the VI, allowing for data to be passed between the FPGA control program and the data acquisition VI. This allows for variables such as the set engine speed, injector control pulse duration, and spark timing parameters to be monitored and logged from the acquisition program. The last improvement on the code that has been made is that a text file gets saved with every set of acquired data. This allows for the parameters for each test to be saved for easier evaluation and organization by the operator.

The LabView program records 300 consecutive engine cycles. Previous studies have shown that 300 cycles will give 99% confidence in average values of recorded data [30] and is picked to be consistent with previous work on this engine. Data is acquired as raw signals from LabView and saved in the Technical Data Management Solution (TDMS) format. All data is post-processed in the Matlab code described in Section 2.6.5.

2.6.5 MATLAB Post-Processing

Data analysis is done using a MATLAB program written by the author. Three separate files that were generated by the LabView^{TM} code are imported into MATLAB for analysis. The text file that was generated during the data acquisition is imported for the purpose of bookkeeping. The text file contains information about the operating parameters of the engine such as spark timing, engine speed and equivalence ratio. The other two imported files are for the crank angle dependent and time dependent signals.

Data Filtering

Imported pressure signals must be filtered in order to remove any unwanted noise from the signal. Care must be taken during the design of the filter in order to remove the noise from the signal without removing any combustion characteristics. Relevant work has shown that the filtering will have little effect on the cycle averaged parameters such as IMEP, however metrics evaluated on a crank angle basis can be greatly effected by filter choice [34].

It is also necessary to select a filter that does forward and backward filtering. A filter will inherently cause a phase shift of the data if unidirectional, which will cause errors with calculation of combustion phasing and IMEP calculation [35]. Therefore a filter with forward and backward filtering must be selected.

The selected filter for analysis was a butter-worth low-pass filter with forward and backward filtering. The selected cut off frequency is 3500 Hz. This filter provides adequate filtering for the data with no phase shift.

Chapter 3

Engine and Combustion Performance Metrics

In this section the engine and combustion performance metrics will be discussed. Metrics are evaluated on a cycle-by-cycle basis and the values for individual cycles are used to perform statistical analysis on engine operation. Data is acquired from the LabView^{TM} VI, analyses using a MATLAB program written by the author and statistics for each test exported automatically to a master EXCEL sheet

3.1 Indicated Performance

Mean effective pressure is the selected method of evaluation of the indicated engine performance. Mean effective pressure is a normalized value which allows for comparisons to be made to engines of larger displacement, number of cylinders or running at different engine speeds.

3.1.1 Indicated Mean Effective Pressure

The Indicated Mean Effective Pressure (IMEP) is the work transferred from the in-cylinder gas to the piston, normalized by the displacement volume of the engine. The equation for the IMEP is given in Equation 3.1.

$$IMEP = \frac{\oint P(v)dV}{V_d} \tag{3.1}$$

In this equation V_d is the displacement volume and Pressure (P) is acquired with respect to volume. The integral is evaluated as a line integral for the entire cy-

cle. Acquired data was numerically integrated in this work using the Simpson's 1/3 method. Simpson's method was selected to maintain consistency with previous work and to minimize truncation errors [36].

The split-cycle engine requires that the IMEP be evaluated method unique to this engine. Cylinder 1 performs intake and compression strokes while cylinder 2 performs expansion and exhaust. This means that the first cylinder represents work input while cylinder 2 represents work output. As a result the IMEP must be evaluated for each cylinder and net IMEP calculated as in Equation 3.2.

$$IMEP_{Net} = IMEP_{Cyl.1} + IMEP_{Cyl.2} \tag{3.2}$$

The necessity of the calculation of $IMEP_{Net}$ can be better understood by observing Figure 3.1. In this figure two real pressure traces are given from a random cycles representative of average operation of the engine. The area enclosed by the compression cylinder trace represents the work input and the expansion cylinder the positive work.

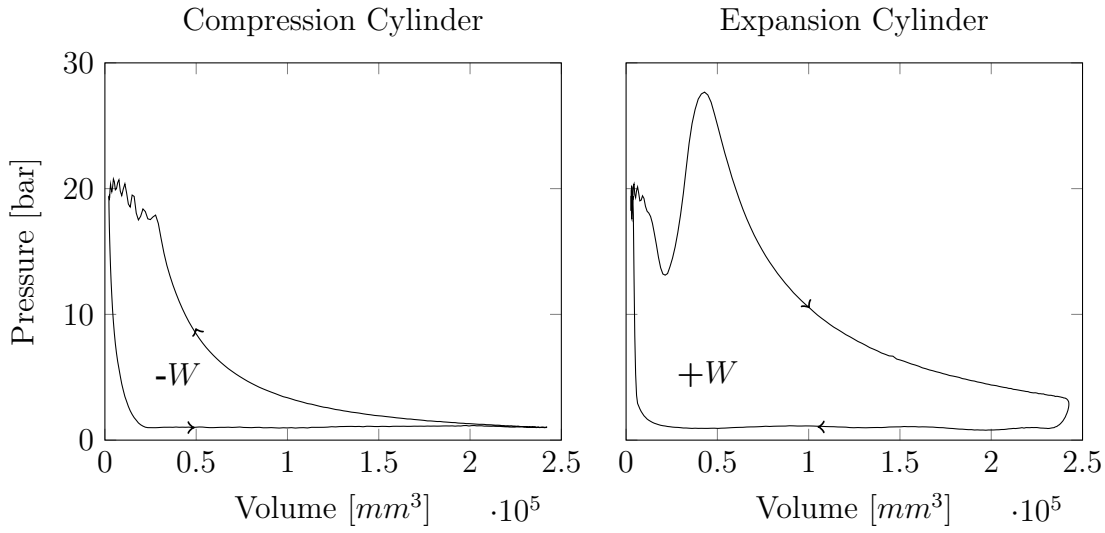

Figure 3.1: Compression and Expansion Cylinder Pressure Traces

3.1.2 Brake mean Effective Pressure

The Brake Mean Effective Pressure (BMEP) is another MEP variable that can be calculated for engine operation. Similar to the IMEP, the BMEP is calculated normalizing for cylinder displacement. The difference between the two is that the BMEP

will be calculated using the brake torque. The equation for BMEP is given in equation 3.3.

$$BMEP = \frac{W_b}{V_d} \tag{3.3}$$

In the preceding equation W_b is the brake work per cycle cylinder and V_d is the displacement volume. This is a useful parameter to study the work output of the engine while accounting for frictional losses.

As the split-cycle is currently setup, the BMEP is not suitable for evaluation due the engine being connected to the dynamometer via a belt drive. This results in high friction losses from the belt, resulting in decreased torque and BMEP values. As a result, the IMEP will be the reported value in this work.

3.2 Mass Fraction Burned (MFB)

Given that the main motivation behind the investigation of the split-cycle engine was to achieve short burn durations the calculation of Mass Fraction Burned (MFB) is of great interest. The MFB is used to compute the crank angle burn duration in terms of °CA. The Normalized Pressure Ratio (PR_n) method is the selected evaluation method for this work, maintaining consistency with previous works on this engine. The PR_n was selected over methods such as the Rassweiler and Withrow method [37] as the PR_n method was found to give more accurate results in previous works on this engine [11].

Normalized Pressure Rise Method

The PR_n method is a way of evaluating the burn durations in an engine. The methodology of the PR_n is by establishing the deviation of the pressure trace between a fired engine cycle and a motored one. The equations and methodology of the PR_n method are described in the following equations [38].

$$PR(\theta) = \frac{P_f(\theta)}{P_m(\theta)} - 1 \tag{3.4}$$

Equation 3.4 is the equation for evaluating the Pressure Ratio (PR) of each cycle. The pressure rise $PR(\theta)$ is calculated for each measured crank angle point for every data set. P_f is the fired engine pressure trace and P_m is the motored engine pressure

trace. As such, with the PR_n method it is necessary to obtain motored engine pressure traces for the engine speed that the analysis is being performed at.

After the PR has been calculated for each cycle they must be normalized. With this method the cycle with the maximum PR is taken as the normalizing cycle. This assumes that this cycle has complete combustion and all other cycles are incomplete with respect to this one. The equation for the PR_n is given in Equation 3.5

$$PR_n(\theta) = \frac{PR(\theta)}{Max[PR(\theta)]} \tag{3.5}$$

The advantage of the use of the PR_n method is that the motoring trace inherently includes the effects of the flow occurring into the cylinders of the engine. Given that ignition occurs before the valves are closed it is believed that this can cause issues when using more traditional methods of MFB.

3.3 Combustion Phasing

Combustion phasing is of great importance to the operation of an engine. Combustion phasing provides information to the burn durations and phasing of the durations. The evaluated phasing parameters are described in the following sections.

CA10

The CA 10 is a measure from the ignition timing to the point where 10% of mass has burned in cylinder as determined using the PR_n method. The CA 10 is referred to as the flame development period.

CA10-90

The CA10-90 is the measure of the duration of the 10-90% burn. This is referred to as the main burn duration. The duration is measured to the 90% value as after this the evaluation becomes unreliable for analysis. This is the accepted methodology applied to all engines.

CA90

The CA90 is the sum of the CA10 and CA10-90, representing the total burn duration. CA90 will be used to evaluate the total burn duration of the split-cycle engine.

Location of Peak Pressure

The Location of Peak Pressure (LPP) is the absolute crank angle position of the maximum fired pressure. Indication of the combustion phasing and the combustion stability. The LPP and the peak pressure are indicated in Figure 3.2.

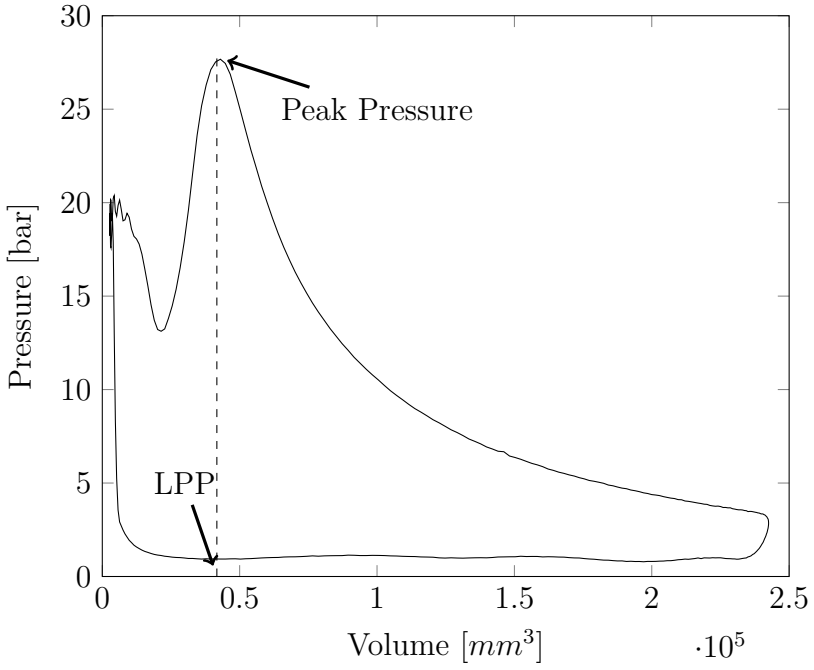

Figure 3.2: LPP Measurement Location

3.4 Combustion Stability

Combustion stability is important for the determination of the stability of the engine, especially as the lean limit of operation is approached. The main parameter used to evaluate the stability is the Coefficient of Variation (COV).

Coefficient of Variation

The coefficient of variation (COV) is a statistical measure of the dispersion of a measured value. The COV is used to measure the cycle-cycle variations of various parameters. The COV is the ratio of the standard deviation (σ) normalized with respect to the mean value ($\overline{x}$). The formula for the COV is given in Equation 3.6.

$$\%COV = \frac{\sigma}{\overline{x}} \times 100 \tag{3.6}$$

The COV is an accepted indicator of combustion stability [1, 22]. In this work the % COV of the IMEP, and LPP have been used for evaluation.

3.4.1 Lean Limit Definition

As the main focus of this work on this engine is the lean limit of operation, the definition of the limit is essential. There is no formal definition of the lean operating limit of an engine, therefore it is left up to the discretion of the operator. Stone has noted that the typical acceptable limit of COV_{IMEP} ranges from 5-10% [1]. After this point engine fluctuations become prevalent and can lead to issues with the durability of engine components if run for an extended period of time at this condition. Furthermore, an increase the number of misfires and durations of combustion can be seen as the lean limit of operation is approached.

For this work the author has chosen to define the lean limit at the point when COV_{IMEP} begins to rapidly increase beyond 5%. This point corresponds with an increase in misfires and COV_{LPP} , as well as the AFR meter reading becomes unstable. The results pertaining to the stability of operation will be presented later in this work.

3.5 Volumetric Efficiency

The volumetric efficiency is a measure of the amount of fresh air brought into an engine cylinder normalized with respect to the swept volume of the cylinder. This parameter indicates the efficiency of the gas exchange process during the intake stroke. High volumetric efficiency is desired in engines as the more charge brought into the engine, the greater the amount of fuel that can be used, and therefore the greater output that can be achieved. Volumetric efficiency is calculated using Equation 3.7

$$\eta_v = \frac{\dot{m}_a}{\rho_\infty V_d N} \times 100\% \tag{3.7}$$

where:

$\dot{m}_a$ = Mass Flow Rate of Air [kg/s]
ρ_∞ = Density of Air at Standard Conditions [kg/m^3]
V_d = Displacement Volume of Compression Cylinder [m^3]
N = Engine Speed [rev/s]

Chapter 4

Engine Operations Benchmark

In this chapter the engine has been tested as configured in previous work[11] and the results will be presented as evaluated by this author. The engine has been tested at engine speeds of 850, 1000 and 1200rpm and best achievable ignition timings for each engine speed. An emphasis is given to the lean limit of operation, with analysis performed by the author. Further discussed in this section is the head gasket failure that occurred and its effects on engine operation.

The best achievable ignition timing(BAT) of this engine is the ignition timing that will provide the greatest work output at stoichiometric conditions and a given engine speed. This value is similar to the minimum advance for best torque value presented in other works on combustion engines. However given the very retarded ignition occurring well after engine TDC, the use of this parameter would not be fully accurate. With the split-cycle the BAT occurs at the ignition timing closest to engine TDC where any further advancement would allow the flame to propagate into the XOVR passage and ignite pre-mixed fuel.

4.1 Operating Characteristics

4.1.1 Indicated Output

Indicated output for the engine is given in terms of the IMEP. Figure 4.1 shows the output of the engine at the three tested engine speeds.

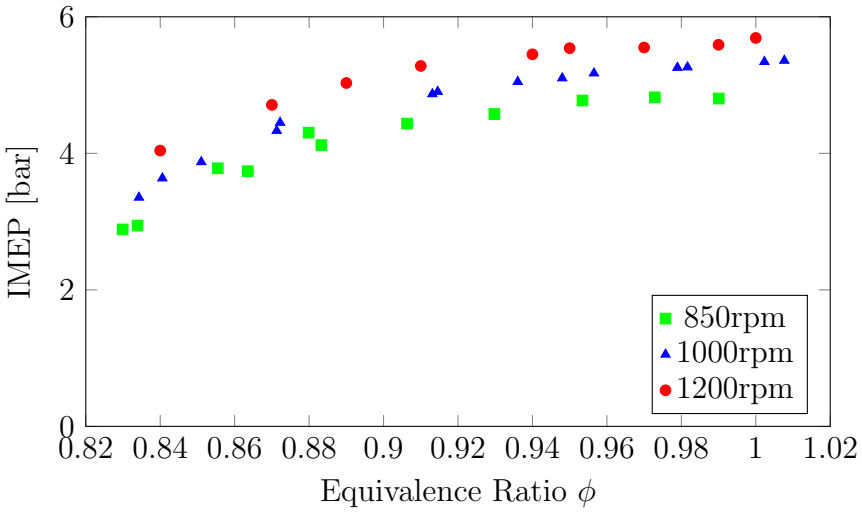

Figure 4.1: Engine IMEP [bar]

Compared to other state of the art engines the indicated IMEP produced is low. In comparison, an efficient spark ignited engine would have a full load IMEP of above 10 bar [39]. Limitations are attributed to the fact that this is still an experimental engine with several factors limiting load. Changes in valve timing may yield better indicated output and will be explored later in this work. A major limiting factor with this engine is the RPV valve train. Currently the valve will open under high peak pressures, limiting the load. This limits the advancement of ignition under the current operating regime of the engine.

4.1.2 Rates of Combustion

With the split-cycle engine the total burn durations are of great interest. Burn durations are calculated using the PR_n method described in the combustion metrics. In Figure 4.2 the total burn duration for the best achieved ignition timings are presented.

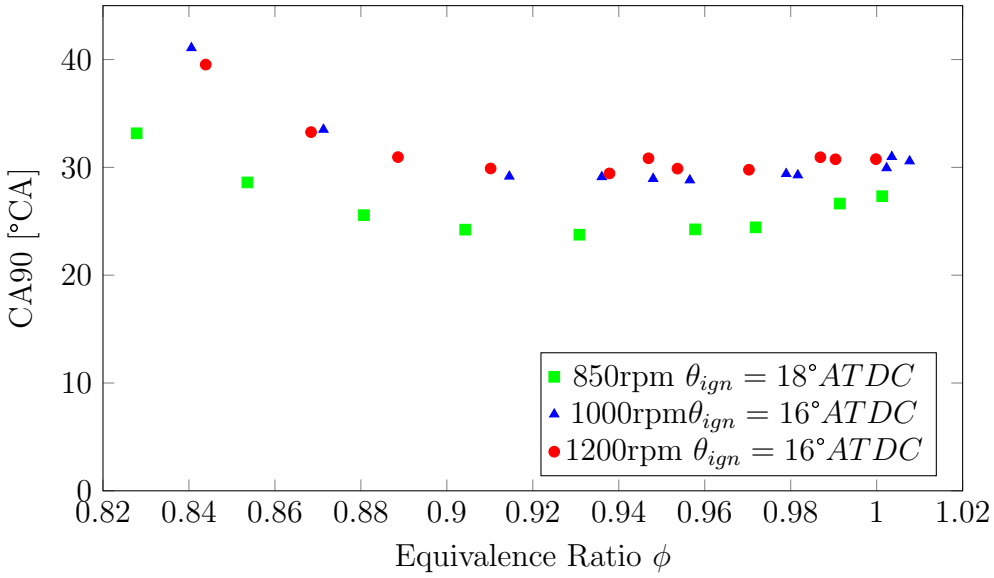

Figure 4.2: CA90

From this figure one can see that fast burn durations can be achieved with the split-cycle engine despite the late ignition. Burn durations of approximately 30°CA have been achieved for a range of equivalence ratios and engine speeds. The duration of combustion does not begin to increase until the equivalence ratio (ϕ) is less than 0.9. This is evidence of the engine beginning to reach the lean limit of operation.

Flame Development Period and Main Burn Durations

As discussed in Section 4.1.2 the total burn duration can be separated into the flame development period (CA 10) and the main burn duration (CA 10-90). The difference in the duration of these two periods is of interest to the engine operation. Figure 4.3 shows the breakdown of the burn at stoichiometric conditions and best achievable ignition timings.

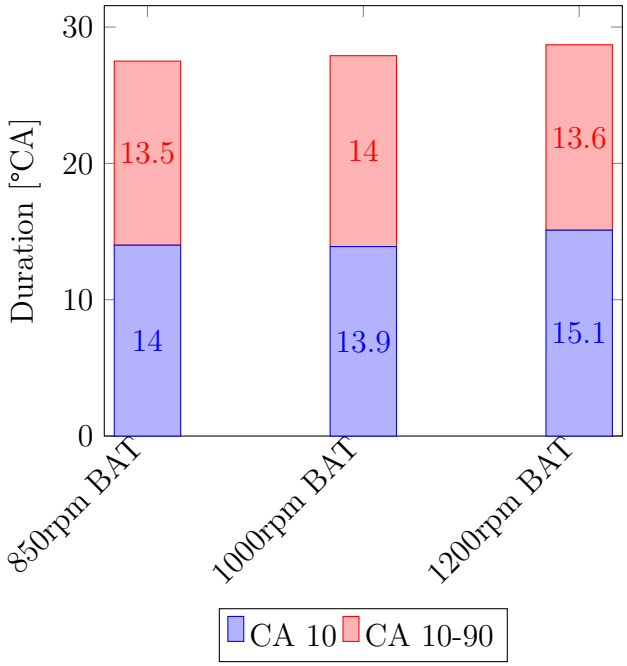

Figure 4.3: Burn Durations at Stoichiometric Conditions and Best Achievable Ignition Timing

From figure 4.3 it is possible to see that each portion of the burn takes roughly half of the total burn duration. The development of the kernel takes a significant portion of the total burn, totaling roughly half the burn. The CA 10-90 suggests that once the flame is a certain size the turbulence is successful at improving rates of combustion. It is believed that the kernel is relatively unaffected by the turbulence until it reaches a critical size at which point the turbulence can wrinkle the flame front and accelerate flame growth.

Comparison to Similar Engines

The overall burn durations achieved by the split-cycle engine are amongst the fastest when compared to other natural gas engines in literature. A comparison to other similar engines is conducted with the results presented in Table 4.1

Table 4.1: Comparison of Split-Cycle Burn Durations to Literature

Authors	**Ignition Delay**	**Main Burn**	**Total**
Rousseau et al. [18]	10°	40°	50°
Johansen & Olsson [23]	14°	15°	29°
Ma et al. [40]	N/A	N/A	43°
Ma et al.*[40]	N/A	N/A	30°
Huang et al. [41]	22.5°	26°	48.5°
Split-Cycle Engine	13.9°	14°	27.9°

* Fuelled with 50% H_2 content

From Table 4.1 one can see that the split-cycle engine is amongst the fastest NG fueled engines in literature. The engines that the split-cycle have been compared to often have combustion enhancing characteristics that the split-cycle does not have. Given examples are turbocharged and have complex combustion chamber geometries leading to enhanced combustion. The work by Johansen & Olsson [23] was able to achieve burn durations similar to the split-cycle engine. This example used a complex combustion chamber with large squish areas to achieve the fast rates of combustion. While this design led to fast combustion rates in a 4-stroke arrangement, the chamber construction is so complex that it would likely not be practical for mass production.

Another example that did achieve similar combustion rates was the second example by Ma et al. [40]. This engine was a dual-fuel engine which was fuelled with hydrogen as well as NG. This arrangement relies on a pilot injection of hydrogen which is used to ignite the mixture. Since hydrogen is a faster burning fuel, shorter burn durations can be achieved when using dual fuel strategies. This result shows how impressive the split-cycle burn durations are, given that comparable durations are achieved despite not using this enrichment.

In contrast to given examples the split-cycle does not rely on turbo-charging, complex geometries or hydrogen enrichment to achieve fast combustion rates. The current split-cycle engine has a simple flat piston design and operates at low engine speeds. With an improvement on any of these areas of the design the split-cycle engine may be able to achieve faster burn rates.

4.1.3 Combustion Stability

The overall combustion stability of the split-cycle engine is on average for well running spark ignited engines near stoichiometric operating conditions (2-3% COV_{IMEP}) [1]. For the tested best achievable ignition timings the COV_{IMEP} remains under 3%. The COV_{IMEP} for the tested ignition timings from stoichiometric to the lean operating limits is given in Figure 4.4.

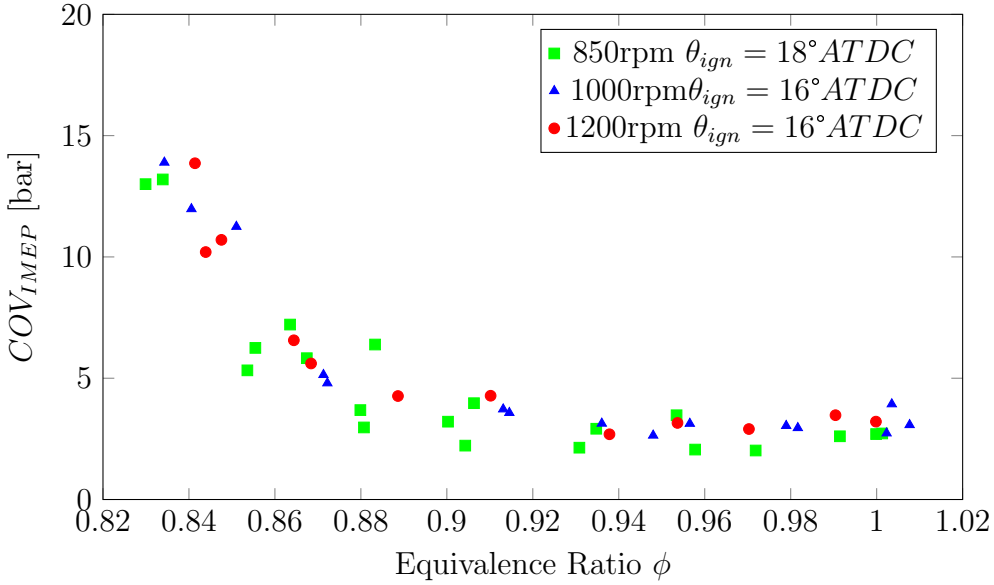

Figure 4.4: COV_{IMEP} at tested ignition timings

As can be seen from the figure COV_{IMEP} will remain under 5% for the equivalence ratios in the range of $\phi = 1 - 0.9$. After the equivalence ratio has decreased below $\phi = 0.9$ the coefficient of variation begins to increase, showing decreasing combustion stability. This trend also occurs with the COV_{LPP} as shown in Figure 4.5.

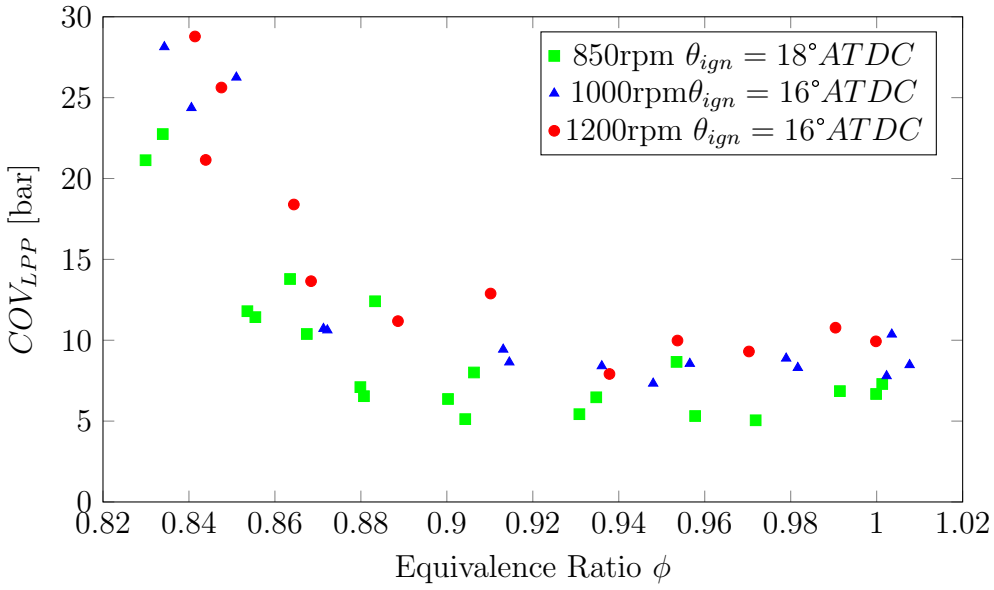

Figure 4.5: COV_{LPP} at tested ignition timings

As with the COV_{IMEP}, the COV_{LPP} only begins to increase at $\phi < 0.9$. Before this limit is reached the COV_{LPP} remains below 10%. After this point the COV begins to increase until the lean limit of operation is reached around $\phi \approx 0.85$. The engine can not be run at leaner equivalence ratios than those presented as the number of misfires increase and stability decreases to the point where the engine can not be run without potential damage occurring.

Overall the Coefficient of Variation (COV) for the engine near stoichiometric are on par for spark ignited engines. With the late ignition timing and large amounts of in-cylinder turbulence it was believed that the split-cycle may suffer from unstable combustion, however the results at stoichiometric operating conditions do not indicate this.

Of interest from these results is the lean limit of operation. Typical spark ignited NG engines can run at equivalence ratios of $\phi \approx 0.6$, significantly leaner than that of the split-cycle engine [6, 18, 24]. The proposed reason for this higher than expected lean limit are explored in Section 4.2

4.1.4 Volumetric Efficiency

As has been noted before, the overall volumetric efficiency of this split-cycle engine is low. The volumetric efficiency is 71-72% for tested engine speeds. When compared

to the volumetric efficiency of the Kubota Z482 it is based off of, this is a significant reduction. Volumetric efficiency ranges from 80-90% with the stock Kubota engine, meaning that the split-cycle has a large drop in volumetric efficiency when compared to normal 4-stroke operation. It should be noted that poor volumetric efficiency is a characteristic of the split-cycle type designs and is a noted obstacle to achieve high overall efficiencies with such poor volumetric efficiency.[42].

4.2 Lean Limit of Operation

The lean limit of operation can be attributed to two effects caused by the operation of the split-cycle engine. The first one is the effects of early exhaust valve closure in the engine. The second is the effects of turbulence which were previously attributed as the leading cause of the high lean limit in this engine.

4.2.1 Exhaust Valve Timing Effect on Lean Limit

To understand the effect of the exhaust valve closing (EVC) on the engine performance one has to first understand the valve timing of the combustion cylinder. The nominal valve timings are given in Table 4.2. Due to fluid boundary layers, the valve must be open a certain amount before the flow can pass through the valve. This results in fluid quenching which changes the effective valve opening and closing times.

Table 4.2: Nominal Expansion Cylinder Valve Timings

Valve	Opening	Centerline	Closing
XOVR Outlet	15°BTDC	6°ATDC	27°ATDC
Exhaust Valve	21°BBDC	108°BTDC	12°BTDC

One of the key factors when deciding on the valve timing for the split-cycle engine was to avoid valve overlap between the EVC and the XOVR outlet opening. This timing is desired for two reasons. The first is to prevent the short circuiting of fresh charge into the exhaust. This would be caused by the compressed charge rapidly flowing through an open exhaust valve. The second issue is that the exhaust must be closed before the XOVR opens as it could result in compressed products expanding into the exhaust resulting in lost potential work. With the XOVR outlet opening at 15°BTDC, exhaust valve timing has been conservatively set at 12°BTDC. The effects of this early valve closure can be seen in Figure 4.6.

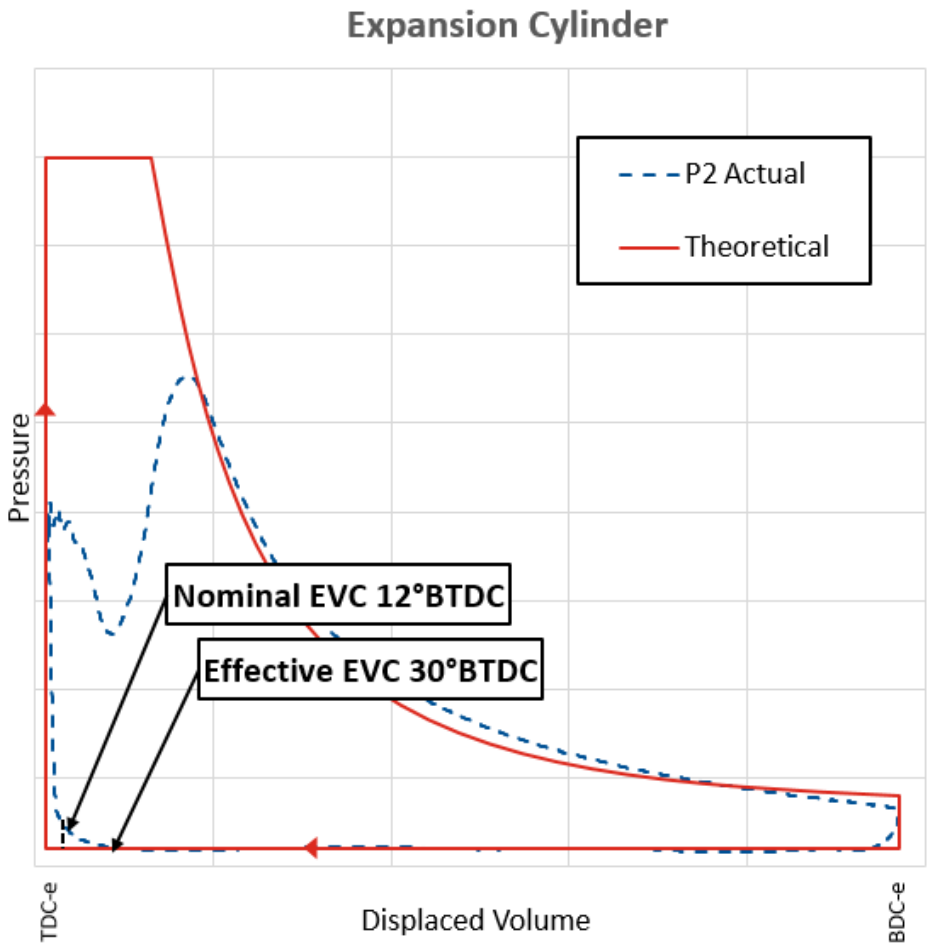

Figure 4.6: Pressure Trace Highlighting the EVC

As the valve timing is set at 12°BTDC, some of the combustion products are trapped in the cylinder for each cycle. This is evidenced by the pressure rise which occurs after valve closes and before engine TDC. Given the location of the pressure rise it has been determined by the author that the valve is effectively closed around 30°BTDC due to fluid effects. The effective valve timing is defined as the point where the in-cylinder pressure exceeds the measured exhaust pressure. It is conservatively estimated using ideal gas assumptions that the engine is operating with 15-25% of the mass of combustion products trapped per cycle. This trapped mass acts similarly to Exhaust Gas Recirculation (EGR), slowing down the rate of combustion in the following cycle and making mixtures harder to ignite [43].

This amount of trapped combustion products in-cylinder, henceforth referred to as Internal Gas Recirculation (IGR), is detrimental to the operation of the engine. Firstly, the IGR will make it more difficult to ignite lean mixtures. This is most likely the

leading cause of the higher-than-expected lean limit of operation. The amount of IGR in this engine (15-25%) is excessive for engine operation. Typical amounts of EGR for NG engines range from 12-20% before becoming detrimental to combustion [44, 45].

The second reason this amount of IGR can be detrimental to the engine is that the mass trapped in-cylinder restricts the amount of fresh charge brought into the cylinder during each cycle. Typical engines rely on valve overlap to ensure that all the exhaust products are removed from the cylinder after each cycle [1]. Since valve overlap does not result in combustion products removed from the cylinder, the fresh mixture transfer from the XOVR is limited, therefore limiting the engine performance.

The problems presented by the early valve closure and high IGR will be addressed with two new strategies in this work. The first way is with the use of alternative ignition strategies as discussed in Chapter 5. The second way this will be evaluated is with a change in EVC timing in order to vary the amount of trapped mass. This will be explored in the results of Chapter 6.

4.2.2 Turbulence Effect on Lean Limit

The second feature of the split-cycle that will contribute to the lean limit of the engine is the amount of turbulence at the time of ignition. Various works have shown the effect of increasing turbulence intensities on ignition, both in IC engines and other combustion setups. In the work of Shy et al. [46] kernel development was studied under increasing turbulence intensity, showing increasing ignition difficulty with high intensities. Given the high amount of turbulence generated by the split-cycle engine architecture this may contribute to the high lean limit. Work by Atibeh at al. [47] studies lean limit ignition in an experimental engine. Their work concluded that with lean and dilute mixtures the probability of flame quench increased with increasing in-cylinder turbulence levels. Given the excessive amount of turbulence in the split-cycle when compared to typical IC engines it is possible to suggest that the turbulence can lead to flame quenching during kernel development.

The typical spark ignition process begins from the initial ignition of a kernel using the spark plug. At the time of ignition the kernel growth is unaffected by turbulence as it is smaller than the smallest scale turbulent eddy. However, it can be extinguished by a turbulent eddy. Once the kernel grows to a critical size the small scale turbulent

eddies can wrinkle the flame front leading to enhanced flame growth. At this point it is not possible for an eddy to extinguish the flame.

In order to deal with the large amounts of in-cylinder turbulence alternative ignition strategies that deposit more energy to kernels are explored in Chapter 5. With this strategy an increase in energy will result in greater stability in the case of lean turbulent mixtures.

4.3 Head Gasket Failure

During routine testing of the split-cycle engine it was noted that operation was deteriorating. The COV of the engine kept increasing compared to previous tests and misfires occurred more frequently, even at stoichiometric equivalence ratios. The cause of these misfires was determined to be excessive oil leakage caused by a failed engine head gasket. The engine gasket that failed is the copper gasket located between the two pieces of the engine head. This gasket is required for sealing the crossover passage, cooling and oil passages. An analysis of the failure of the gasket is given, followed information on the re-design of the new copper head gasket. Finally, an assessment of the engine operation with the failed gasket is given with results compared to the new, properly functioning gasket.

4.3.1 Evidence of Gasket Failure

Fouled Spark Plug

During testing of the engine it became evident that an excessive amount of oil leakage had been occurring. What first led to the discovery of the oil leakage was that the engine had ceased firing. Upon investigation it was determined that the spark plug had completely bridged as shown in Figure 4.7.

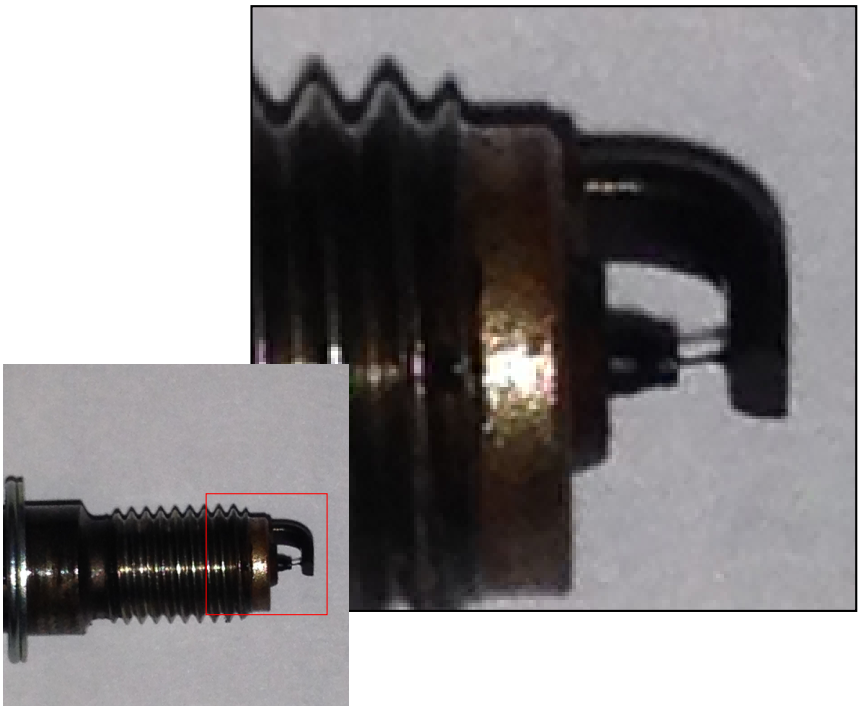

Figure 4.7: Bridged Spark Plug

This was initially a perplexing thing to occur with the split-cycle engine. Gaseous fuels such as NG do not typically form solid particulate when burning, making a bridged spark plug a completely unexpected. This solid build up was determined to be caused by a leakage of oil that had made its way into the combustion cylinder and undergoing incomplete combustion resulting in the carbon build up discovered on the spark plug.

Decreasing Combustion Stability

Upon subsequent testing it was noticed that the combustion stability had begun decreasing. The number of misfires had increased at stoichiometric equivalence ratios, testing provided less consistent results than earlier tests and higher engine speeds (1000 and 1200rpm) became challenging to run at. Further evidence was the increasing rate at which the spark plug was fouling, where evidence began showing on the spark plug at under 20 hours of use. In order to stop the oil leakage, the engine was taken apart in order to determine the cause of it.

4.3.2 Head Gasket Failure

Failed Head Gasket

Upon removal of the engine head it was evident that a complete failure of the head gasket had occurred. Mass leakage of oil was evident in both the lower parts of the engine head and on the gasket itself.

Evidence of the leakage was easy to spot on the engine head. The crossover passage was coated with a carbon build up. In the coolant passages there was a sludge build up that is evidence of the mixing of lubricating oil and engine coolant. Figure 4.8 shows the lower portion of the head after removal from the engine.

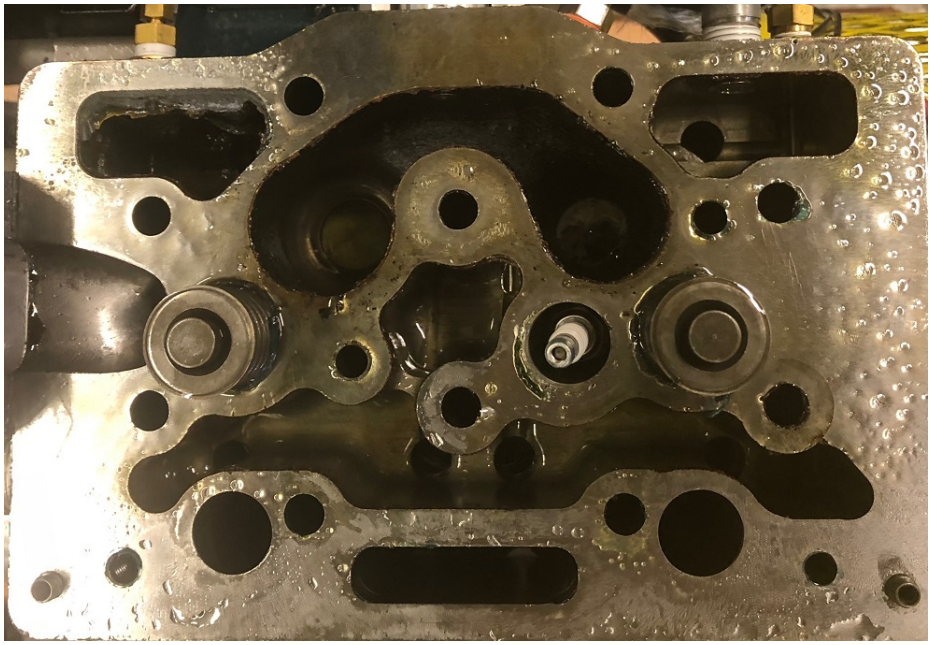

Figure 4.8: Lower head portion after removal

As can be seen in the figure a total head gasket failure occurred. Oil coated all surfaces of the head and evidence of oil leakage was shown into the XOVR and coolant passages. In the top left coolant passage the build up of sludge from the mixture of coolant and oil can be seen. The black carbon build up coating the XOVR can be seen in the top center of the image. This was attributed to the oil leaking into the passage and oxidizing on the hot walls of the XOVR. This most likely caused some amount of particulate matter or vaporized oil to enter into the combustion chamber with fresh charge. It would have been this particulate matter and oil entering the chamber during each cycle that could lead to the measured combustion instabilities. Evidence

of the particulate entering the combustion chamber can be seen on the engine head around the combustion chamber. The combustion chamber after removal from the engine can be seen in Figure 4.9.

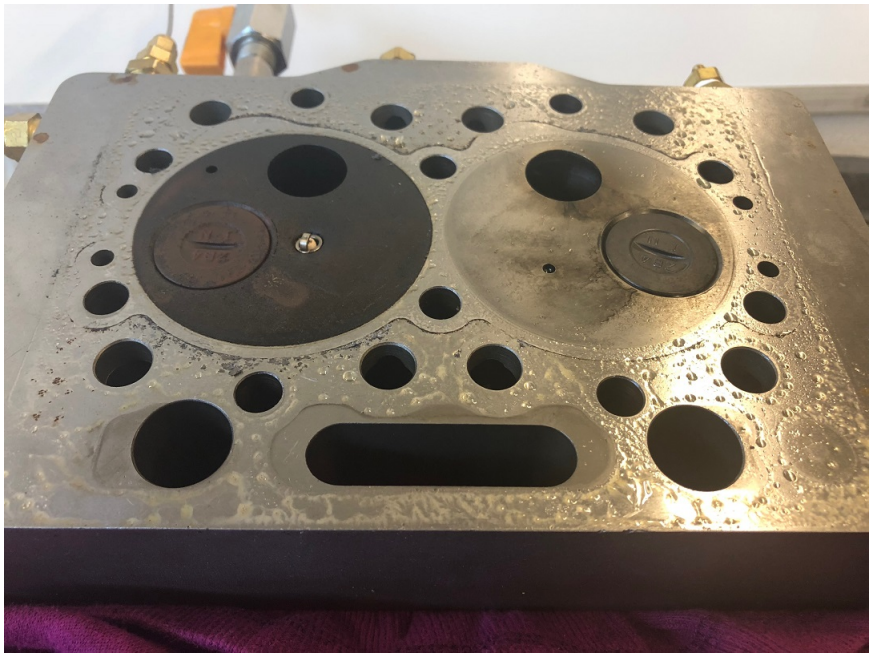

Figure 4.9: Cylinder Head exposed to Combustion Chamber

In this figure the chamber on the left is the combustion chamber. As is obviously apparent in the image a large build up of carbon was deposited on the cylinder head. The layer of carbon was thick and had to be cleaned off before reconstruction could occur. This thick layer of carbon build up is further evidence of the oil entering the combustion chamber.

4.3.3 Head Gasket Re-Design

Failure Analysis

An analysis of the failed copper gasket was conducted. Figure 4.10 shows the XOVR side of the failed gasket with key points of failure annotated .

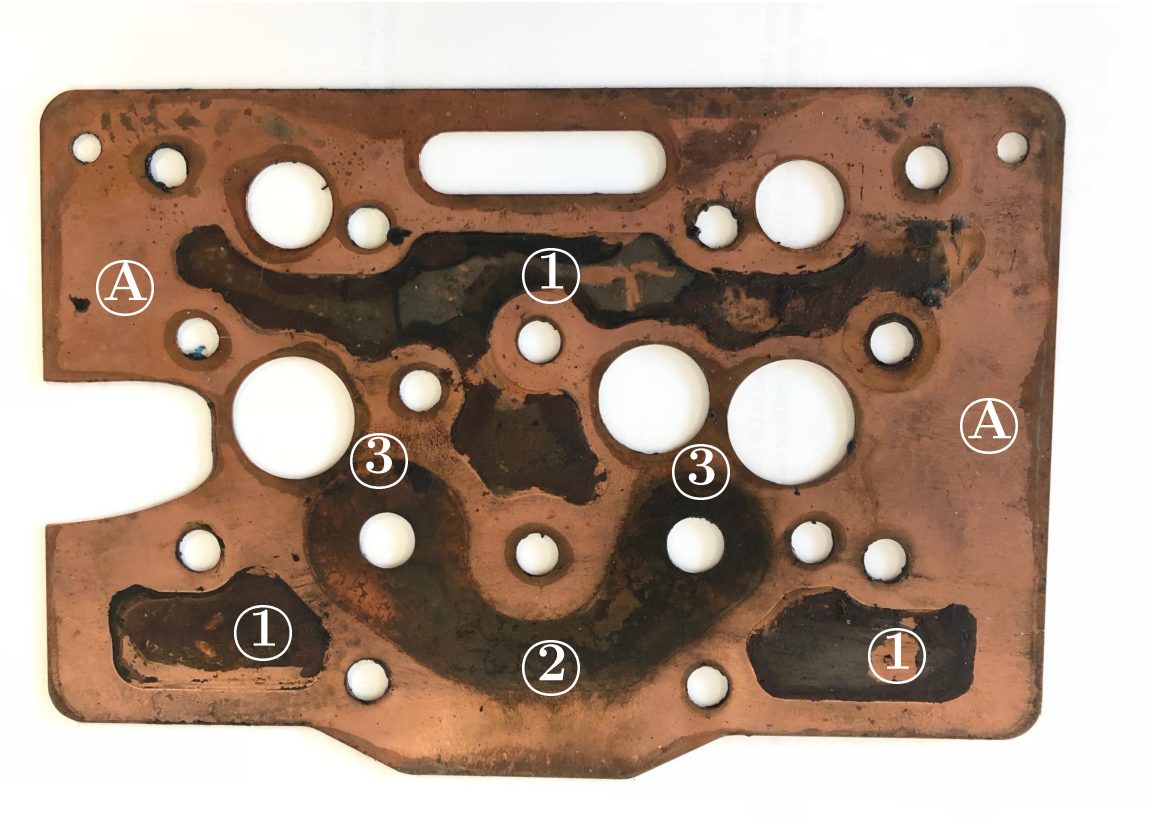

Figure 4.10: Failed Gasket on side exposed to XOVR

These three key areas of the failure are:

1. **Coolant Passages:** On the gasket the passages are dark, discoloured and covered with a sludge.

2. **XOVR Passage:** Coated with soot on both sides of gasket. Pressure reaches the back side of the gasket through valve stem clearance holes. This pressure reaching the back side of the gasket may be a location for failure propagation to begin.

3. **Gasket Failure Locations**: Indicated by discolouring of copper gasket. Occurred where the XOVR and other sealing surfaces had minimal contact area in between sealing surfaces.

Gasket Re-Design

When re-designing the gasket three criteria were developed.

1. Maximize the sealing area between the XOVR and any other features
2. Minimize the surface area of the gasket, increasing the average pressure throughout the clamped areas
3. Remove any areas where pressure can enter the backside of the gasket leading to propagation

With these criteria in mind the gasket was modified with reference to Figure 4.10. The clearance holes for the valves were reduced, giving more material in the areas indicated ③. All material has been removed from the XOVR in area ② in order to minimize the chance of the pressure propagating from underneath the gasket. Material around the coolant passages ① was left in the revised gasket design in order to prevent coolant from corroding the aluminium upper head. Material was removed from areas indicated Ⓐ in order to reduced the clamped area and increase pressure in the rest of the gasket. A new gasket was manufactured out of a sheet of 1mm thick copper sheet. After manufacturing the surface was run over with a stone in order to minimize any burs near the edges. The new gasket is shown in Figure 4.11.

Figure 4.11: New Copper Head Gasket

4.3.4 Comments on Combustion with Failed Head Gasket

What initially obscured the failed engine head gasket was that the combustion was similar to the results that were presented in Sections 4.1.1 and 4.1.2. While it was evident that combustion was less stable than earlier tests it was not as detrimental as the author would have expected given the outright failure of the gasket. This interesting behaviour would suggest that the intense turbulence created by the split-cycle architecture is not only able to speed up rates of combustion for gaseous fuels, but also to partially overcome the oil and solid particulate during combustion.

The first parameter that can be looked at is the COV_{IMEP} . At 850rpm the COV_{IMEP} ranged from 3-5% with the failed gasket at equivalence ratios closer to stoichiometric. In comparison, the new gasket has a $COV_{IMEP} = 2 - 3\%$ at these conditions. While there is evidence of some amount of instability, the COV_{IMEP} is still within the range of what would be considered stable using the criteria set by Stone [1]. Furthermore, with the failed gasket the lean limit of operation was determined to be $\phi \approx 0.87$. This does not represent a significant change from that with the new gasket.

Chapter 5

Alternative Ignition Strategies

To address issues with the lean limit of operation alternative ignition strategies have been experimentally tested with the split-cycle engine. With these strategies the overall goal is to increase the amount of energy at the time of ignition or improve the delivery of energy to a developing flame kernel. A review of alternative ignition strategies is conducted, followed by the experimental results of the selected strategies.

5.1 Review of Alternative Strategies in Literature

5.1.1 Conventional Ignition Coil Based Strategies

The spark plug is the conventional method of ignition for engines operating on the Otto cycle, hence the name spark ignited engines. There are two main components to a spark ignition system; the spark plug and the coil. The spark plug functions by having two electrodes, one ground and one (the center electrode) connected to a high voltage source. When a spark is desired a high voltage is generated by the coil and sent to the center electrode. When a high enough voltage is achieved the voltage will form a bridge across the gap between the two electrodes and initiate a spark. It is this high voltage spark that will ignite the air-fuel mixture [1]. Figure 5.1 shows the voltage profile of a single spark event.

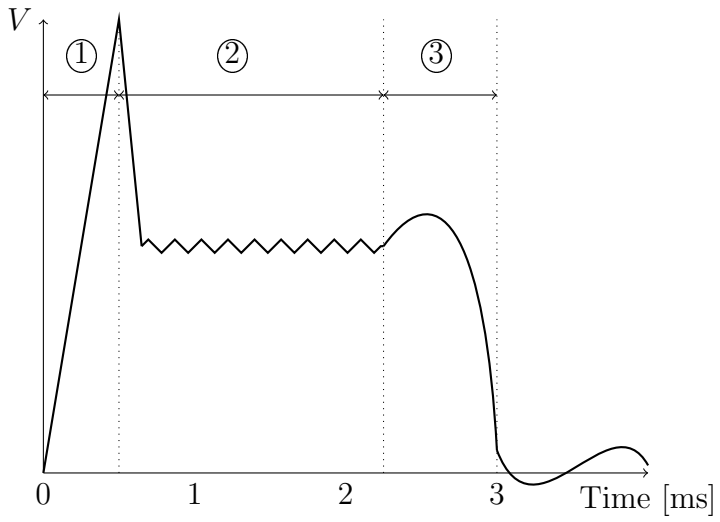

Figure 5.1: Voltage Profile of a Typical Spark Event

As shown in the preceding figure, the spark event can be broken down into three phases. They are as follows [48].

1. **Breakdown** Highest voltage achieved during an ignition event, however only occurs for very short period of time. What initially ignites the kernel.

2. **Arc Discharge** Longest portion of an ignition event. Voltage potential across the gap remains relatively constant. Provides supplemental energy to the kernel

3. **Glow Discharge** End of the ignition event as voltage across the gap drops to zero. Smallest amount of energy deposited into kernel during this phase.

The energy profile of an ignition event is also important to look at. During the initial breakdown event a large amount of energy is deposited to the kernel in a short period of time. After the initial breakdown, the energy will decline to zero at a constant rate as shown in Figure 5.2.

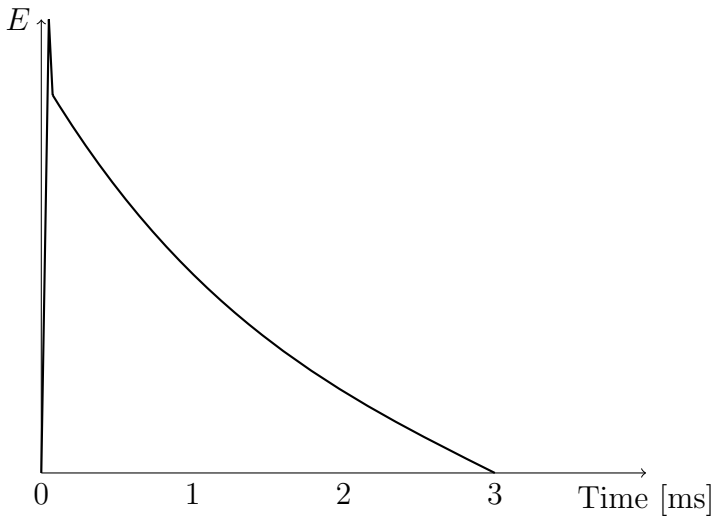

Figure 5.2: Energy Profile of a Coil Strike

The initial energy deposition (or the peak) is significantly greater than that of the rest of the ignition event. This initial spike is not displayed on the graph as the peak is too large to accurately display.

Multiple Coil Re-Strikes Ignition

The multiple strike ignition strategy consists of re-striking an ignition coil multiple times in a single ignition event. This process is visually represented in Figure 5.3 .

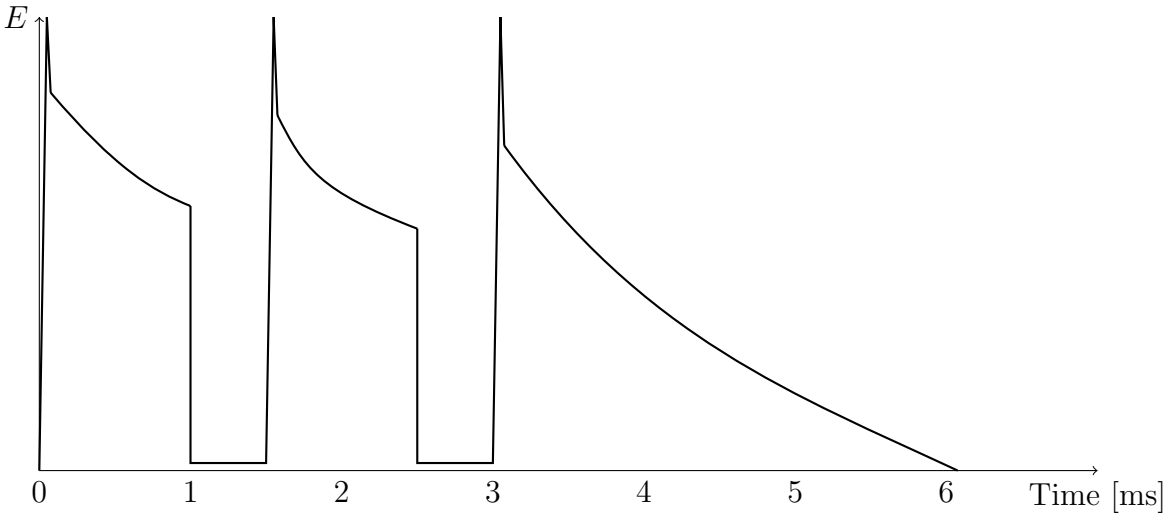

Figure 5.3: Energy Profile of a Multiple Strike Ignition Event

In this particular example a coil is re-struck twice during a single ignition event to

give a total of three sparks. Before the coil can fully discharge it is re-dwelled for a period of time, allowing for subsequent sparks to be discharged in rapid succession. The goal of this ignition strategy is to create two separate spark kernels that can increase probability of ignition.

The work of Zhang et al. [49] used a strategy where two sparks were created per ignition event in diluted a mixture. The work showed that there was an ideal phasing required for the timing between the strikes in order to ignite at leaner mixtures. Two sparks were created with the goal of igniting two kernels that would interact with one another to create a single, larger more stable kernel. The work found that this method was highly dependent on the phasing of the two coil strikes. If the strikes were too close to one another the second strike would discharge into the existing kernel or combustion products and a second kernel was not formed. If the second strike came too late, two kernels would form however they would not interact and stability would not increase.

A similar approach has been studied in the work of Poggiani et al. [50, 51] In these works a single coil is struck up to nine times per ignition event. In this work the method of the extension of the lean limit was determined to be by increasing the probability of ignition by having the multiple strikes. The work concluded that local rich or lean pockets of the mixture existed and that with nine strikes it was more probable that an ignition kernel could be successfully formed. This method did not initiate the formation of nine separate kernels. The work expressed doubt that such a strategy would work in a very homogeneous mixture such as the split-cycle engine as local variations of the mixture would not be as significant.

The advantage of a multi-strike system is the relative simplicity. Beyond acquiring a coil with the ability to be re-dwelled before all the charge had been fully dissipated, no special equipment is required. All that is required for implementation in an ignition system would be a change to the control software.

Dual Coil Ignition

A dual coil ignition strategy consists of discharging two coils simultaneously through a single spark plug. Effectively the dual coil ignition strategy increases the amount of energy supplied to a spark plug. Practical setup requires that two coils be simultaneously fired through a single spark plug with the use of a diode block to combine

outputs from the coils. Work done by Alger et al. [52] has shown the effectiveness of the dual coil strategy at extending lean limits of operation and tolerance to dilution. The reason for discharging two coils over using a single larger coil is that a larger coil with the equivalent energy would have discharge characteristics that would result in longer ignition events. Implementation requires a second coil with a diode block to combine energy from the two coils.

5.1.2 Non-Conventional Ignition Strategies

Corona Ignition

A corona discharge is a type of electrical discharge which ionizes surrounding air to fuel mixture, leading to the formation of unstable chemical radicals which in turn ignite the mixture. The theoretical advantage of a corona discharge is that it can lead to more stable ignition while requiring less energy input than a typical spark plug and coil arrangement. The corona will also ignite a volume of air-fuel mixture, which results in multiple ignition sites in a volume as opposed to a single kernel.

In testing at ambient conditions [53] it has been shown that the increased volume that the corona mixture ignites leads to greater combustion stability and faster flame development periods for both stoichiometric and lean conditions. However, the volume of the mixture was relatively the similar to the kernel of a spark plug when igniting under engine like conditions, meaning that results are similar to those of a conventional spark plug system. While theoretically possible to achieve the large ignition volume in engine like conditions, it will require significantly more development before corona ignition is feasible for engine applications.

Laser Ignition

Another proposed method of ignition is the use of a laser ignition system. In these systems a high-energy laser pulse is directed to the combustion volume to ignite a volume of air-fuel mixture [54]. While these systems have shown the ability to ignite both leaner mixtures and those at higher pressures, issues with implementation into internal combustion engines are prevalent. In particular the large power requirements would be problematic for a non-stationary application. Furthermore, the large amounts of heat generated by the laser make mounting in the cylinder head impractical [55]. While laser ignition is a promising technology, problems with packaging have made it impractical for commercial availability to this point.

Rail Plug Ignition

Another type of experimental ignition system is the rail plug ignition system. A working example of this type of system has been developed by the University of Texas [56]. A rail plug system will work similarly to a spark plug in that a large voltage is applied to an electrode that will jump across a gap to ground igniting a mixture. The difference with this system is that the charge is not built up by an electrical coil, but through a continuous electrical current applied to the electrode, creating an electromagnetic force. Eventually this electromagnetic field will break down, creating a high energy spark. This spark has been shown to be effective at igniting mixtures under lean equivalence ratios. The rail plug ignition is unable to be successfully implemented into engines as they are susceptible to high amounts of wear and very large energy requirements [57].

5.1.3 Selected Ignition Strategies

Given that it is desired to implement a strategy that can extend the lean limits of engine operation in the split-cycle engine, all of the proposed strategies present viable options. The split-cycle is an existing engine and any physical modification to the engine is not desired given tight packaging constraints and the cost of modifications. Of further interest to the author is the availability of the systems for design and construction. For the five systems discussed in this chapter, how they fit into this criteria compared to the traditional coil ignition strategy is shown in Table 5.1.

Table 5.1: Comparison of potential ignition systems

System	Energy Deposited	Durability	Packaging	Availability	Cost
Multiple Re-Strikes	Similar over larger volume	Good	Existing hardware	Software Change	Low
Dual Coil	Double	Good	Fits in existing packaging	Good	Low
Corona Ignition	Less than over a larger volume	Good	Similar to spark plug	No	High
Laser Ignition	Significant Increase	Unknown	Not feasible	No	High
Rail Plug Ignition	Significant Increase	Poor	Similar to spark plug	No	High

It can be noted from this table that many of the alternative ignition systems have a flaw that would make implementation into the split-cycle impractical. Primarily, it is the lack of commercial availability of parts to construct these systems. This would require that significant work and development be done to make them feasible for the split-cycle. The rail plug has mostly been deemed infeasible due to the large amounts of energy required to operate it. The laser and corona ignition systems have been demonstrated primarily in combustion chambers and not in reciprocating engines, meaning significant work that is outside the scope of this work would be required for implementation. For this reason alternative strategies using the multiple coils have been implemented.

5.2 Implementation of Selected Coil Strategies

5.2.1 Engine Coil

The engine coil selected for use in this work is an AEM 30-2853 high energy inductive smart coil as used in previous works on this engine. The coil is capable of driving the multiple re-strikes and was therefore deemed suitable for this work. The coil is capable of up to 100mJ per spark which makes it a high energy spark coil. Manufacturer provided specs are given in Table 5.2 [58].

Table 5.2: AEM Coil Manufacturer Specifications

AEM 30-2853	
Output Energy	103 mJ
Dwell	3.0 ms
Arc Duration	2.9 ms
Control	5V TTL

5.2.2 Multiple Coil Strike Implementation

Once the coil was verified as capable of handling multiple re strikes, implementation of the strategy only required a software change via LabView. The LabView control program was updated to allow up to 5 coil re-strikes per ignition event. Though previous work with this strategy has used up to 9 re-strikes [51], this was not deemed necessary for the split-cycle engine due to the short flame development period of under 15°CA. Any attempt to achieve this with the existing hardware would likely result in spark being discharged into an already developed flame. For this reason a limit of 5 strikes was selected and implemented to the LabView code.

5.2.3 Dual Coil Ignition Implementation

Implementation of the dual coil ignition strategy required a second ignition coil to be discharged and energy output combined with the existing coil. A second identical AEM 30-2853 coil was connected and necessary modifications made to the LabView program to control the second coil. The outputs were connected via an electrical diode block which will allow energy to flow through the block and combined, however not back into the coils. A MSD 8210 Auto Coil Selector was selected as the electrical diode block for the system. The auto coil selector is for a redundant ignition system in an auto racing setting, however it was determined that the part would function as needed for this system. A schematic of the system is shown in Figure 5.4

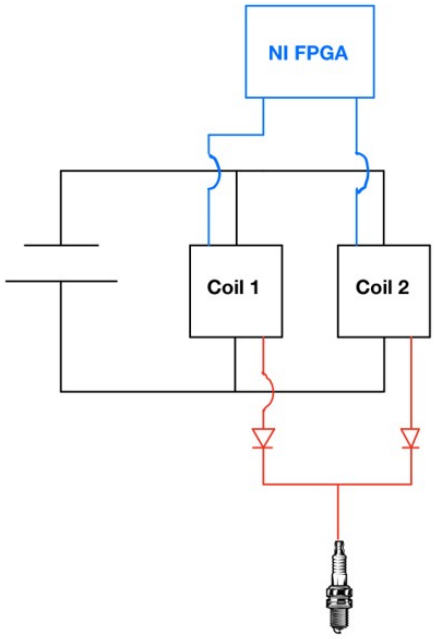

Figure 5.4: Schematic of the Dual Coil Ignition System

5.3 Spark Energy Measurements

With the selected strategies measurement the amount of energy inputted by the coil is of interest two reasons. Firstly, it will allow for the numerical quantification of the energy inputted to the system. Secondly, it ensures that the energy required to be inputted to the system is not greater than any gains made from the selected strategy.

The energy across a gap is defined as the change in voltage and current with respect to time. Equation 5.1 gives the integral used to calculate energy.

$$E = \int Vidt \tag{5.1}$$

From this equation it is apparent that in order to measure energy across the gap both the voltage and current need to be measured. However this is not practical to do directly as the peak voltage across the spark gap is on the order of kV, much higher than the capabilities of an oscilloscope. In order to measure the voltage and current the circuit as shown in Figure 5.5 is required.

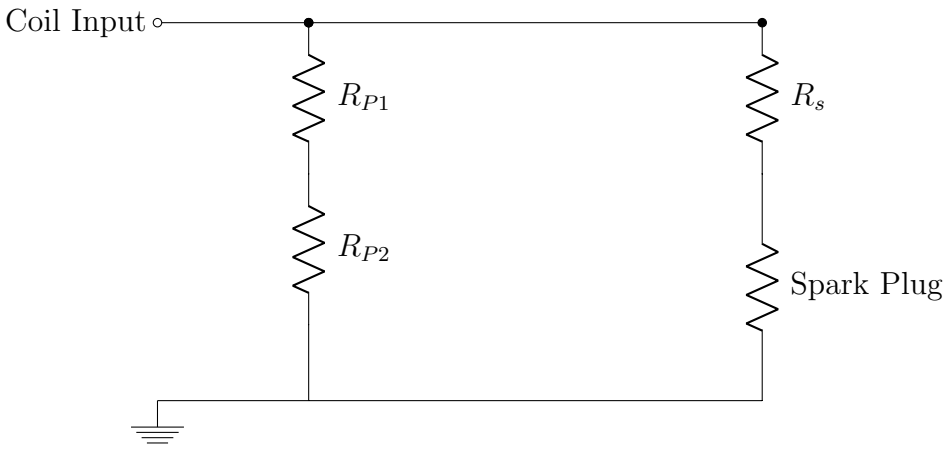

Figure 5.5: Circuit used for measuring spark energy

Using this circuit the energy can be determined for the spark plug using known resistor values. Given that in a parallel circuit the voltage drop for each branch will be the same, this circuit can be solved to determine the current and voltage of the spark plug.

The first side of the circuit that is solved is the spark plug side. A small value resistor is used to allow a small voltage drop which can be measured. Since the current across the resistor R_s and spark plug is the same, the current can be determined for this

loop of the circuit using $i_{SparkPlug} = V_R/R_s$.

The loop of the circuit that is in parallel with the spark plug is used to determine the voltage drop. Using two known values of resistance the voltage drop can be calculated for this loop, which will be equal to the voltage drop of the spark plug side of the circuit. The first resistor, R_{P1}, must be large enough to cause the majority of the voltage drop. If this value is not large enough, a large voltage drop will occur over R_{P2} that will exceed the capacity of the oscilloscope. The voltage is measured at R_{P2} which can then be used to calculate spark plug voltage using the following series of equations.

$$\begin{aligned} V_{Total} &= V_{P1} + V_{P2} \\ &= i_P \times R_{P1} + i_P \times R_{P2} \\ &= i_P(R_{P1} + R_{P2}) \end{aligned} \tag{5.2}$$

where

$$i_P = V_{P2}/R_{P2} \tag{5.3}$$

Then substituting equation 5.3 into 5.2.

$$\begin{aligned} V_{Total} &= \frac{V_{P2}}{R_{P2}}(R_{P1} + R_{P2}) \\ &= \frac{V_{P2} \times R_{P1}}{R_{P2}} + V_{P2} \end{aligned} \tag{5.4}$$

Values for the resistances had to be determined experimentally. As the system is unique for each spark plug and coil set it took trial and error to determine values that would give good experimental results. The three chosen resistor values are given in Table 5.3

Table 5.3: Selected resistor values for Spark Energy Circuit

Resistor	**Value**
R_{P1}	2.2 M ohm
R_{P2}	10.2 ohm
R_S	10 ohm

5.3.1 Energy Measurements

For the purpose of this work energy has been measured for three different types of spark events. First the standard single coil event, followed by a multiple re-strike

strategy and lastly the dual coil strategy. The spark energy is measured using the methodology described in the previous section. The two voltage measurements are taken using an oscilloscope capable of data logging. The two voltage traces for a spark event are then imported into MATLAB and used to calculate instantaneous current and voltage of a spark event. The total energy measured is given in Table 5.4.

Table 5.4: Measured Energy Values of Spark Strategies

Spark Method	**Energy**
Single Spark	50 mJ
5 Re-Strikes	65 mJ
Dual Coil Simultaneous	78 mJ

A couple of interesting things can be noted from the results. Firstly, the energy produced by a single spark is half of what the manufacturer specifications say the coil is capable of producing. The reason for this discrepancy is that when measuring the voltage across the gap there is are significant losses though the circuit that would not be accounted for if just measuring the coil. Furthermore, the methodology of measuring the energy is not prescribed by the manufacturer and therefore may result in different measured outputs.

Also what can be noted is that with the dual coil strategy the energy measured at the gap is not doubled despite the fact that twice the energy is being inputted from the second coil. This can be related to the fact that the increase in voltage will change the characteristics of the spark event through the entire system. This could be causing the energy not actually doubling with the use of the second coil.

5.4 Multi-Strike Testing Results

The first tests conducted were on the use of the multi-strike ignition capabilities on the extension of the lean limit of operation. Tests were done at a range of ignition timings from stoichiometric to the leanest equivalence ratios. Tests were performed primarily at an engine speed of 850rpm. Nomenclature used in this section for describing the spark timing is described in Figure 5.6. The strike is the position at which the coil begins to discharge, the tail length is the discharge period and the re-dwell is the period between two strikes when no discharge is occurring.

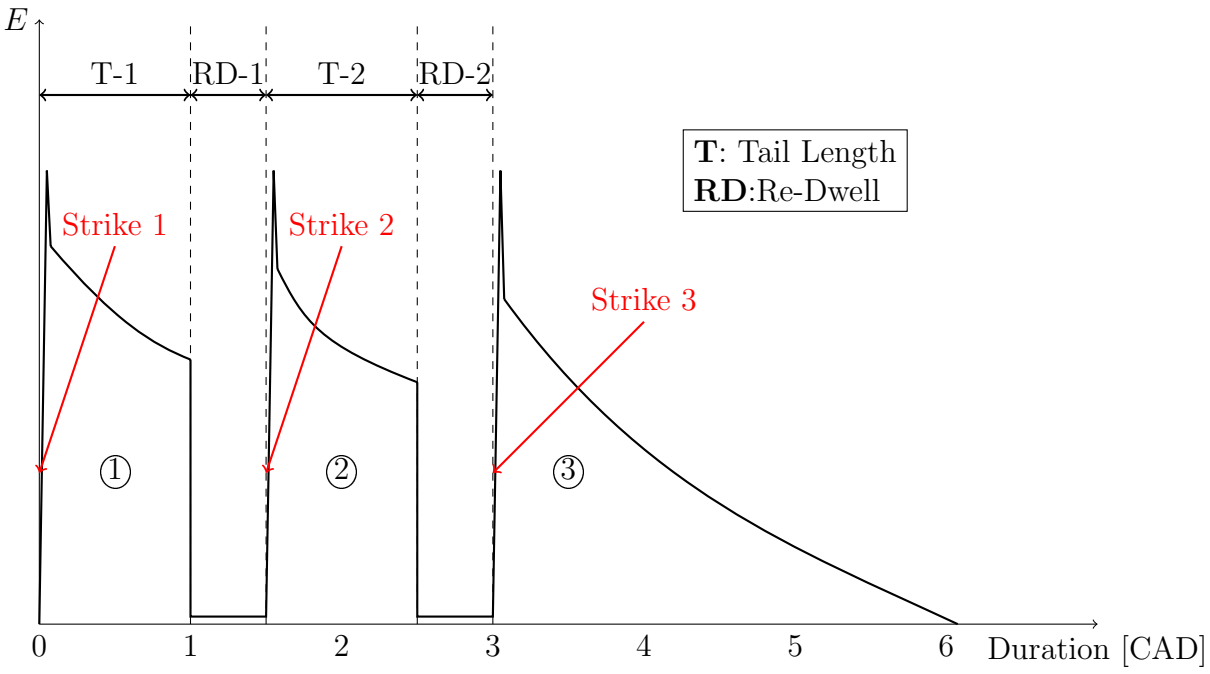

Figure 5.6: Nomenclature Used for Multiple Strike Ignition Event for example with three strikes

5.4.1 Single Re-Strike Strategy

The first tests were done to determine if an extension could be achieved via the method described by the work of Zhang et al. [49], with two kernels interacting to form a single, larger stable kernel. In order to achieve this an iterative strategy was attempted to determine ideal phasing. Since the ideal duration of the first spark and the dwell between the sparks is unknown, multiple tests at multiple phasings were conducted. In the testing performed the duration of the first spark ranged from 1-5°CA and the dwell from 1-5°CA. Durations were selected to keep the majority of the ignition event occurring within 10°CA to be within the flame development period of this engine. In Figure 5.7 the COV_{LPP} is presented for tests at $\theta_{StrikeOne} = 20°ATDC$, T1=1°CA, varying re-dwell lengths and $n_{engine} = 850rpm$.

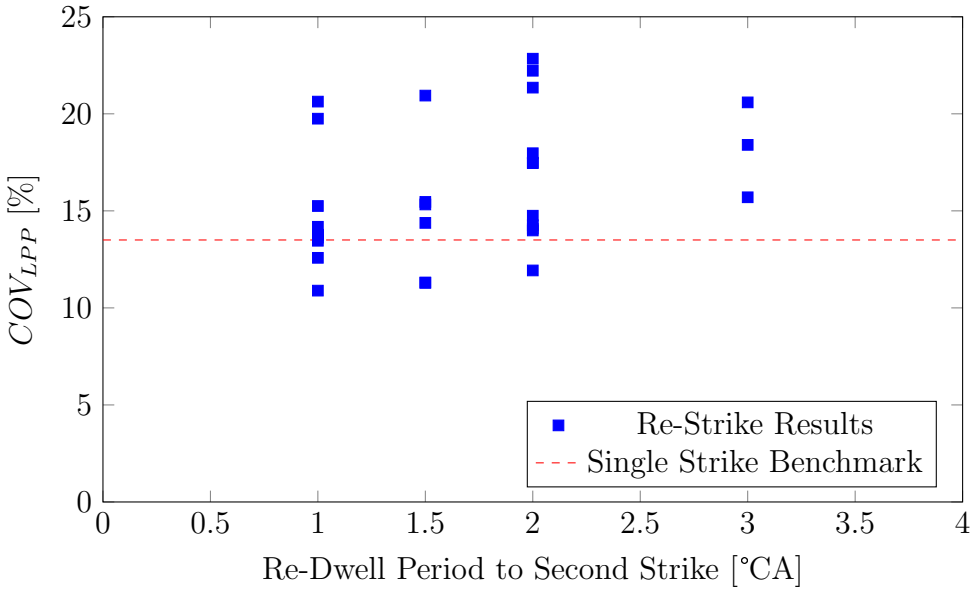

Figure 5.7: COV_{LPP} at $\phi = 0.83$, $\theta_{StrikeOne} = 20°ATDC$, T1= 1°CA and $n_{engine} = 850rpm$

As can be seen from this example not only is there no improvement in the results noted, but most of the results are worse than the benchmark case of a single ignition strike at these conditions. Also given the large spread of multiple runs of the tests would further indicate that this is an ineffective strategy for this engine. Furthermore, no improvements in the COV_{IMEP} or number of misfires was noted for any tested case with two ignition strikes. Figure 5.8 shows the COV_{IMEP} at the same tested conditions as in Figure 5.7.

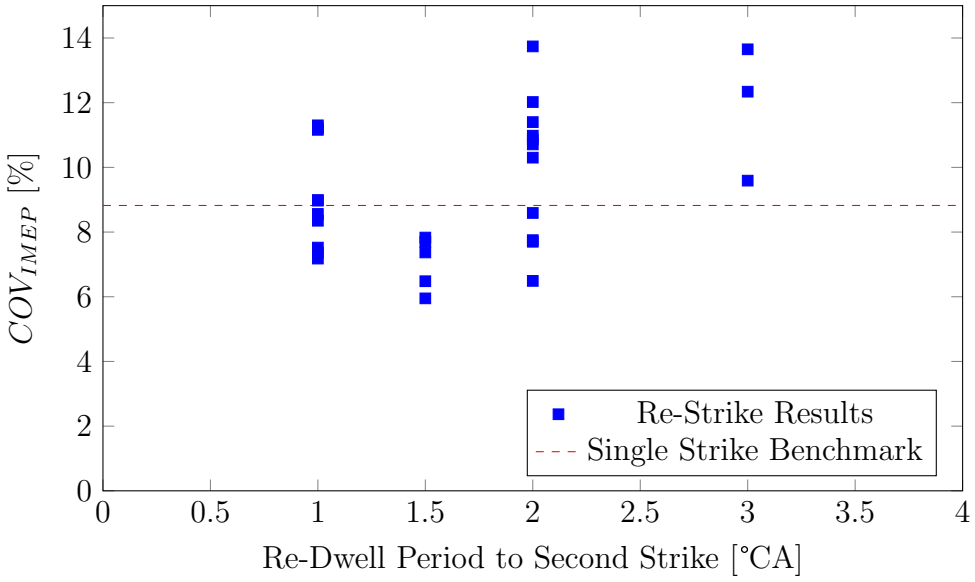

Figure 5.8: COV_{IMEP} at $\phi = 0.83$, $\theta_{StrikeOne} = 20°ATDC$, T1 = 1°CA and $n_{engine} = 850rpm$

While it may be noted that the case with the 1.5°CA Re-Dwell period has produced an decrease in COV_{IMEP} , the change is not large enough to be called an extension of the operating range of the engine. Given that the increase is only in the range of 1-2% and no other combustion characteristics improve (COV_{LPP} has increased), this is not considered to be an improvement in stability by the author.

Tests using two coil strikes have been repeated with varying operating conditions for the engine producing similar results to the cases observed here. Given that no noticeable increase has been noted under any circumstance the ability to use two coil strikes for a lean limit extension of operations has been unsuccessful. Reasons for this failure are discussed further in Section 5.4.3.

5.4.2 5 Coil Re-Strikes Results

Testing with five coil re-strikes has been conducted. As with the two re-strikes strategy no operating conditions were found which could cause an extension in the lean operating limit of the engine. For example, in tests that were performed at $\theta_{StrikeOne} = 20°ATDC$, T1=1°CA, RD=1°CA, lean equivalence ratios and $n_{engine} = 850rpm$. It was found that in these tests the five strike ignition strategy degraded the quality of combustion when compared to the single spark strategy. The COV_{IMEP} increased in the range of 1-2% and the COV_{LPP} increased by up to 5%. Furthermore, the flame

development period (CA10) actually increased by 2-3 °CA for the tests occurring with the 5 coil strikes.

5.4.3 Ineffectiveness of the Re-Strike Strategies

The reasons for the ineffectiveness of these strategies have been attributed to three factors by the author.

1. The transition from the flame development period to the main burn of the split-cycle engine already occurs in a short period of time. The flame development period has been determined to be in the range of 10-15°CA. Any improvement in the flame development period will have to improve upon an already short development period. This makes the successful implementation of any strategy challenging and any improvements difficult to measure.

2. Previous works where this strategy has been effective was on engines fueled with liquid fuels [49, 50]. Engines tested in were port injected which may lead to local inhomogeneities in the air-fuel mixture. In these engines it may be that locally rich or lean pockets of mixture are present, meaning that either of the discussed strategies could be attributed to re-strike representing a chance for a spark to occur in a more favourable condition. In the work of Poggiani et al. [50] they expressed doubt that the multiple re-strike strategy would work in an engine where the charge is very homogeneous. This work would affirm the postulate of Poggiani.

3. The required duration of each of the ignition events. Since this strategy requires the re-dwelling of the coil, any of these strategies increases the total duration of an event compared to a normal spark. The manufacturer specifies the coil discharge time is 3ms (roughly 15/degree CA at 850rpm), meaning that any amount of re-dwelling results in energy delivered into an already developed flame kernel at the end of the ignition event. The spark strategy duration can exceed the period of flame development, leading to the ineffectiveness of these strategies.

Given that the split-cycle has an already short flame development period and a very homogeneous charge the reason for the failure of these selected strategies is apparent. Any level of benefit that has been noted in other works using these strategies is not present in the split-cycle engine.

5.5 Dual Coil Testing Results

5.5.1 Engine Output

Engine output for this section of the work will be presented in terms of engine IMEP. Results are compared between the best achievable ignition timing for the single coil strategy and the dual coil simultaneous discharge at the same timing. In Figure 5.9 the output is compared between the two strategies at $\theta_{Ignition} = 18°ATDC$, $n_{Engine} = 850rpm$ and a range of equivalence ratios.

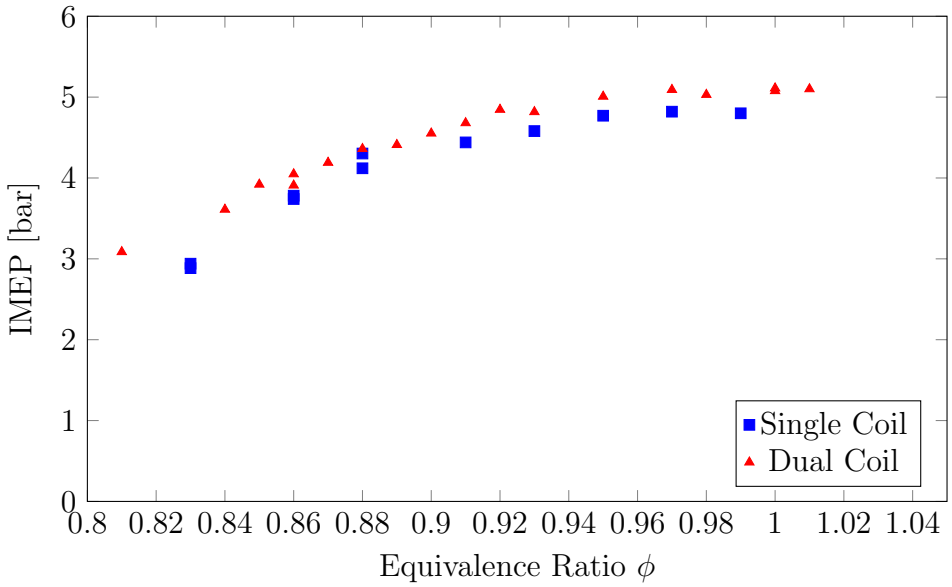

Figure 5.9: $IMEP$ for Dual Coil Ignition at 850rpm $\theta_{Ignition} = 18°ATDC$

As can be seen in the preceding figure engine output is marginally improved across all operating points with the dual coil strategy. In particular greater output is measured when running at the leanest equivalence ratios. The trend of increasing lean output is also evident when running at 1000 and 1200 rpm as seen in Figure 5.10 and Figure 5.11 respectively.

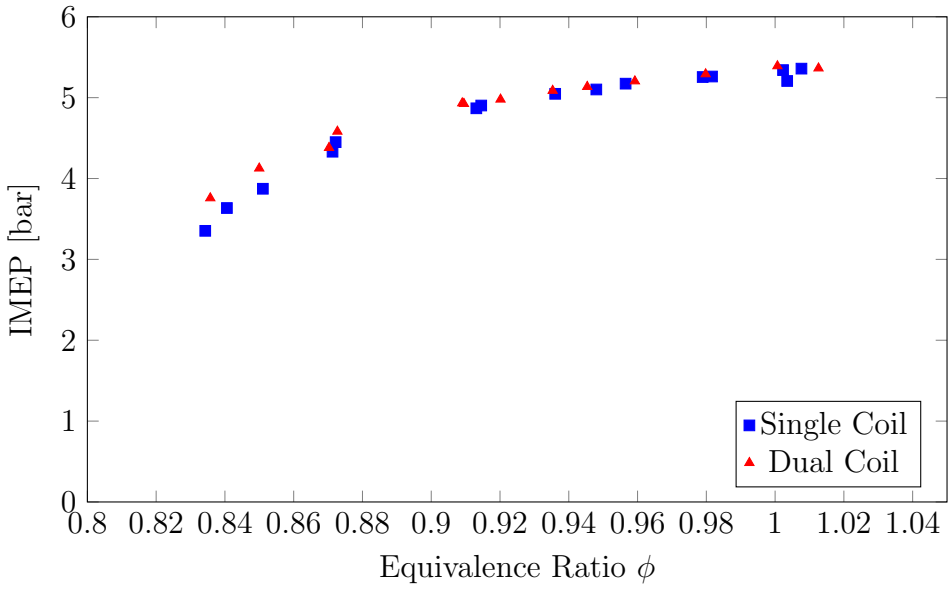

Figure 5.10: $IMEP$ for Dual Coil Ignition at 1000rpm $\theta_{Ignition} = 16°ATDC$

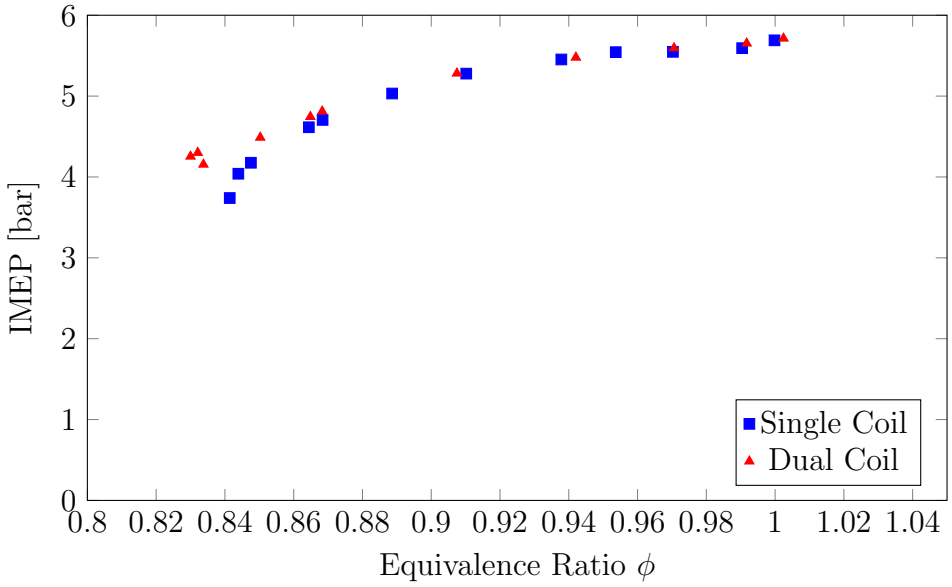

Figure 5.11: $IMEP$ for Dual Coil Ignition at 1200rpm and $\theta_{Ignition} = 16°ATDC$

While the increase in IMEP is not large, noticeable improvements have been made. The output is great enough to exceed the spark energy that has been inputted by the second coil. While the 1000rpm and 1200rpm case do not show improvements for $\phi > 0.9$, the 850 rpm tests show minor improvements at all equivalence ratios. One potential reason for this is that the 1000 and 1200 rpm cases are both ignited

at the same ignition timing and the 850rpm ignition occurs later. This may result in different in-cylinder turbulence, resulting in different results with this strategy.

5.5.2 Burn Durations

Given that IMEP is increasing with the usage of the dual coil ignition strategy it could be reasoned that an improvement in the total burn duration could be measured as well. Figure 5.12 shows the total burn duration of the tests performed at 1000rpm.

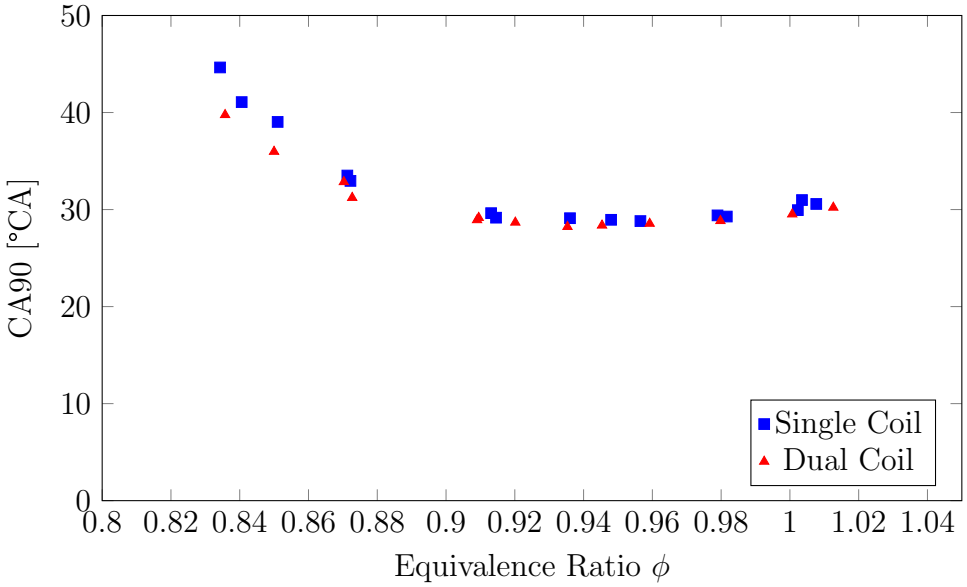

Figure 5.12: Total Burn for Dual Coil Ignition at $n_{engine} = 1000rpm$ and $\theta_{Ignition} = 18°ATDC$

Differences in the burn durations can be seen at $\phi < 0.9$. After this point the average burn duration of the single coil strategy will begin to deviate from the dual coil strategy. By observing the flame development period in Figure 5.13 the same trend can be observed.

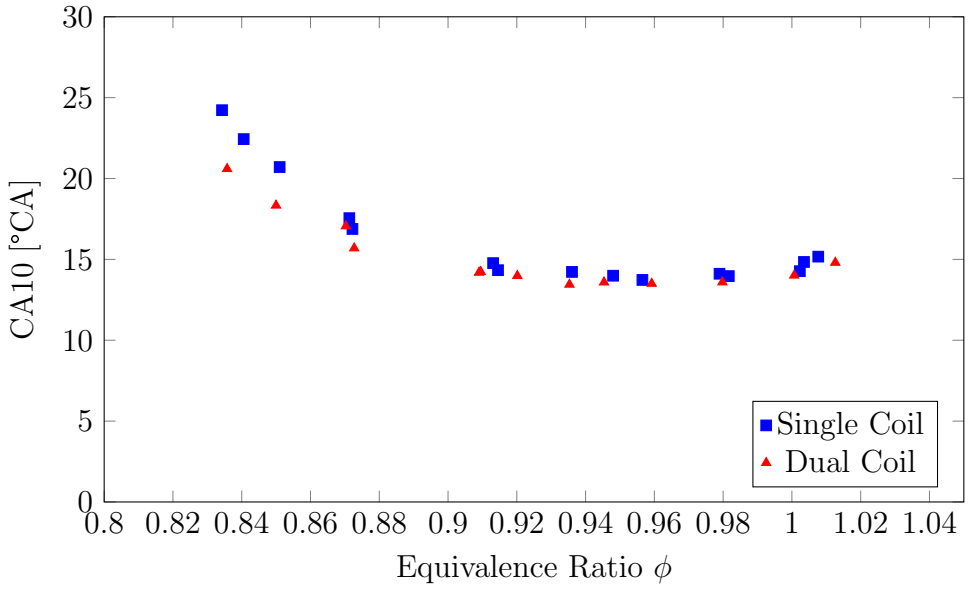

Figure 5.13: Flame Development Period for Dual Coil Ignition at $n_{engine} = 1000rpm$ and $\theta_{Ignition} = 18°ATDC$

However when observing the main burn period of the engine, it can be noted that this portion of the burn is unaffected by the ignition strategy. This effect can be seen in Figure 5.14 for the tests at 1000rpm.

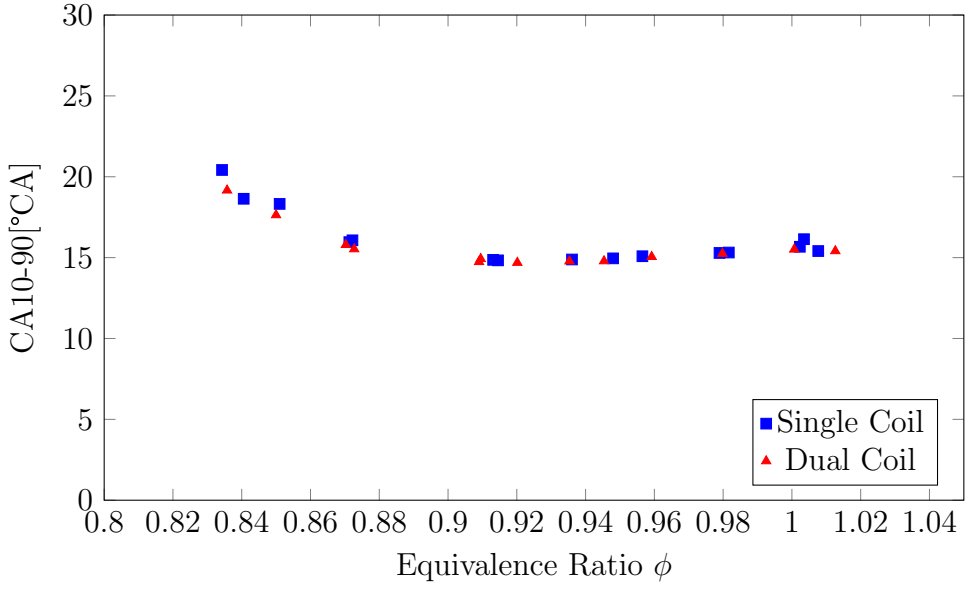

Figure 5.14: Main Burn Period for Dual Coil Ignition at $n_{engine} = 1000rpm$ and $\theta_{Ignition} = 18°ATDC$

This behaviour is indication that a more stable kernel is being formed at lower equiv-

alence ratios by the dual coil strategy. Since the kernel is more stable, the CA10 is more consistent and therefore the flame development period is on average shorter. The CA10-90 of the cycle is unaffected by the ignition strategy as once the kernel has reached a critical size the burn characteristics are determined by engine turbulence and the equivalence ratio. This results in the CA10-90 being similar for the same engine equivalence ratios despite differing ignition strategies.

Results for 850 and 1200rpm are similar to results at 1000rpm, with the same trends exhibited at all engine speeds.

5.5.3 Combustion Stability

As the goal of using alternative ignition strategies is to improve the operational stability of the engine, the COV_{LPP} and COV_{IMEP} are of interest. Any increase in overall output will be accompanied by an increase in the combustion stability. The results for the COV_{IMEP} are presented in Figure 5.15 for a range of equivalence ratios, $\theta_{Ignition} = 18°ATDC$ and $n_{engine} = 850rpm$.

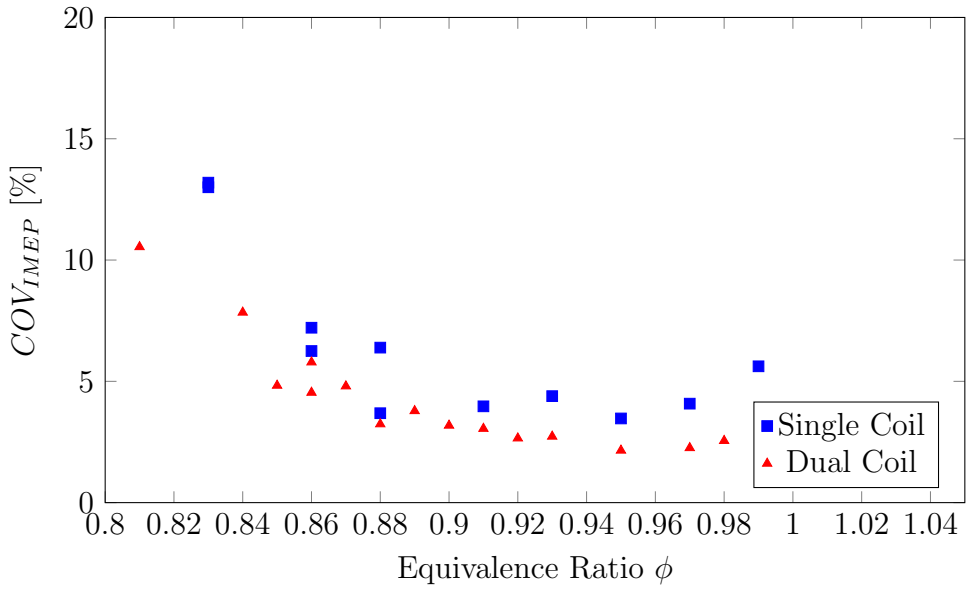

Figure 5.15: Total Burn for Dual Coil Ignition at $n_{engine} = 850rpm$ and $\theta_{Ignition} = 18°ATDC$

The tested results at 850rpm show that the COV_{IMEP} is consistently lower than that of the single coil strategy. This trend with the COV_{IMEP} can be further seen in Figure 5.16 which shows results for the 1200rpm at $\theta_{Ignition} = 16°ATDC$.

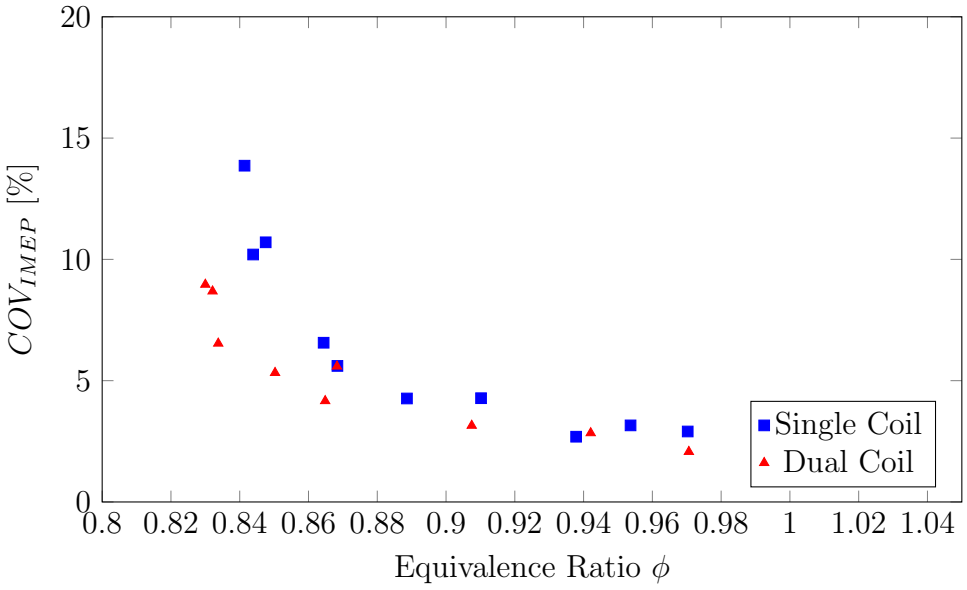

Figure 5.16: COV_{IMEP} for Dual Coil Ignition at $n_{engine} = 1200rpm$ and $\theta_{Ignition} = 16°ATDC$

At 1200rpm it can be seen clearly that the COV_{IMEP} decreases leaner equivalence ratios with the dual coil strategy. In this case the COV_{IMEP} remains under 10% for equivalence ratios $\phi > 0.82 - 0.83$. Given that stability increases rapidly at $\phi = 0.85$ with the single coil strategy, this is an indicator of the effectiveness of the dual coil discharge.

The COV_{LPP} can also be looked at as an indicator of combustion stability. Figure 5.17 shows the COV_{LPP} for testing conducted at 1200rpm and $\theta_{Ignition} = 16°ATDC$.

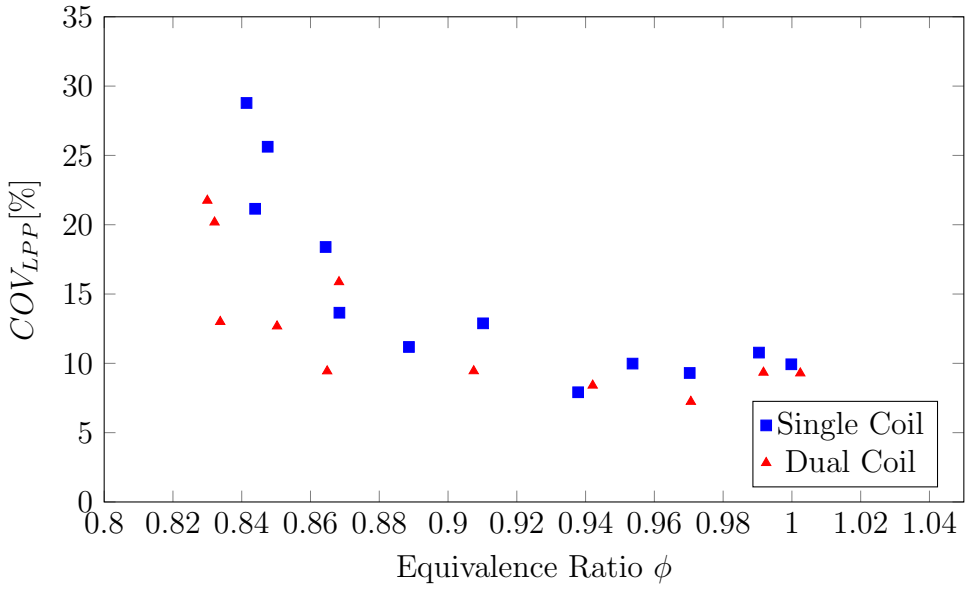

Figure 5.17: COV_{LPP} for Dual Coil Ignition at 1200rpm $\theta_{Ignition} = 16^{\circ}ATDC$

As can be seen in this figure the dual coil strategy results in a lower COV_{LPP} at lean operating points during split-cycle engine operation. The trend of decreasing COV_{LPP} is also evident in data collected at 850 and 1000 rpm.

The notable decreases in both the COV_{LPP} and COV_{IMEP} at lean equivalence ratios show the effectiveness of the dual coil ignition strategy. The decrease in these measured COV occur for the entire range of engine speeds and spark timings. As with the burn durations presented in the previous section, the trends are present at all tested engine speeds.

5.5.4 Misfires

Another potential indicator of combustion stability is the number of misfired engine cycles. Under normal operation the tendency of the engine is to see an increase in the number of misfires at $\phi < 0.9$. Any increase in combustion stability will result in a decrease in the frequency of misfires. Figure 5.18 shows the number of misfires per 300 cycles for an engine speed of 1000rpm and $\theta_{Ignition} = 16^{\circ}ATDC$.

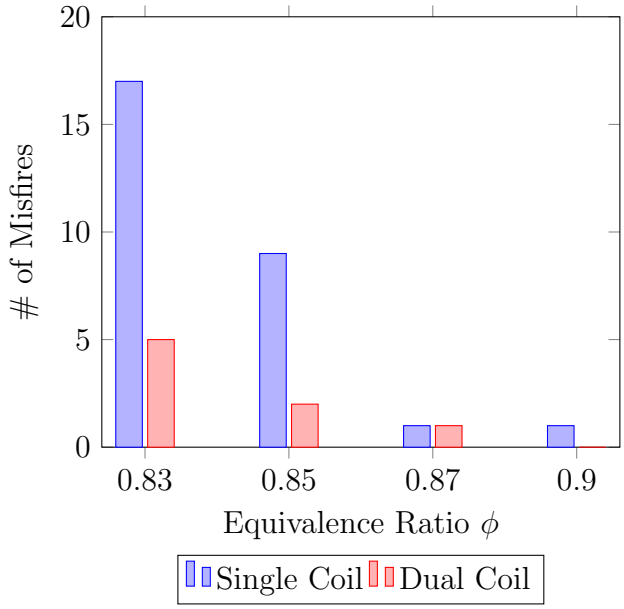

Figure 5.18: Average number of Misfires per 300 cycles at $n_{engine} = 1000rpm$ and $\theta_{Ignition} = 16°ATDC$

As can be seen from the preceding figure, the average number of misfires per 300 cycle significantly decreases with the dual coil strategy. It is important to note that even at what is considered borderline stable with the single coil strategy, ($\phi = 0.85$), the total number of misfires decreases with the dual coils.

This trend of decreasing misfires occurs at all tested engine operating points. At $\phi = 0.85$ the average number of misfires per 300 cycles decreases from 9.5 to 2 at 1200rpm. At even leaner equivalence ratios the number of misfires decrease more dramatically. At 850rpm and $\phi = 0.83$ the number of misfires will decrease from an average of 22 to 5.

5.5.5 Dual Coil Ignition Conclusions

The dual coil ignition strategy has a positive effect on engine operation, most evidently as the lean limit of operation is approached. Overall output in IMEP increases; burn durations, number of misfires and the coefficients of variation all decrease. These factors all demonstrate the effectiveness of this strategy.

Evidence of the dual coil strategy improving the stability of the ignition kernel is evidenced by the reduction of the flame development period. This indicates that the

increases measured are caused by an overall more stable kernel. Furthermore, the added benefit of decreasing the number of misfires is especially advantageous for the split-cycle engine. Given that it is fuelled with NG, which is a potent greenhouse gas with high global warming potential, the benefit of decreased misfires is significant. If implemented on a large scale the impact of decreasing the number of misfires for all methane fueled engines would be significant.

While the extension of ϕ is not large enough to run at extremely lean equivalence ratios, improvements made are on the scale of improvements made with similar research [52]. The advantage of the dual coil strategy as implemented is the relative ease at which it could be installed engines. The hardware for this set-up is simple and reliable and would not require significant changes for implementation. Even though the advantages of this strategy are at the lean limit, the simplicity and costs to implement for these ratios is small so the benefit out-weighs the cost. Furthermore, this strategy is applicable to any engine that has any combination of lean, dilute and extreme turbulence at the time of ignition.

Chapter 6

Valve Timing Effects and Modifications

6.1 Valve Timing Effects

The effects of the valve timing effects for each of the four valves is discussed in following section. The compression cylinder features an intake valve and crossover passage inlet valveXOVI. The expansion cylinder includes the exhaust valve and crossover passage outlet valveXOVO. The valve timing diagram in Figure 6.1 can be referenced to better understand the effects of the valve timing.

Intake Valve

The intake valve timing is the most similar in behaviour to typical IC engines. The valve ideally opens near the TDC of the compression cylinder and draw fresh air into the cylinder. The valve will close after BDC of the cylinder to maximize fresh charge entering the cylinder. The effects of intake valve closure time are not explored in this work.

Crossover Inlet Valve

The XOVI must open before TDC of the expansion cylinder and ideally close at TDC. The ideal timing of the opening of this valve is when the XOVR pressure is equal to the pressure in cylinder. The valve timing is set so that the XOVR pressure remains as close to constant as possible during mass transfer processes. Opening the valve too late results in $P_{Cyl} > P_{XOVR}$, leading to sonic flow across the valve and increased heat losses. Opening the valve too early when $P_{cyl} < P_{XOVR}$ would result in back

flow from the XOVR, resulting in charge from the XOVR being re-expanded and re-compressed, resulting in increased work input.

Crossover Outlet Valve

The crossover outlet needs to be set so that the mass transfer will occur as close to TDC as possible. This will maximize the turbulence intensity and allow ignition to occur as close as possible to TDC, thus maximizing work output. If the XOVO valve opens to early (ie.before TDC), mass enters the expansion cylinder early and is re-compressed by the upward piston motion, decreasing work output.

This valve closing needs to occur as close to TDC of the expansion as possible to allow for ignition of the mixture as close to TDC as possible. If the valve closes too late, the piston will have begun its downward motion when the volume of the combustion chamber is rapidly expanding, creating worse conditions for combustion. The conditions are worsened due to decreased pressure and temperature. This behaviour of XOVO is challenging for the split-cycle. Due to the finite amount of time needed for the valve opening, optimizing opening and closing times present a trade off with each other. A later valve opening time results in a later closing time and vice versa. Thus, an optimization needs to occur between the XOVO opening and closing to maximize the engine IMEP.

Exhaust Valve

The exhaust valve closure effects have been discussed briefly in Section 4.2.1. The contribution by the author with regards to the split-cycle engine operation is noting the amount of trapped combustion products that the exhaust valve closure causes in the split-cycle engine operation.

The purpose of the early exhaust closure is to prevent short circuiting (fresh charge entering the exhaust). In the case of the split-cycle short circuiting would be detrimental to engine operation for two reasons:

1. Compressed charge from the XOVR would enter exhaust, not allowing for expansion work to be performed on the cylinder
2. Since fuel is premixed, methane would enter exhaust. This would result in wasted fuel as well as be detrimental to the environment due to methane's potency as a greenhouse gas. [20]

Initial setting of the exhaust valve closing was set conservatively to prevent these two effects from occurring. This timing was set in initial testing nominally at 12°BTDC, however effective closing of the valve has been determined to be around 30°BTDC. This effective valve timing was found to by determining the point at which the in-cylinder pressure deviates from the pressure measured with the exhaust pressure transducer. This timing increases the IGR and limits fresh charge entering into the cylinder. With the exhaust valve closing an ideal timing must be found to close exhaust valve as close to TDC as possible (limiting the trapped mass) and preventing short circuiting between the XOVR and exhaust.

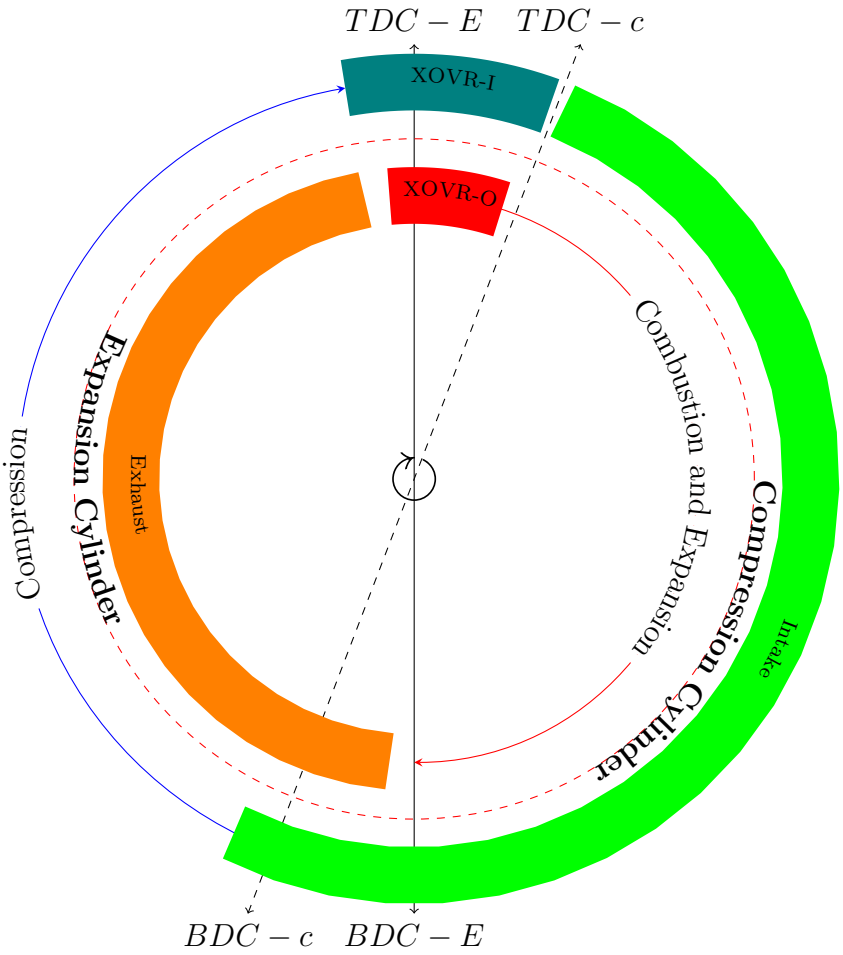

Figure 6.1: Split-Cycle Valve Timing Diagram

6.2 New XOVR Cam Profiles and Timing Design

6.2.1 Cam Profiles

With the work from benchmarking and use of the AVL model as described in previous work on this engine [11], new XOVR valve timings new cam profiles have been designed and constructed. There are two goals that are desired with the new cam profile design.

1. **Increase the pressure in the XOVR Passage:** Increasing the pressure in the XOVR passage will result in increased pressure on the back side of the reverse poppet valves. This will allow for more advanced ignition timing, higher combustion pressures and greater work output.

2. **Shorten the Opening of the XOVR Valve:** Due to the high rates of mass transfer from the XOVR, it has been determined that the XOVO only needs to be open for 10°CA to fill the cylinder. Also, given that XOVO closes at 27°ATDC, an increase in output could be obtained with earlier valve closing, allowing for earlier ignition.

The new cam profiles were selected but not tested by the previous graduate student working on this engine using a combination of an AVL-Boost 1-D model and the MATLAB code used to design the profiles for the RPV. The dynamics of the RPV valve train are extreme when compared to conventional valve trains and limit the designs possible for the cam profiles. Unlike with the initial design, the intake and outlet valves will have different profiles and durations. In Table 6.1 description the new profiles for the XOVI and XOVO are given and compared to the initially implemented profiles.

Table 6.1: Cam Profile Specifications for XOVI and XOVO

	Lift [mm]			**Duration [CAD]**		
	New	Old	Change	New	Old	Change
XOVI	2.7	3.5	-23%	30	55	-45%
XOVO	1.3	3.5	-57%	20	55	-63%

The valve durations for the new cams have been significantly shortened. Furthermore, as a result of the shorter durations, the maximum lift achieved by the RPV has been decreased.

6.2.2 Cam Phasing

Cam phasing for the split-cycle engine was selected by the author based on the known characteristics described in Section 6.1. It was desired that the XOVI closed just after TDC and the majority of the mass transfer occurred at TDC. The selected valve timings are shown in Table 6.2.

Table 6.2: Valve Opening Locations with Modified Cam Profiles

Valve	Opening	Centreline	Closing
Intake*	36°ATDC	132°ATDC	38°ABDC
XOVI*	8°BTDC	7°ATDC	22°ATDC
XOVO	5°BTDC	5°ATDC	15°ATDC
Exhaust	12°BBDC	95°BTDC	2°BTDC

* Locations measured with respect to TDC-e. Subtract 20°CA for compression cylinder

One thing that should be noted is the change in the exhaust valve timing from testing done with the old cam profiles (refer to Table 4.2). The exhaust valve now closes 10° later than previous test to minimize the IGR ratio and achieve the leanest operation possible. Results given in Section 6.6 have been performed with original valve closing at 12°BTDC to determine the effects of valve closure and as a result trapped combustion products on engine operation.

6.3 New Profiles Testing Results

6.3.1 Test Conditions

Testing conditions for the split-cycle engine have changed with respect to previous testing done on the engine. The conditions that the engine was tested at are given in Table 6.3.

Table 6.3: Test Condition for Split-Cycle Engine with New Cam Profiles

Parameter	Value
Engine Speed	850, 1000, 1200 rpm
Equivalence Ratio	0.85-1.00
Ignition Timing	10-15°ATDC-e
Injection Timing	90°ATDC-e
Injection Duration	3.5-4.2 ms
Ignition Strategy	Single Coil

6.3.2 Operating Characteristics

With the new valve timing, changes to the working pressures have been noted. These changes can be compared to the results that have been presented in Chapter 4 of this thesis.

Compression Cylinder

Given the change in the cam profiles and timing of the valves of the compression cylinder, higher pressures are achieved in this cylinder. Peak pressure in the compression cylinder has increased to approximately 30 bar. The increased pressure in the compression cylinder results in greater work input from the cylinder. Average compression cylinder work input has increased to 4.3 bar, up from 3.9 bar with previous valve timings. This increase in compression cylinder input should be compensated for with an increase in work output from the expansion cylinder.

Crossover Passage Pressure

With the new valve timing an increase in the crossover passage pressure has been noted. Average XOVR pressure varies from 27-30.5 bar, depending on the tested engine speed. As with the previous valve timing pressure drops occurs in the XOVR when both valves are closed. This is most likely caused by a combination of mass and heat transfer loss in the XOVR. A cycle representative of an average XOVR pressure trace is shown in Figure 6.2.

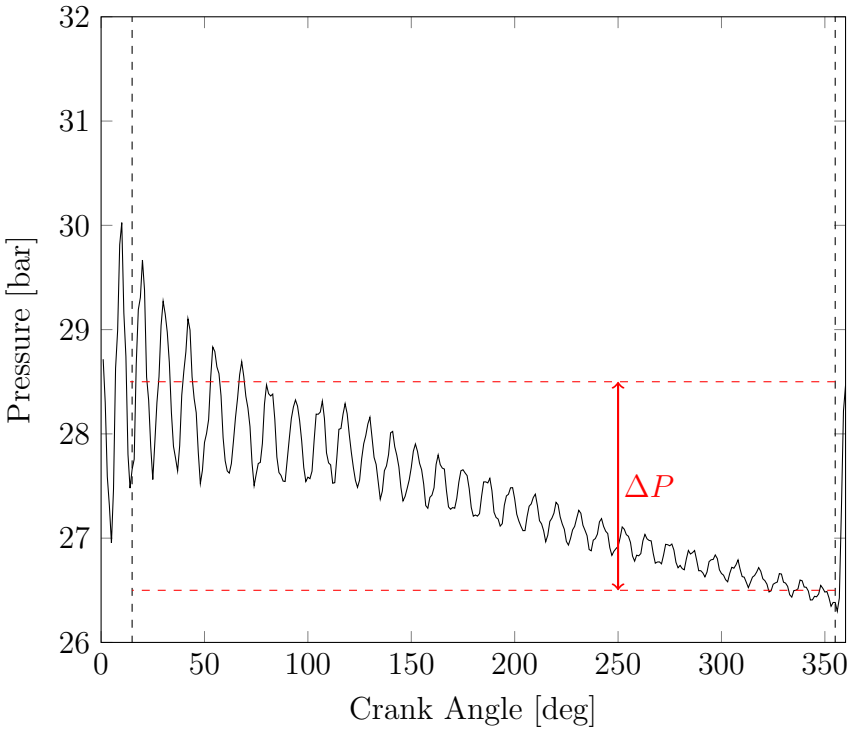

Figure 6.2: Crossover Pressure for a Single Cycle

The vertical lines indicate the position at which both valves are closed. Also indicated on the graph is the pressure drop experienced by the XOVR. The oscillation that is measured is not a characteristic of the XOVR passage, but due to the quick connect fitting that connects the pressure transducer to the XOVR. With the new valve timing the average pressure drop is roughly 7% per cycle. With the increase in pressure in the XOVR the temperature of the gas has also increased to 300°C, an increase of 50°C from the previous profiles. The values for the average XOVR pressure and pressure drop are given in Table 6.4.

Table 6.4: XOVR Pressure Characteristics

Engine Speed	**Cycle Mean**	**Pressure Drop**
850rpm	27.9 bar	1.5 bar
1000rpm	28.9 bar	1.7 bar
1200rpm	30.5 bar	1.9 bar

Ignition Timing

With the earlier closing time of the XOVO, the ignition timing in the engine can be significantly advanced. Best achievable ignition timing has been improved to 12, 11 and 10 °ATDC for 850, 1000 and 1200rpm respectively. This advancement in

ignition timing is advantageous for combustion as it will allow for combustion to be initiated closer to TDC in a smaller volume and with more intense turbulence, potentially leading to greater output and efficiency. The improvement in the best achievable ignition timing is significant, however ignition advancement is still limited by the peak pressure capabilities of the RPV. Further ignition advancement could be achieved with improvements to the RPV valve train.

Fired Cylinder Pressure Traces

The effect of the new cam profiles can be seen in Figure 6.3 where a fired cylinder pressure trace from cycles representative of normal combustion are compared between the new and old profiles.

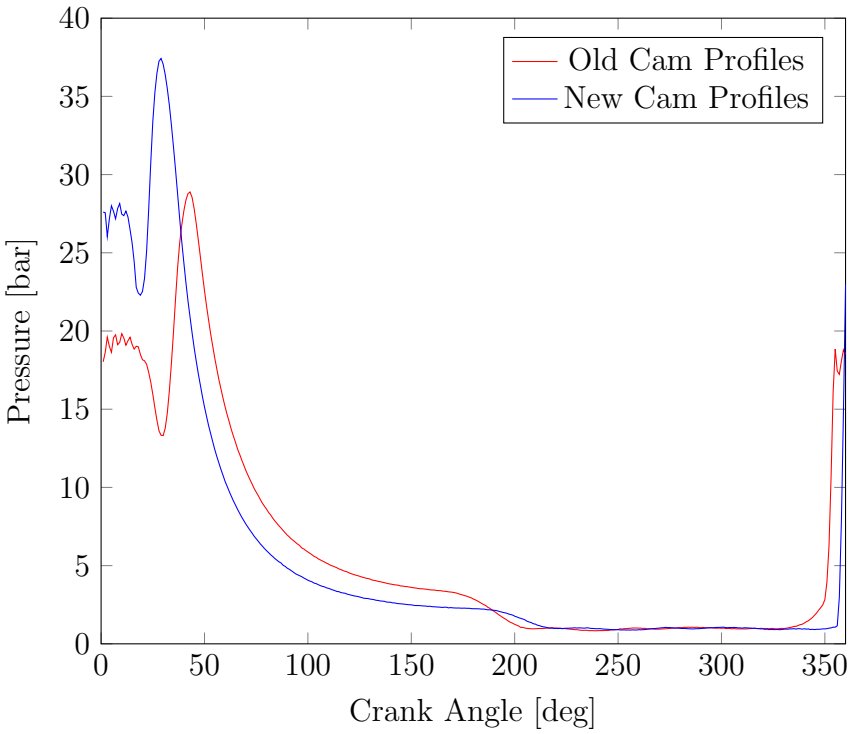

Figure 6.3: Fired Cycles with New and Old Cam Profiles

As can be seen from these example pressure traces, the new cam profiles appear to give better combustion characteristics. The peak pressure occurs closer to TDC and is greater. These two characteristics are evidence of improved combustion, which should result in greater overall efficiency. It would appear that by looking at these pressure traces that an improvement in the combustion has been achieved by the new timings.

6.3.3 Indicated Output

Net engine IMEP with the new cam profiles is lower than expected. Despite ignition occurring closer to TDC, gains are not made in $IMEP_{net}$ when compared to the old cam profiles. Figure 6.4 shows the $IMEP_{net}$ at the best achievable ignition timings for the range of engine speeds and equivalence ratios tested.

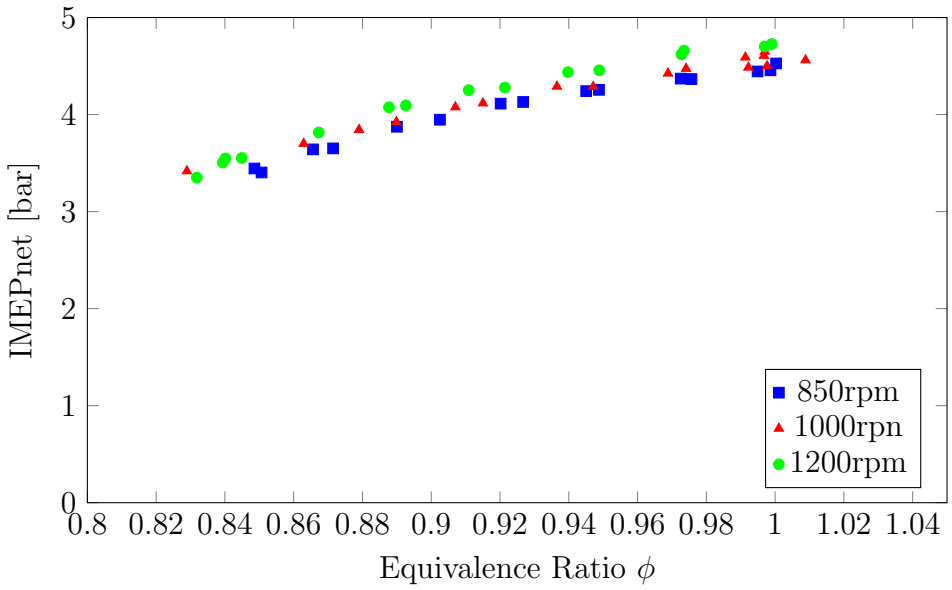

Figure 6.4: $IMEP$ for Best Achievable Ignition Timing with New Cam Profiles

Overall the engine output has decreased with the usage of the new cam profiles despite ignition occurring closer to TDC and higher peak pressures being achieved. With the new valve timing the maximum $IMEP_{net}$ achieved is 4.5 bar. In comparison, an $IMEP_{net} = 5.8bar$ has been achieved with the old profiles. The maximum $IMEP_{net}$ occurs at an engine speed of 1200rpm as the $IMEP_{net}$ is moderately increasing with engine speed. A comparison of the best achievable $IMEP_{Net}$ at 1000rpm for both cam profiles is given in Figure 6.5.

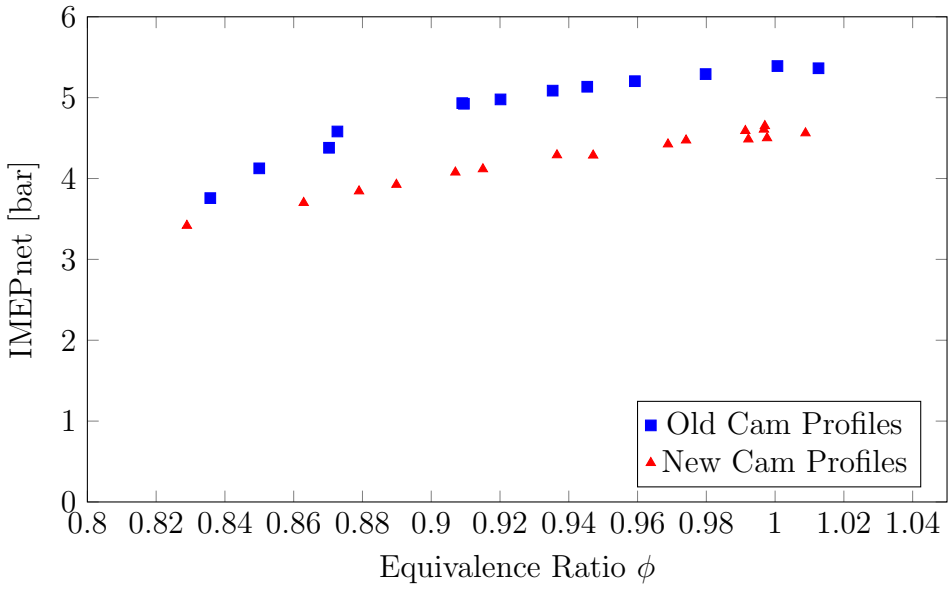

Figure 6.5: $IMEP_{net}$ Comparison at $n_{engine} = 1000rpm$ with New Valve Timing

From figure 6.5 it is evident that there is a significant decrease in the net output of the engine. Part of this decrease can be attributed to the increased pressures in the compression cylinder resulting in greater compression work. The work in terms of IMEP of the compression cylinder has increased to 4.3 bar at all tested engine speeds, an increase of 0.4-0.5 bar. However this does not attribute for the full decrease in output, as the IMEP of the expansion cylinder has decreased at tested engine operating points as well. The IMEP of the expansion cylinder is compared at 1000rpm in Figure 6.6.

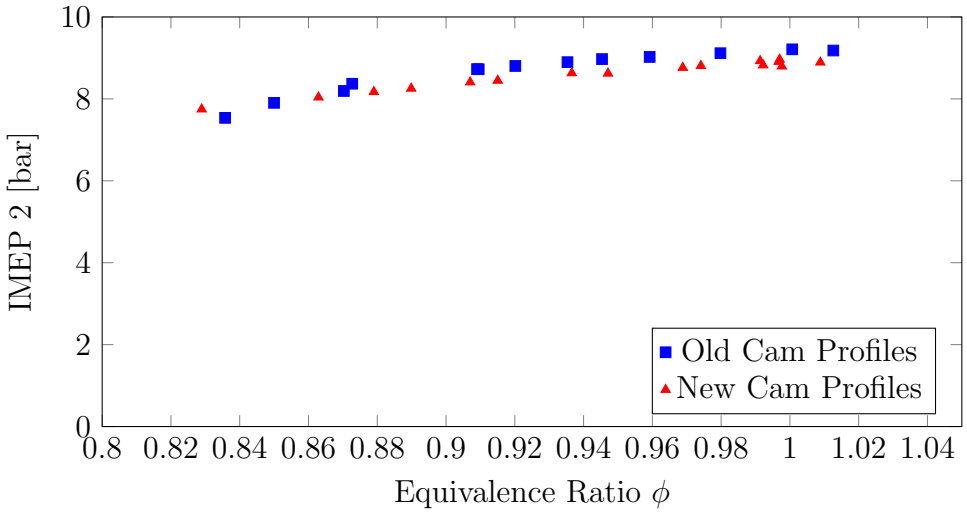

Figure 6.6: $IMEP_{Cyl2}$ Comparison at $n_{engine} = 1000rpm$ with New Cam Profiles

As can be seen from this figure a moderate decrease in the $IMEP_{Cyl2}$ is measured. On average for any given equivalence ratio the value has dropped by approximately 0.1-0.2 bar. While not a significant drop in engine output, it is expected that with the advanced ignition timing would lead to a significant improvement in the output from the expansion cylinder.

6.3.4 Burn Durations

Given that the engine is now operating with ignition occurring closer to TDC it should also be noted that overall burn durations have decreased at all measured operating points. Figure 6.7 shows the total burn durations at best achieved ignition timings at 850, 1000 and 1200rpm.

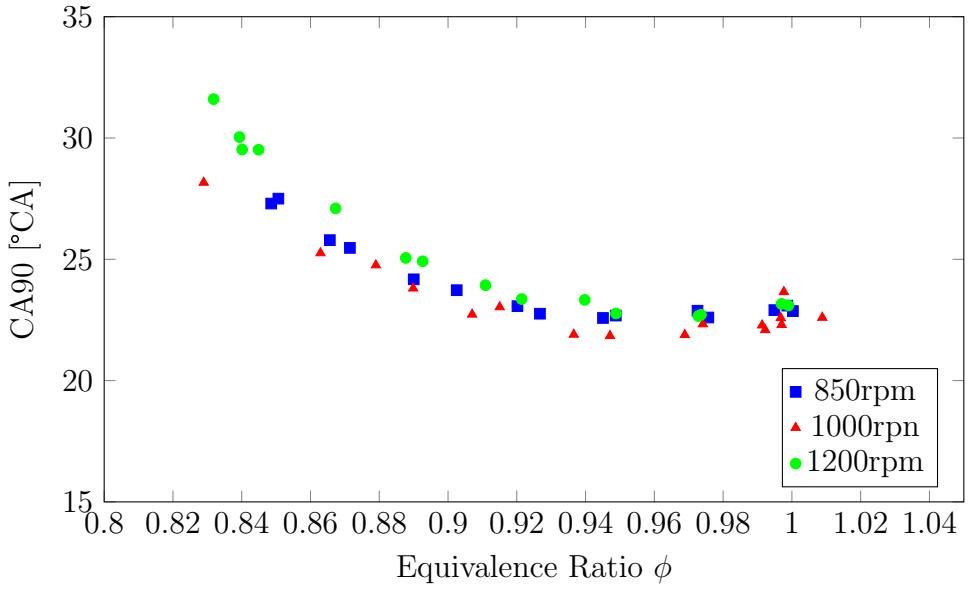

Figure 6.7: $IMEP$ for Best Achievable Ignition Timing with New Cam Profiles

What is particularly impressive with these results in the decrease in overall burn durations is that a large improvement is measured despite what would be considered fast burn already being achieved under previously tested conditions. Figure 4.2 can be referenced to see the burn durations achieved with the old profiles. Using the old profiles durations of 30°CA were achieved at stoichiometric equivalence ratios which have been decreased to 22-23°CA. This decrease of 8°CA is impressive on its own, is more impressive considering that this is almost at 30% reduction. Furthermore, this reduction in burn duration is accompanied by burn occurring nearer to engine TDC, leading to significantly better conditions for combustion.

6.3.5 Combustion Stability

Also of interest with the change in valve timing was how the combustion stability is effected. Since ignition occurs closer to TDC it is likely that more in-cylinder turbulence is present which may make ignition more difficult. However, the COV_{IMEP} shows that overall stability has improved, with reductions occurring at all tested equivalence ratios. Combustion stability results from old valve timings can be referred to in Figure 4.4. This COV_{IMEP} is shown for best achievable ignition timings at tested engine speeds in Figure 6.8

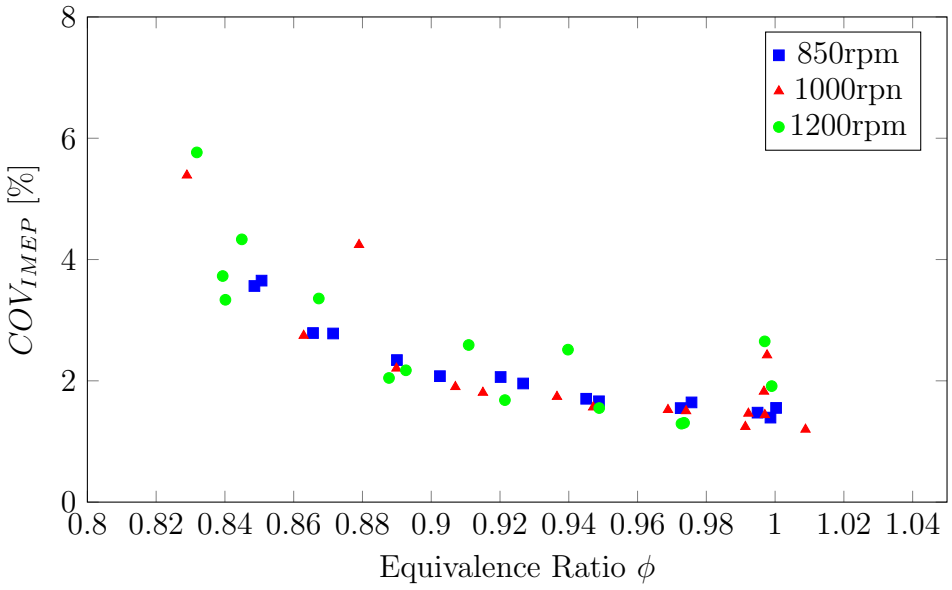

Figure 6.8: COV_{IMEP} at Best Achievable Ignition Timing with New Cam Profiles

As shown in this figure the COV_{IMEP} is under 2% near stoichiometric equivalence ratios and is generally low throughout the tested engine regime. The COV_{IMEP} is lower for these equivalence ratios than it was with previous valve timings as shown in Figure 6.9 comparing results at 1000rpm.

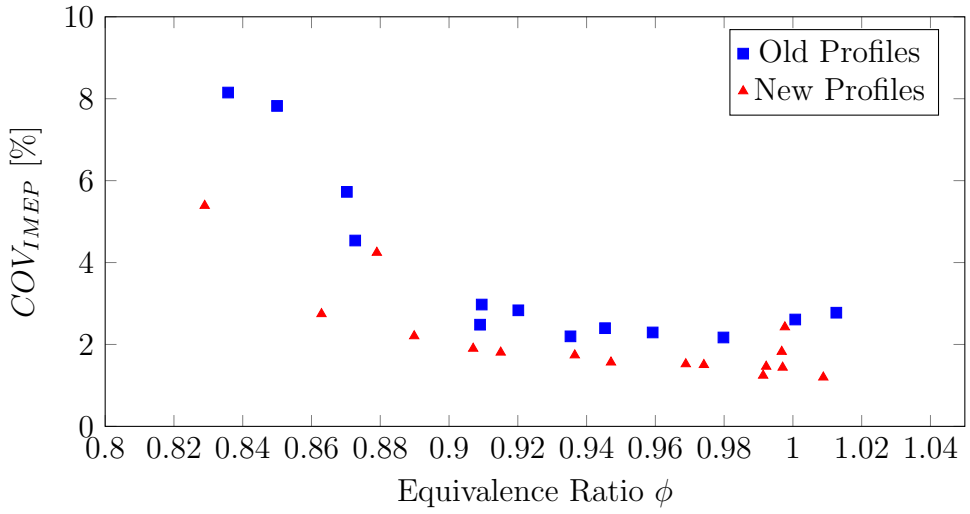

Figure 6.9: COV_{IMEP} at a $n_{engine} = 1000rpm$ comparison between cam profiles

The decrease in COV_{IMEP} can be seen at all tested equivalence ratios with the new cam profiles. With the new profiles stability has improved significantly for the combustion cylinder, with COV_{IMEP} as low as 1% being achieved.

The other measurement of stability is the COV_{LPP}. Figure 6.10 shows the variation for tested engine speeds and equivalence ratios. As with the COV_{IMEP}, the COV_{LPP} is shown to be within acceptable limits (under 15%) at tested equivalence ratios. While it can be noted that several of the test results have a higher COV_{LPP}, the values do fall within acceptable limits. Upon closer inspection of the tests themselves it was noted that there were one or two late phased cycles in these data sets. These would not be enough to say that the engine operation is unstable, however they could negatively impact a statistical measure such as the COV.

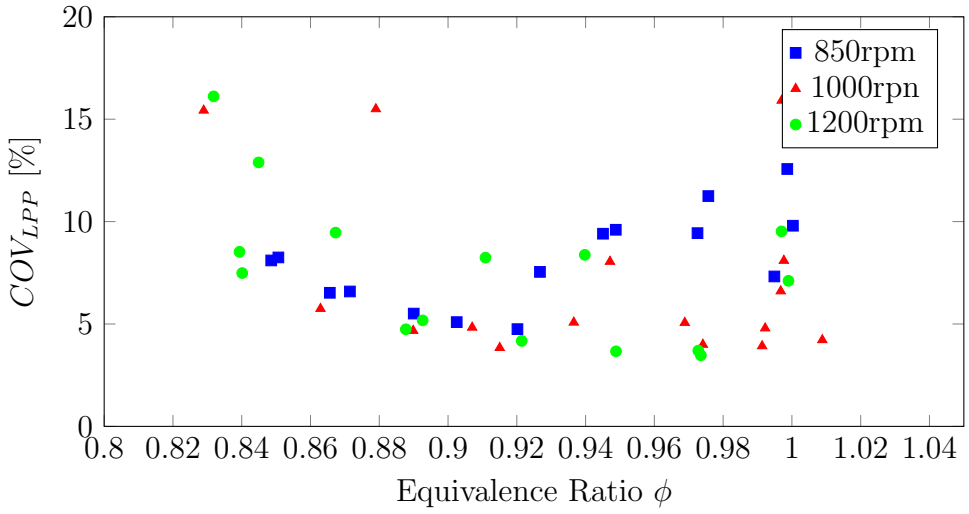

Figure 6.10: COV_{LPP} at Best Achievable Ignition Timing with New Cam Profiles

6.3.6 Volumetric Efficiency

As with previous testing on this engine volumetric efficiency remains poor. Volumetric efficiency has experienced a significant reduction with the new valve timing to 62-64% within the range of 850-1200rpm, an 8-10% drop in efficiency. This number will be further explored in Section 6.5.

6.4 Combustion Cylinder Performance Analysis

The results presented in the previous section are quite peculiar compared to what would normally be expected from a combustion system. What is perplexing from a combustion point of view is that the ignition occurs closer to TDC, burn durations are shorter and greater peak pressures are realized, yet the overall work outputted by the cylinder has decreased. It would be expected that these conditions would lead to significant improvements in combustion, yet they have resulted in no gains in output. To begin explaining what is occurring in the combustion cylinder it is necessary to better understand what the effect of the crossover passage outlet valve closing (XOVO-c) is on the combustion cylinder. Figure 6.11 has annotated the pressure traces of two combustion cycles representative of normal combustion, one with old timing and one with new.

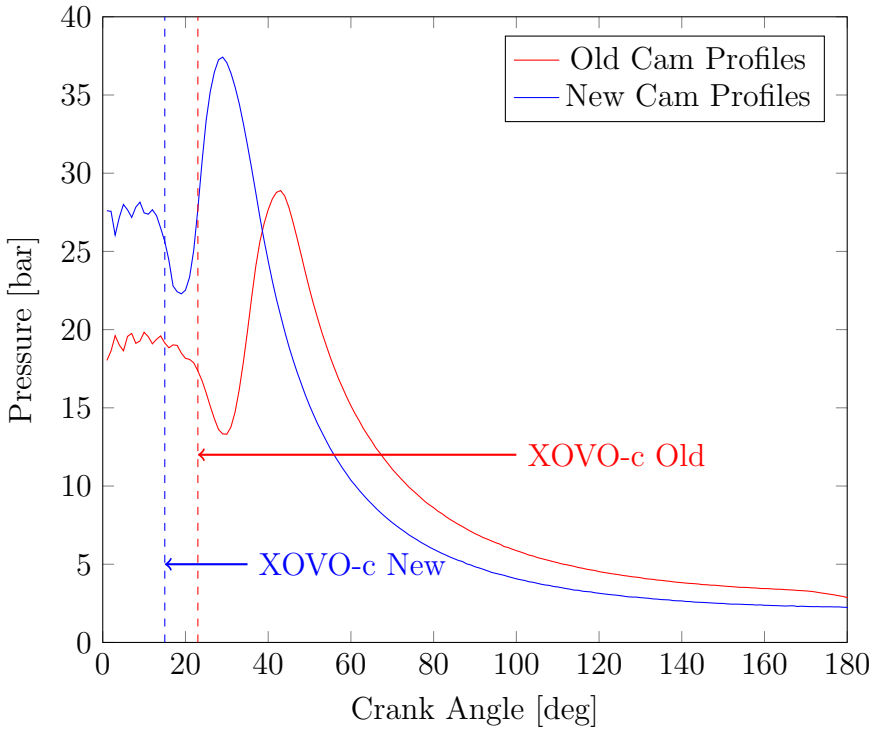

Figure 6.11: Fired Expansion Stroke with XOVO-c noted

As can be seen in this figure, the XOVO-c closes earlier than with the old timing. As shown in previous sections this change in valve timing will result in better combustion characteristics than with the old timing. However, what was not fully noted before was the change of the volume of the combustion cylinder when the valve closes. When the engine is at 25°ATDC, the volume of the expansion cylinder is approximately 19 mL. In comparison, at 15°ATDC the volume of the cylinder is approximately 7.5mL, roughly half the total volume. The amount of fresh charge in cylinder is determined by two factors; the pressure of the XOVR and the volume it is transferring into. As the valve is open and the volume expanding, mass is continuously transferred to the combustion cylinder. This results in the amount of mass transferred being dependent on pressure and volume. This means that the total mass is not guaranteed to be the same with a change in valve timing. An analysis on the mass transfer can be done using ideal gas law as in Section 6.4.1.

6.4.1 Ideal Gas Law Analysis

Using the volume and pressure at the time of XOVO-c the amount of mass in-cylinder can be estimated. In order to eliminate complexities in evaluation motored engine cycles (with no combustion) are evaluated. The mass analysis has been performed for

motored engine cycles at 850rpm for XOVO-c new and old valve timings respectively. Volume of the combustion cylinder is taken as the volume when the XOVO-c for each valve timing case. The in-cylinder mass has been evaluated assuming ideal gas properties of air. The values used for analysis are given in Table 6.5.

Table 6.5: Values Used for Cylinder Ideal Gas Analysis

	Old Timing	**New Timing**
Volume at XOVOc	$19038mm^3$	$7580mm^3$
Pressure	17 bar	22 bar
Temperature	250°C	275 °C
R	287.05 $kJ/kg \cdot K$	

Using the values as given in the table the mass could be calculated using ideal gas law as presented in Equation 6.1. It should be noted that the pressure in-cylinder is actually lower using the motoring trace than with the fired combustion cycles. This is due to the combustion that is occurring preceding the valve closing, which will cause the pressure to be higher. This combustion would effect mass transfer, however the motored cycles were selected as the analysis method as the complexities that arise from combustion fall outside the scope of this work.

$$m = \frac{PV}{RT} \tag{6.1}$$

Using this equation the in-cylinder mass with the old valve timing is determined 0.214 g/cycle, while with the new valve timing the total mass is reduced to 0.119 g/cycle. This is approximately a 50% reduction in total mass per cycle. However, with the old valve timing the maximum $IMEP_{Cyl2} = 9.2$ bar, compared to 9 bar with the new timing; only a reduction of 2.2%. On a mass basis the new valve timing represents a significant improvement in the quality of combustion.

This decrease in mass admitted to the expansion cylinder also partially explains the decreased temperature and pressure at the end of the expansion stroke. Given that the pressures are occurring at the same volume, an explanation for the decrease in temperature and pressure is a decrease in mass. Using $PV = mRT$ it can be understood that in order to keep the equation balanced for a fixed volume a decrease in mass will be met with a decrease in pressure. It is also possible that further contributing to the decreased pressure and temperature is the increased time the combustion products have to expand due to the advanced ignition timing. Further mass losses that could have changed with the new valve timing are blow-by losses in

the compression and expansion cylinders, or mass leakage in the XOVR.

6.4.2 Indicated Specific Fuel Consumption

Given that the mass burned per cycle has decreased, it could be reasoned that the fuel consumption will also decrease for this engine. This is true as the average mass fuel flow rate has decreased from 0.163g/s to 0.157g/s with the new valve timing. However, the question is whether this decrease in fuel consumption is significant enough to offset the the decrease in power output. In order to determine this, a parameter called Indicated Specific Fuel Consumption (isfc) is used. Indicated specific fuel consumption is the rate of consumption per unit output power. It is calculated as in equation 6.2 [1].

$$isfc = \frac{\dot{m_{fuel}}}{\dot{W}} \tag{6.2}$$

Units used for the isfc are g/kWh. The work input to the engine will be the indicated performance, IMEP. It will be cused to calculate $\dot{W}$ using equation 6.3.

$$\dot{W} = IMEP \times V_s \times N \tag{6.3}$$

In this equation V_s is the swept volume of the engine and N is the engine speed in rev/s. Indicated specific consumption will be calculated for both $IMEP_{net}$ and $IMEP_{Cyl.2}$. Results for best achievable ignition timings are presented in Table 6.6 at all tested engine speeds.

Table 6.6: Indicated Specific Fuel Consumption of the Split-Cycle Engine in g/kWh

	Net		**Cylinder 2**	
	Old	**New**	**Old**	**New**
850rpm	328.7	371.1	191.9	187.3
1000rpm	312.4	348.1	181.5	178.6
12000rpm	295.2	329.6	172.1	171.0

The specific fuel consumption of the engine show some interesting results. The net isfc increases when changing for the old valve timing to the new one. This behavior could be attributed to the increased compression work present with the new valve timing. The expansion cylinder does show a decrease in specific consumption, however the decrease is marginal at best. A decrease of $3g/kWh$ would not be considered significant in terms of the consumption. Once again, referring back to combustion characteristics discussed previously, this was not the expected behaviour for the com-

bustion cylinder. What this could be attributed to is the increased mass loss in the XOVR passage, which will be calculated in the following section.

6.4.3 Crossover Mass Loss

As has been noted in previously, the XOVR is the source of a significant amount of mass loss per cycle. This is primarily evidenced by the discrepancy in calculating the AFR using the mass fuel and mass air flow rates verse using the lambda sensor. With the new valve timing it could be hypothesized that due to the increase in XOVR pressure, more mass is lost per cycle in the XOVR than at previously tested conditions. While it is possible that heat transfer does account for some of this pressure drop, the pressure drop per cycle is to large for heat transfer to account for the entire pressure drop.

As with the mass transfer calculations done previously, the mass loss from the crossover passage will be calculated using ideal gas law. Mass will be calculated for the volume of crossover passage when both valves are closed, once when the valves have just closed and immediately preceding them opening. The calculated masses will then be used to determine the mass loss per cycle. This will be calculated for both sets of valve timing to provide an estimate of the increase in mass loss between the two cam profiles. Heat transfer losses will be assumed to account for 30% of the pressure drop. Temperature will be assumed to be the average XOVR temperature as measured experimentally.

The calculations for this set of data have been performed at 850rpm using the motoring traces. Using the motoring traces allows for standard air assumptions to be used to determine properties of the air. Air temperature is assumed to be constant at 250°C for the old profiles and 275°C for the new ones. Total mass loss in the XOVR is estimated to increase from 0.81g/s to 1.15g/s with the new valve timing, an increase of 0.34g/s total. Using the stoichiometric AFR of methane 17.2:1, the mass loss of methane is estimated to increase by 0.02g/s between the new and old cam profiles. This value is then used to compensate the mass fuel flow rate for the tests with the new cam profiles. Using the compensated mass fuel flow rate the isfc_{Cyl2} will decrease to 163.3 g/kWh. For the isfc_{net} the specific fuel decreases to 323.6 g/kWh. Accounting for the extra mass loss that occurs due to the increase in XOVR pressure, the specific output of the split-cycle engine improves for both the net and

combustion cylinder. Table 6.7 shows the specific fuel consumption of the engine with the mass loss compensation performed for all tested engine speeds at best achievable stoichiometric operating conditions.

Table 6.7: Indicated Specific Fuel Consumption of the Split-Cycle Engine in g/kWh with adjustments for mass leakage

	Net		**Cylinder 2**	
	Old	**New**	**Old**	**New**
850rpm	328.7	323.6	191.9	163.3
1000rpm	312.4	308.6	181.5	158.3
12000rpm	295.2	289.8	172.1	150.3

This mass loss shows the need to improve the design of the XOVR passage to decrease the mass loss occurring. The change in consumption is significant and minimizing this loss would lead to improved performance. It is believed that the cause of this leakage is the valve stem seals. Since they come from a production 4-stroke engine, they are only designed to withstand pressures of up to 3 bar, significantly less than the pressures in the XOVR. It is believed that by redesigning these seals the leakage could be minimized and overall performance could be further improved.

6.5 Engine Mass Balance Analysis

One way to gain better insight to the split-cycle engine operation is through the use of a mass balance. By doing a mass balance on the split-cycle engine certain aspects of the engine will be better understood and the best methods to optimize its operation though future designs realized. For this simplified analysis the system will be evaluated as an ideal system where no mass or energy enters or leaves the system after air has entered the compression cylinder. With respect to the performance of this split-cycle, it means that the issues with mass and heat loss in the compression cylinder are neglected.

Since the purpose of this mass balance is to analyze the relationship of the compression and expansion cylinder, two defining rules are set for there performance.

1. The amount of mass entering or exiting the system can be restricted by either the compression or expansion cylinder. The mass that is compressed is the mass present in the compression cylinder when the intake valve closes. The mass that is expanded is the mass in the expansion cylinder when the XOVO-c.

2. The amount of mass to be compressed is the mass in-cylinder at the intake valve closing. Any mass not transferred to the XOVR is therefore re-expanded

These two rules show an interesting characteristic of the split-cycle engine. As shown in section 6.4 the amount of mass transferred to the expansion cylinder, and therefore exhausted out of the system, is determined by XOVO-c. However, this is largely unrelated to mass compressed as that amount will be determined by the geometry of the engine. This creates a difference in the mass expanded versus the mass compressed. Using this concept a new parameter has been defined by the author, the Mass Compressed Ratio (MC_r).

$$MC_r = \frac{m_{eCyl.2}}{m_{cCyl.1}} \tag{6.4}$$

The MC_r is defined as the expanded mass in the expansion cylinder $m_{eCyl.2}$ divided by the mass compressed in the compression cylinder $m_{cCyl.1}$. The expanded mass is the mass at the XOVO-c as determined using a motored engine trace and standard gas assumptions. The compressed mass is the theoretical mass in the compression cylinder calculated using SATP assumptions. In a normal 4-stroke engine this value would be unity assuming no blow-by, however with the split-cycle or any split-engine design this value can vary. A $MC_r < 1$ will result in poor volumetric efficiency and mass being re-compressed on each cycle in the compression cylinder. This occurs as mass flow will be limited by the compression cylinder, meaning that the expansion cylinder is over-sized and performing excessive work. It is not theoretically possible for $MC_r>1$ as this would violate the conservation of mass in the system. Hence this value would approach one and could never practically exceed it.

What should be noted about the MC_r is that it is not a parameter that can be calculated using the geometry of the engine. It is a function of the displacement volume and valve timing, thus resulting a value largely dependent on the working pressures of the engine. This means it can only be practically calculated after tests have been performed on the engine.

6.5.1 Mass Compressed Ratio Evaluation

Using the engine performance data the MC_r can be determined. Results from this evaluation are presented at engine speed of 850rpm for both sets of valve timings. Using the nominal valve timing of intake valve closing and XOVO-c, volumes at these

locations are determined. Temperature of the air is estimated using the temperatures measure by thermocouples instrumented to the engine. Using ideal gas law $m_{eCyl.2}$ and $m_{cCyl.1}$ can be estimated. With the old valve timings the $\mathrm{MC}_r = 0.69$. With new valve timing the $\mathrm{MC}_r = 0.42$. This value shows that how with the new valve timing a significant increase in the excess mass being compressed for each cycle is being done with the new valve timing. The values presented by the MC_r suggest that an excess of mass is being compressed for both valve timings. Output has decreased with the new valve timing as the MC_r ratio is decreasing for the new valve timings.

6.5.2 Relationship of MC_r to Volumetric Efficiency

As shown in section 6.3.6 the volumetric efficiency has decreased with the change in valve timing. A possible explanation for this decrease in volumetric efficiency, and the poor volumetric efficiency of split-cycle engines in general, could be linked to the MC_r. As can be understood from the MC_r the expansion cylinder is the restricting element for the flow in the split-cycle engine. Given that less mass is being expanded with the new valve, timing a decrease in the overall volumetric efficiency of the engine would be expected.

Given the large reduction in the MC_r it could be expected that a larger decrease than 10% would occur in the volumetric efficiency. The reasons for the significant discrepancy in this number are due to the actual split-cycle engine not being an ideal system. Mass leakage is known to happen in the XOVR and a large amount of blow-by is present, making direct comparisons inaccurate. Also, usage of ideal gas law for this analysis would not be fully accurate as it only provides an estimate of the in-cylinder mass. Ideally usage of this value should be accompanied by more sophisticated methods of evaluation.

6.5.3 Ideal Expansion Cylinder Volume

From the results given by the MC_r it is apparent that the mass ratio of compression to expansion is not correct for this engine. To maximize volumetric efficiency and output, the MC_r needs to be optimized for the split-cycle engine. Given that an ideal MC_r would be one it is obvious that a change in the expanded mass needs to be achieved. While valve timing could be retarded this is not ideal from a performance standpoint. One thing that could achieve a $MC_r = 1$ would be to have differing vol-

umes for the compression and expansion cylinder, assuming working pressures remain the same.

Differing volumes for compression and expansion stroke is a noted design feature that has been mentioned in literature that could improve engine efficiency [1]. One of the advantages the split-cycle is that it is a relatively simple way to achieve this [12, 42]. However, the exact effects differing volumes have never been evaluated in literature. The results from the MC_r suggests is that differing volumes are not a desired feature of this design, but a required one. With this design change one could expect improved engine performance.

For the current design the ideal volume has been calculated for the split-cycle engine at the new valve timing. An ideal bore can be estimated using $PV = mRT$ (assuming that a change in volume would not change in working pressures. Using the m_c calculated in earlier sections as the m_e, the ideal bore of the expansion cylinder of this engine would be 102mm. Given that the bore is currently 67mm, the current expansion cylinder is vastly undersized. Changing to a larger bore on the expansion cylinder could result in better volumetric efficiency, thus resulting in greater engine output. This number should only be used to give an idea of the ideal cylinder size. Were any design changes to be made to the engine a study with a numerical model of the engine should be undertaken.

6.6 Exhaust Valve Timing Closure Effects

As discussed in section 4.2.1 the split-cycle engine design inherently traps a significant amount of mass in cylinder. This leads to more dilute mixtures which will contribute to the high lean limit of the engine. With the new valve timing, the exhaust valve was set to close at 2°ATDC. This was the latest timing that the valve could be set at without fresh charge expanding into exhaust or the valve contacting the piston. As such, valve timing has been changed to close much earlier at 12 °BTDC-e. New motored pressure trace of the expansion cylinder for the advanced valve timing is given in figure 6.12.

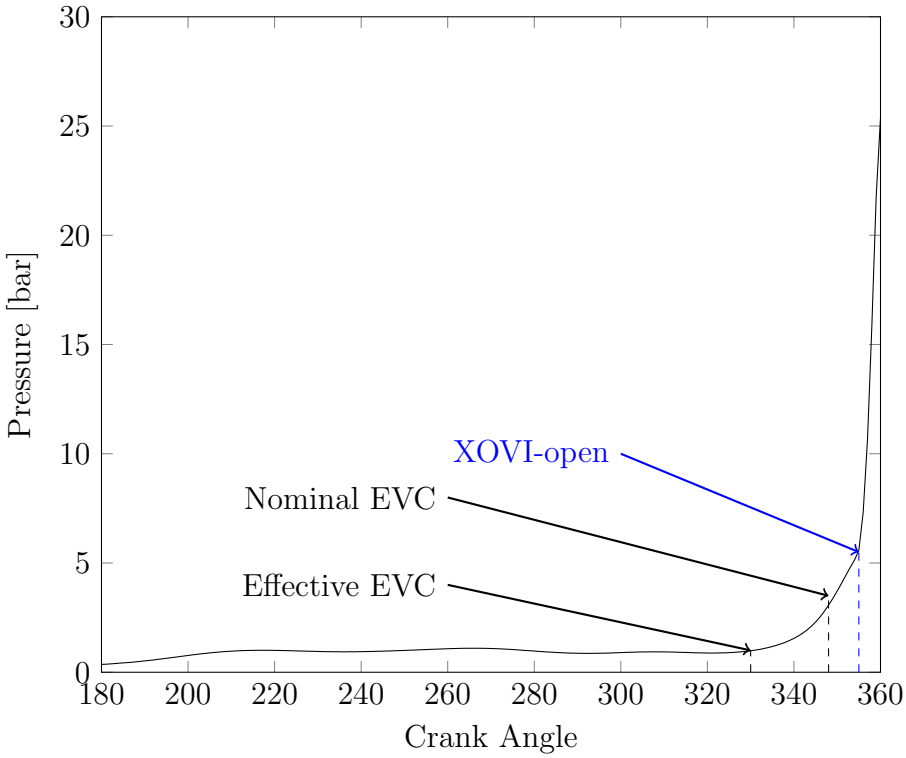

Figure 6.12: Motoring Trace for New Exhaust Valve Timing Closing Event

As evidenced by the pressure rise significantly before engine TDC the valve is closing and trapping a significant amount of combustion products. This amount of IGR is so significant that it is not possible to get the engine to running with this exhaust valve timing. The pressure rise as indicated begins at roughly 330°BTDC, marking the point of effective valve closing. This point was determined ads the point which the compression cylinder pressure trace deviates from the measured exhaust pressure transducer. This is the same effective valve timing as with the old cam profiles meaning the same amount of mass is trapped in cylinder. However, given that the amount of mass transferred in at TDC is roughly half, this will result in the % IGR doubling. As such, using the same criteria as in previous IGR estimations the IGR = 30-50%. This amount is extremely excessive and would be an explanation for why ignition is no longer possible.

This exhaust valve closing effect shows that the IGR ratio can be effected negatively enough to no longer allow for ignition. With the current design of the engine a new exhaust valve closure time between the two tested values is not possible. Fine adjustment is not possible between the intake/exhaust cam and the crank shaft and would require an eccentric idler gear or similar mechanism to be designed installed

between the two shafts. Thus adjustment is limited by the pitch of the timing belt, which results in adjustments in 10°CA increments. In order to achieve the finer adjustment major engine components would need to be relocated. Given that results showed the effects of the valve closure conclusively and the amount of work necessary to modify for finer adjustment, it was deemed not necessary to further investigate exhaust valve closure effects.

6.7 Future Design Considerations

Given the results discussed in this section several design recommendations can be made for future works on this engine.

Exhaust Valve Adjustment

To minimize the trapped combustion products in-cylinder, a mechanism should be designed to give finer adjustment to the exhaust valve closing and allow for optimal exhaust valve timing to be achieved.

Crossover Mass Leakage

The leakage in the XOVR has been noted as a significant loss of both fuel and compression work in this engine. The most likely cause of the leakage is the valve stem seals which should be redesigned accordingly to minimize the pressure loss.

Differing Compression and Expansion Cylinder Volumes

The expansion cylinder is undersized for the amount of compressed mass in this engine. Either the compression cylinder volume should be decreased or expansion cylinder increased. This will result in less mass re-compression, better volumetric efficiency and improved output. An accurate numerical study should be undertook to come up with the best possible changes in the volume of these cylinders.

Chapter 7

Summary, Conclusions and Recommendations

The primary goal of this research was to provide greater insight into the operation of the split-cycle engine constructed at the University of Windsor. While previous work on this engine provided an excellent basis for the start of this research many questions pertained to the operation of this engine. The two questions that this work attempted to solve were:

1. **Lean Limit of Operation:** One unanswered question from previous testing was the relatively high lean limit of operation at $\phi = 0.85$. No definitive answer was given for the cause of this high operational limit.

2. **Valve Timing Effects:** Very low output has been achieved by the split-cycle engine. With the primary testing completed it was determined that the engine could have an improvement in efficiency and output with a change in valve timing. New cam profiles have been tested and implemented in this work.

7.1 Conclusions on Operational Lean Limit

Previous to this work it was hypothesized that the lean limit could be attributed to intense in-cylinder turbulence at the time of ignition. As has been presented by this work a large contributing factor of this lean limit is early exhaust valve closure. Early closure traps mass in the cylinder of the engine and dilutes the mixture making it more difficult to ignite.

In order to achieve leaner operation different ignition strategies have been tested. Due to cost and practicality coil based ignition strategies were tested. A short summary of the tested strategies is presented.

- **Multiple Re-Strike Ignition:** A single coil is re-struck multiple times in a single ignition event. Implementation of this strategy degraded the quality of ignition with increased misfires, higher COV and lower output. This was concluded to be inefficient due to the extended discharge period of this strategy.
- **Dual Coil Ignition:** The discharge of two coils simultaneously through a single spark plug was shown to be an effective way of extending the lean limit of operation. This strategy results in more energy being deposited to the ignition kernel. This strategy has shown to be moderately effective at extending the lean limit and improving near lean limit performance in the split-cycle engine. Number of misfires have decreased along with measured COV.

The dual coil strategy proved to be effective at moderately extending the lean limit of operation. The true effectiveness of this strategy comes from reducing the number of misfires in the engine, particularly beneficial considering the engine is fuelled with methane. However, the most likely cause of the high lean limit is the high amount of trapped mass (estimated at 15-25%). With this knowledge exhaust valve timing is crucial for the split-cycle engine.

7.2 Conclusions on Valve Timing Effects

The results of changing valve timing have had mixed effects in terms of performance on the split-cycle engine. Overall output has decreased, however combustion characteristics such as burn duration, indicated fuel consumption and coefficients of variation have all improved. It has been determined that the expansion cylinder acts as a restriction to the flow. Since the valve closes earlier less volume is present, resulting in a reduction in mass on the cylinder. Doing a mass balance analysis reveals that the engine is compressing significantly more gas than it is expanding, resulting in more re-compression work and lower output.

7.3 Recommendations and Future Work

It is the recommendation of the author that the following improvements could be made to the split-cycle engine:

1. Fix the mass leakage in the XOVR. This is a significant loss of work in the engine and could lead to better engine performance. Mass leakage is most likely around the valve stem seals so the valve stem seals should be improved

2. Explore a change in the displacement volume of either the compression or expansion cylinder. A simple mass balance analysis has shown that more mass is being compressed per cycle then can be expanded due to the engine valve timing. This potentially causes numerous negative effects such as poor volumetric efficiency and needless compression work. An in-depth numerical study should be performed to determine a change in volume that would result in better operational characteristics for the split-cycle engine.

3. Though not discussed in depth in this work, the closure force of the RPV is a limiting factor for engine performance on this engine. In order to further advance ignition closer to TDC and achieve better combustion the valve train should be modified to enable higher peak pressures before further testing is done.

Bibliography

[1] Richard Stone. *Introduction to Internal Combustion Engines: 4th Edition*. SAE International, Warrendale, PA, 2012.

[2] Fanourios Zannikos, Evangelos Tzirakis, K Pitsas, and S Stournas. Vehicle emissions and driving cycles: Comparison of the athens driving cycle (adc) with ece-15 and european driving cycle (edc). 8:282–290, 01 2006.

[3] Proposal for post-2020 co2 targets for cars and vans. `https://ec.europa.eu/clima/policies/transport/vehicles/proposal_en`. Accessed: 2018-04-23.

[4] J.C. Guibet and E. Faure-Birchem. *Fuels and engines: technology, energy, environment*. Number v. 2 in Publications de l'Institut français du pétrole. Éditions Technip, 1999.

[5] Luz Dondero and José Goldemberg. Environmental implications of converting light gas vehicles: the brazilian experience. *Energy Policy*, 33(13):1703 – 1708, 2005.

[6] Haeng Muk Cho and Bang-Quan He. Spark ignition natural gas engines—a review. *Energy Conversion and Management*, 48(2):608 – 618, 2007.

[7] T. Korakianitis, A.M. Namasivayam, and R.J. Crookes. Natural-gas fueled spark-ignition (si) and compression-ignition (ci) engine performance and emissions. *Progress in Energy and Combustion Science*, 37(1):89 – 112, 2011.

[8] R Tilagone and S Venturi. Development of natural gas demonstrator based on an urban vehicle with a downsized turbocharged engine. 59:581–591, 11 2004.

[9] David Lancaster, Roger B. Krieger, S.C. Sorenson, and William L. Hull. Effects of turbulence on spark-ignition engine combustion. 85:689–710, 02 1976.

[10] A. Das and H. C. Watson. Development of a natural gas spark ignition engine for optimum performance. *Proceedings of the Institution of Mechanical Engineers*, 211(5):361, 1997. Copyright - Copyright Mechanical Engineering Publications, Ltd. 1997; Last updated - 2012-03-19.

[11] Iain A.S. Cameron. *Development and Analysis of a Spilt-Cycle Engine Fueled with Methane*. PhD thesis, University of Windsor, 2015.

[12] Ford Phillips, Ian Gilbert, Jean-Pierre Pirault, and Marc Megel. Scuderi split cycle research engine: Overview, architecture and operation. 4:450–466, 06 2011.

[13] Ettore Musu, Riccardo Rossi, Roberto Gentili, and Rolf Reitz. Clean diesel combustion by means of the hcpc concept. 3:964–981, 08 2010.

[14] Oded Tour et al. Steam enhanced double piston cycle engine, September 25 2007. US Patent 7,273,023.

[15] Jukka Tiainen, Ari Saarinen, Tore Grönlund, and Martti Larmi. Novel two-stroke engine concept, feasibility study. oct 2003.

[16] Carmelo J Scuderi. Split four stroke cycle internal combustion engine, April 8 2003. US Patent 6,543,225.

[17] SERGEY PALTSEV, JOHN M. Reilly, HENRY D. JACOBY, ANGELO C. GURGEL, GILBERT E. METCALF, ANDREI P. SOKOLOV, and JENNIFER F. HOLAK. Assessment of us ghg cap-and-trade proposals. *Climate Policy*, 8(4):395–420, 2008.

[18] S Rousseau, Bernard Lemoult, and Mohand Tazerout. Combustion characterization of natural gas in a lean burn spark-ignition engine. *Proceedings of the Institution of Mechanical Engineers, Part D: Journal of Automobile Engineering*, 213(5):481–489, 1999.

[19] DF Quinn and JA MacDonald. Natural gas storage. *Carbon*, 30(7):1097–1103, 1992.

[20] Jos Lelieveld, Stefan Lechtenböhmer, Sergey S Assonov, Carl AM Brenninkmeijer, Carmen Dienst, Manfred Fischedick, and Thomas Hanke. Greenhouse gases: Low methane leakage from gas pipelines. *Nature*, 434(7035):841, 2005.

[21] Christine M. Vagelopoulos and Fokion N. Egolfopoulos. Direct experimental determination of laminar flame speeds. *Symposium (International) on Combustion*, 27(1):513 – 519, 1998. Twenty-Seventh Sysposium (International) on Combustion Volume One.

[22] John B. Heywood. *Internal Combustion Engines Fundamentals*. McGraw-Hill, New York, 1988.

[23] Krister Olsson and Bengt Johansson. Combustion chambers for natural gas si engines part 2: Combustion and emissions. *SAE transactions*, pages 499–511, 1995.

[24] Takeshi Kato, Kiyoaki Saeki, Hiroto Nishide, and Takashi Yamada. Development of cng fueled engine with lean burn for small size commercial van. *JSAE review*, 22(3):365–368, 2000.

[25] Thermodynamics, Fluid Mechanics Group, and WJD Annand. Heat transfer in the cylinders of reciprocating internal combustion engines. *Proceedings of the Institution of Mechanical Engineers*, 177(1):973–996, 1963.

[26] W Scott Wayne, Nigel N Clark, and Christopher M Atkinson. A parametric study of knock control strategies for a bi-fuel engine. Technical report, SAE Technical Paper, 1998.

[27] Usman Asad, Raj Kumar, Xiaoye Han, and Ming Zheng. Precise instrumentation of a diesel single-cylinder research engine. *Measurement*, 44(7):1261–1278, 2011.

[28] Richard S Davis and Gary J Patterson. Cylinder pressure data quality checks and procedures to maximize data accuracy. Technical report, SAE technical paper, 2006.

[29] Kistler. *TDC Sensor System Type 2629DK*, 2018.

[30] David R Lancaster, Roger B Krieger, and John H Lienesch. Measurement and analysis of engine pressure data. *SAE Transactions*, 84:155–172, 1975.

[31] Sierra Instruments. *Smart-Track 2 Series 100 Mass Flow Meters and Controllers*, c.2 edition, 01 2011.

[32] Dean Ripple. Nist standard reference database 60, version 2.0 (web version). `https://srdata.nist.gov/its90/main/its90_main_page.html`. Accessed: 2018-07-09.

[33] OMEGA Engineering Inc. Thermocouple response time. `https://www.omega.com/techref/ThermocoupleResponseTime.html`. Accessed: 2018-07-09.

[34] P. J. Shayler, M. W. Wiseman, and T. Ma. Improving the determination of mass fraction burnt. In *International Congress and Exposition*. SAE International, feb 1990.

[35] M A Plint A.J. Martyr. *Engine Theory: Testing and Practice*. Butterworth-Heinemann, Oxford, United Kingdom, 3 edition, 2007.

[36] Steven C. Chapra. *Applied Numerical Methods with MATLAB for Engineers and Scientists*. McGraw-Hill Science/Engineering/Math, 2006.

[37] Gerald M. Rassweiler and Lloyd Withrow. Motion pictures of engine flames correlated with pressure cards. In *Annual Meeting of the Society*. SAE International, jan 1938.

[38] Lars Eriksson. Spark advance modeling and control. 1999.

[39] Hikmet Arslan Osman Akin Kutlar and Alper Tolga Calik. Methods to improve efficiency of four stroke, spark ignition engines at part load. *Energy Conversion and Management*, 46(20):3202 – 3220, 2005.

[40] Fanhua Ma, Yu Wang, Haiquan Liu, Yong Li, Junjun Wang, and Shuli Zhao. Experimental study on thermal efficiency and emission characteristics of a lean burn hydrogen enriched natural gas engine. *International Journal of Hydrogen Energy*, 32(18):5067 – 5075, 2007.

[41] Erjiang Hu, Zuohua Huang, Bing Liu, Jianjun Zheng, and Xiaolei Gu. Experimental study on combustion characteristics of a spark-ignition engine fueled with natural gas–hydrogen blends combining with egr. *International Journal of Hydrogen Energy*, 34(2):1035 – 1044, 2009.

[42] Joshua Finneran, Colin P Garner, Michael Bassett, and Jonathan Hall. A review of split-cycle engines. *International Journal of Engine Research*, 0(0):1468087418789528, 0.

[43] G.H. Abd-Alla. Using exhaust gas recirculation in internal combustion engines: a review. *Energy Conversion and Management*, 43(8):1027 – 1042, 2002.

[44] Amr Ibrahim and Saiful Bari. An experimental investigation on the use of egr in a supercharged natural gas si engine. *Fuel*, 89(7):1721–1730, 2010.

[45] Asok K Sen, Sudhir K Ash, Bin Huang, and Zuohua Huang. Effect of exhaust gas recirculation on the cycle-to-cycle variations in a natural gas spark ignition engine. *Applied Thermal Engineering*, 31(14-15):2247–2253, 2011.

[46] CC Huang, SS Shy, CC Liu, and YY Yan. A transition on minimum ignition energy for lean turbulent methane combustion in flamelet and distributed regimes. *Proceedings of the Combustion Institute*, 31(1):1401–1409, 2007.

[47] Payman Abbasi Atibeh, Michael J Brear, Peter A Dennis, Pedro J Orbaiz, and Harry C Watson. Lean limit combustion analysis for a spark ignition natural gas internal combustion engine. *Combustion Science and Technology*, 185(8):1151–1168, 2013.

[48] F. A. Soldera, F. T. Mucklich, K. Hrastnik, and T. Kaiser. Description of the discharge process in spark plugs and its correlation with the electrode erosion patterns. *IEEE Transactions on Vehicular Technology*, 53(4):1257–1265, July 2004.

[49] Anqi Zhang, Khanh Cung, Seong-Young Lee, Jeffrey Naber, Garlan Huberts, Michael Czekala, and Qiuping Qu. The impact of spark discharge pattern on flame initiation in a turbulent lean and dilute mixture in a pressurized combustion vessel. *SAE International Journal of Engines*, 6(1):435–446, 2013.

[50] Claudio Poggiani, Alessandro Cimarello, Michele Battistoni, Carlo N Grimaldi, Massimo A Dal Re, and Matteo De Cesare. Optical investigations on a multiple spark ignition system for lean engine operation. Technical report, SAE Technical Paper, 2016.

[51] Claudio Poggiani, Michele Battistoni, Carlo N Grimaldi, and Adriano Magherini. Experimental characterization of a multiple spark ignition system. *Energy Procedia*, 82:89–95, 2015.

[52] Terrence Alger, Jess Gingrich, Barrett Mangold, and Charles Roberts. A continuous discharge ignition system for egr limit extension in si engines. *SAE International Journal of Engines*, 4(1):677–692, 2011.

[53] Marc Bellenoue, S Labuda, B Ruttun, and Julien Sotton. Spark plug and corona abilities to ignite stoichiometric and lean methane/air mixtures. *Combustion science and technology*, 179(3):477–496, 2007.

[54] Herbert Kopecek, Soren Charareh, Maximilian Lackner, Christian Forsich, Franz Winter, Johann Klausner, Guenther Herdin, Martin Weinrotter, and Ernst Wintner. Laser ignition of methane-air mixtures at high pressures and diagnostics. *Journal of Engineering for Gas Turbines and Power*, 127(1):213–219, 2005.

[55] Bipin Bihari, Sreenath B Gupta, Raj R Sekar, Jess Gingrich, and Jack Smith. Development of advanced laser ignition system for stationary natural gas reciprocating engines. In *ASME 2005 Internal Combustion Engine Division Fall Technical Conference*, pages 601–608. American Society of Mechanical Engineers, 2005.

[56] DK Ezekoye, Matt Hall, and Ron Matthews. Railplug ignition system for enhanced engine performance and reduced maintenance. Technical report, University of Texas, 2005.

[57] J De Dale, MD Checkel, and PR Smy. Application of high energy ignition systems to engines. *Progress in energy and combustion science*, 23(5-6):379–398, 1997.

[58] *Instruction Manual:30-2853 High Output Ignition Coil.*

Vita Auctoris

NAME:	Steven G. Dal Bello
PLACE OF BIRTH:	Windsor, Ontario
YEAR OF BIRTH:	1993
SECONDARY EDUCATION:	Holy Names High School Windsor, Ontario 2007-2011
POST-SECONDARY EDUCATION:	B.A.Sc. Mechanical Engineering with Automotive Option - Co-op University of Windsor Windsor, Ontario 2011-2016
POST-GRADUATE EDUCATION:	M.A.Sc. Mechanical Engineering University of Windsor Windsor, Ontario 2016-2019